SPATIO-TEMPORAL VARIATION OF SOIL MOISTURE: REMOTE SENSING APPROACH AND HYDROLOGIC MODELLING OF SOLANI WATERSHED

Thesis submitted to Andhra University
in partial fulfillment of the requirements for the award of
Master of Technology in Remote Sensing and Geographical Information System

ANDHRA UNIVERSITY

Submitted By:

VIDYA A.

Supervised By:

Dr.V. HARI PRASAD

In-charge, Water Resources Division

Indian Institute of Remote Sensing

Dehradun, India.

iirs

Indian Institute of Remote Sensing (NRSA)
Dept. of Space, Govt. of India,
DEHRADUN – 248001
UTTARANCHAL, INDIA
(FEBRUARY,2008)

DEDICATED TO MY PARENTS

DEDICATED TO MY PARENTS

CERTIFICATE

This is to certify that Ms. Vidya A. has carried out the dissertation entitled "Spatio-temporal variation of soil moisture: Remote sensing approach and Hydrological Modeling of Solani watershed." for the partial fulfillment for the award of Master of Technology (M.Tech.) in Remote Sensing and GIS. The project has been carried out from water Resource Division under the able guidance of Dr V. Hari Prasad, In-charge" at Indian Institute of Remote Sensing, Dehradun, India.

Dr. V. Hari Prasad
Project Guide

Dr. V.K. Dadhwal
Dean, IIRS

ACKNOWLEDGEMENT

First of all, I express my sincere gratitude to Dr. V.K. Dadhwal, Dean, IIRS Dehradun for providing me the opportunity to carry out this project in this institute.

It is a pleasant aspect that I now have the opportunity to express my gratitude to my guide Dr. V. Hari Prasad. His integral view on research and his concepts in this field has made a deep impression on me. I owe him lots of gratitude for having me shown the way of research. His encouragement, suggestions and valuable feedback contributed greatly to this project. I thank him for his endurance, creative thoughts and energetic working mode that influenced me greatly insights. I want to thank him for his patience and perseverance.

I sincerely thank Dr. S.P. Aggarwal for accompanying in field and giving me field knowledge. The field knowledge imparted by him is unforgettable. The valuable suggestions he gave during reviews helped a lot to improve the research work. I also thank Er. Ashutosh Bhardwaj for accompanying to the field and for the moral support and encouragement he always gave. I also want to thank Er. Praveen Takur for accompanying me for LAI field visits.

I would like to express my sincere thanks scientists Dr. S.K. Jain and Dr. J.V. Tyagi, National Institute of Hydrology, Roorkee, for sharing soil texture data and soil moisture meter readings.

Special thanks to Mrs. Shefali Aggarwal for sharing CARTOSAT DEM. I would also like to thank Dr. Anil Kumar for imparting knowledge about DEM generation. Also special thanks to Dr. Samir Saran for sharing ENVISAT ASAR data. Thanks also to Dr. N.R.Patel for sharing LAI instrument and for instructing for its operation.

Many thanks and lots of love goes out to my parents, for their inspiration and encouragement. Moral support given by them is indebt, which is very much necessary during any research work.

A thesis cannot be completed without the help of friends. I would like to first thank fellow trainees of WRD Ms.Ambika Mukund, Ms.Nidhi Mishra and Ms.Rupinder Kaur for giving me valuable suggestions and support throughout my project. Also special thanks to my roommate Ms. Smita Majumdar for giving support and sharing some lighter moments throughout my stay in IIRS. I would like to thank Ms. Aditi Sarkar and Mr. Saurabh Verma for the treasurable moments shared. The fun we had at IIRS can never be forgotten. I also want to take the opportunity to thank Mr.Kailash, Mr. Bhaskar, Mr. Manoj who helped throughout the dissertation work.

Vidya A.
25 April 2008

ABSTRACT

Soil moisture is a key state variable of the energy and water cycle on earth surface. Soil moisture mapping is very difficult task for several reasons. Soil moisture exhibits extreme temporal and spatial variability across landscapes, with unknown scale dependencies. Limitations of acquiring adequate in-situ measurements and the high demand of data makes remote sensing and hydrologic modeling a highly viable option for extraction of knowledge about soil moisture. With the advent of optical and microwave remote sensing data with high spatial and temporal resolution, it is desirable to exploit them for assessing soil moisture. Solani watershed of 539 km^2 was chosen for the study. The study assesses the ability of soil moisture index, Short wave infrared water stress index (SIWSI) and Water deficit index (WDI) developed to infer surface soil moisture status in Solani watershed. Soil moisture index calculated using ASTER and LISS III had a good correlation coefficient of 0.64 and 0.62 with the in-situ soil moisture content. The spatial pattern of soil moisture map obtained using SIWSI derived from MODIS reflectance data had a Cramer's V of 0.64. WDI for the watershed was computed using ? T-NDVI relationship. Cramer's V for the spatial map derived from WDI was around 0.58. Potential of microwave data was also analyzed to assess the soil moisture in the watershed. The correlation of co-efficient between backscattering coefficient and insitu soil moisture after vegetation correction was 0.61 and hence showed a potential application to assess the surface soil moisture condition. MIKE SHE hydrological model was used to obtain the soil moisture at different depths and comparisons were made with in-situ soil moisture obtained from gypsum blocks. Root mean square error of 2.1, 4.2, and 5.6 was obtained for the depths 15, 45 and 75cm respectively. Nash-stucliffe coefficient ranged from 0.70 to 0.89 for the three depths.

Keywords: Soil moisture, Gypsum blocks, Remote Sensing, Hydrologic Modeling, MIKE SHE

TABLE OF CONTENTS

LIST OF TABLES

LIST OF FLOWCHARTS

LIST OF FIGURES

1. INTRODUCTION

1.1. GENERAL OVERVIEW

Hydrologists have a fundamental role to play in the recognition; assessment and resolution of the key theoretical and applied problems within the water cycle that currently limit our ability to ensure a sustainable environment into 21st century and beyond. The term hydrology can be divided in to two terms: hydro, relating to water, and loge, a Greek word meaning knowledge. Thus, hydrology is the study, or knowledge, of water. The Earth holds more than 300 km^3 of water beneath the land surface, on the surface, and in the atmosphere. This vast amount of water is in constant motion, known as the hydrologic cycle. Therefore hydrology is of value not only in the field of engineering, but also in forestry, agriculture, and other branches of environmental sciences.

The hydrologic cycle, illustrated in Figure 1.1, shows the pathways water travels as it circulates throughout global systems by various processes. The components are precipitation, evaporation, transpiration, infiltration, runoff, percolation, groundwater recharge and interflow.

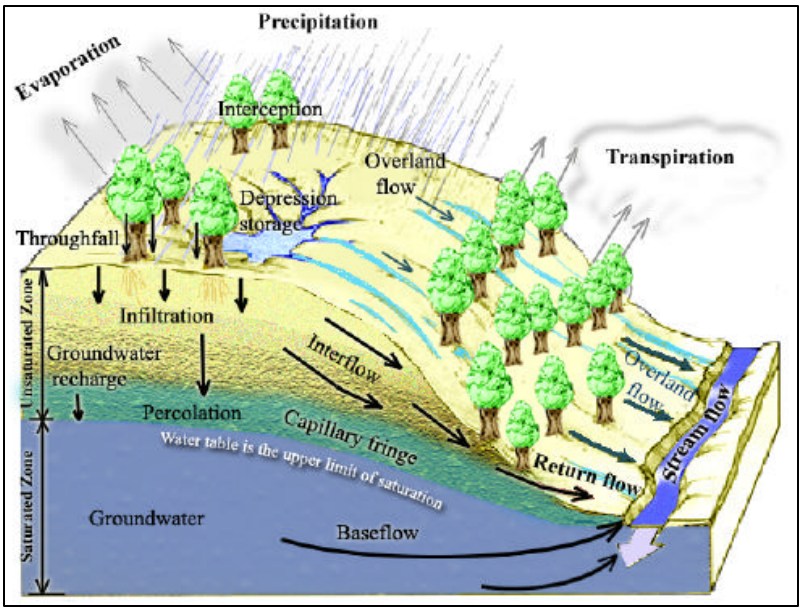

Figure 1.1 The hydrologic cycle in agricultural systems. (Tarboton, 2003)

1.1.1 IMPORTANCE OF SOIL MOISTURE IN HYDROLOGIC CYCLE

Soil moisture controls the partitioning of energy and water related to evapotranspiration and runoff and thereby influences the hydrological response of an area. Soil moisture is a key state variable of the global energy and water cycle as it controls the partitioning of incoming radiative energy into sensible and latent heat fluxes (Engman, 1991). Soil moisture is widely recognized as a key parameter in environmental processes, including meteorology, hydrology, agriculture and climate change. From a hydrologic viewpoint, soil moisture controls the partitioning of rainfall into runoff and infiltration and therefore has an important effect on the runoff behavior of catchments (Aubert et al.,2003). Further its highly variable in space and time. An understanding of the soil moisture balance and its variability (spatial and temporal) is instrumental in quantifying the linkage between regional hydrology, ecology and physiography.

A number of methods for determining soil moisture content both in lab and in the field have been developed. The in-situ methods in this regard include gravimetric technique, nuclear techniques, gamma attenuation, electromagnetic technique, and hygrometric techniques. The neutron scattering method makes use of the thermal or slow neutron density, whereas gamma attenuation is a radioactive technique that can be used to calculate soil moisture content within a 1-2cm soil depth. The electromagnetic techniques include those methods, which depend upon the effect of moisture on the electrical properties of soil. The preferred method for determining soil moisture is gravimetric soil moisture. The low cost expenditure and easy estimation of soil moisture is the advantage of the above-mentioned method.

From the above-mentioned methods the soil moisture values are generally obtained through ground measurements, which are typically, point measurements collected in representative locations and at specific time intervals. Detailed analysis of soil moisture patterns would require a dense network of observations, which is often impractical. Therefore, remote sensing and modeling offers a useful alternative to know the status of soil moisture in a watershed.

1.2. REMOTE SENSING AND SOIL MOISTURE

Soil moisture has a strong influence on the amount and composition of reflected and emitted energy from a soil surface, and thus information about soil moisture condition can be derived from measurements in all parts of the electromagnetic spectrum. In the shortwave region, the major effect of adsorbed water on soil reflectance decreases the reflected energy, making soils darker when moistened, particularly in the water absorption bands centered at 1.45μm to 1.9μm. The decrease in reflectance is proportional to the thickness of the water film around the soil particles and can be related to gravimetric water content as well as the energy status of the adsorbed water (Idso et.al., 1975).

Soil thermal behavior is largely a function of soil moisture, which modulates the heating and cooling of soil through the partitioning of radiant energy in to latent heat and sensible heat components. The difference in the amplitude of the diurinal variation in temperature across soil surfaces result in their differences in thermal inertia, which is related primarily to their moisture content and texture properties (Mulders, 1987). Reginato et al. (1976) showed how daily maximum-minimum surface soil temperatures as well as maximum-minimum soil air-temperatures were inversely related to the soil water content (0-2cm) in soils.

Both active and passive microwave remote sensing can accurately measure surface soil moisture contents in the top 5 cm of the soil. The longer wavelengths (>5cm) are best suited for soil moisture determinations (Ustin et al., 1981; Engman, 1995). The theoretical basis for microwave remote sensing measurements of soil moisture results from the large contrast between the dielectric properties of liquid water and dry soil. An increase in soil moisture content results in higher dielectric constants. In passive microwave remote sensing of soils, the brightness temperature (T_B) is measured, which is the product of the surface temperature and surface emissivity. Surface emissivities can typically vary from 0.95 when dry to less than 0.6 when wet, and are also sensitive to surface roughness. For active microwave remote sensing of soils, the measured radar backscatter, s^o is related directly to soil moisture but is also sensitive to surface roughness.

1.3. MODELLING OF SOIL MOISTURE

A *"model"* is a simplified representation of a physical system. Hydrological simulation models form the basis of information for decisions regarding the development and management of water and land resources in a watershed. Though many hydrological models have been developed in the past, which are mostly lumped, i.e. they refer to the spatially averaged condition of the entire basin (Crawford and Linsey, 1963; Sugawara et.al. , 1984). Furthermore, their parameters have no direct physical meaning and cannot be derived from measurable properties of the basin. Hence, their applicability is limited only to gauged watersheds. To overcome these limitations, considerable efforts within hydrological research have been made towards the development of distributed physically based catchment models. Such models use parameters related directly to the physical properties of the catchment namely topography, soil and vegetation; and spatial variability in both physical characteristic and meteorological conditions.

MIKE SHE (Refsgaard and Storm, 1995), a major development in this direction, is a comprehensive deterministic, distributed and physically based modeling system capable of simulating all major hydrological processes in the land phase of the hydrological cycle. Though it has been widely adopted for catchment studies (Refsgaard et.al., 1992; Jain et.al.,1992), its applicability for soil moisture study has been limited. In the present study MIKE SHE has been adopted for the hydrological modeling of a small watershed (Solani) of about 539 km^2 with special emphasis on soil moisture profiles at different depths and also at different locations.

Soil moisture distribution in the unsaturated zone is calculated by solving the one dimensional Richards' equation. Extraction of moisture for transpiration and soil evaporation is introduced via sink terms at the node points in the root zone. Infiltration rates are found by the upper boundary that may be either flux controlled or head controlled. The lowest node point included in the finite difference scheme depends on the phreatic surface level, and allowance is made for the unsaturated zone to disappear in cases where the phreatic surface rises to the ground surface.

1.4. RELEVANCE OF THE STUDY

The knowledge of distribution of soil moisture has been proven useful for watershed management to determine the allocation of limited resources during times of drought and help co-ordinate relief efforts in times of flooding. The distribution of soil moisture also plays a key role in the prediction of erosion and sediment loads in watershed streams and ponds. In cultivated watershed knowledge of soil moisture can be used for irrigation scheduling, site-specific management of diseases and pests, and improving crop yield prediction. In arid and semi-arid watershed, soil moisture content has been used as an indicator of plant health. Such watershed scale applications have a common set of requirements that define the desired soil moisture product (Table1.1).

Table 1.1: Soil moisture product requirements for application in watershed management

Mapping parameter	Requirement
Spatial resolution	10-100m
Vertical resolution	Root zone, 15cm to >1m
Quantization	3-4 levels, ranging from dry to very wet

(Source: Susan et.al., 2004)

To fully meet the requirements for soil moisture information for the watershed scale applications described above, it is necessary to combine the horizontal coverage and spatial resolution of remote sensing with the vertical coverage and temporal continuity of a soil moisture simulation model (Susan et.al., 2004). Distributed hydrologic model such as MIKE SHE has been used for this purpose. The soil moisture at different depths can be obtained. Since soil moisture distribution is a complex function of not only soil physical properties and topography, but also vegetation type, land use, season, time of day, weather conditions and initial soil moisture content. Thus using MIKE SHE an analysis has been done to see the sensitivity of the parameters above mentioned.

The MODIS and ASTER on the Earth Observing System (EOS) Terra Mission began to produce data from February 2000 acquires data in 36 and 15 bands respectively. In recent years, MODIS has been used extensively for developing a lot of indices from the products offered such as surface reflectance and land surface temperature. This thesis tries to estimate

variability of soil moisture using MODIS and ASTER; its relevance to any further study that aims at watershed management. Also ENVISAT-ASAR data, active microwave sensor data has been used to assess the spatial variability of soil moisture.

1.5. STATEMENT OF SCIENTIFIC PROBLEM

Soil moisture is difficult to define because it means different things in different disciplines. For example, a farmer's concept of soil moisture is different from that of a water resource manager or a weather forecaster. Generally, however, soil moisture is the water that is held in the spaces between soil particles. Surface soil moisture is the water that is in the upper 10 cm of soil, whereas root zone soil moisture is the water that is available to plants, which is generally considered to be in the upper 200 cm of soil.

Soil moisture is of fundamental importance in hydrological processes. How much water infiltrates, evapotranspires, and recharges the subsurface depends on the soil moisture content (Rodriguez-I-turbe,2000; Bashford et.al. 2002). Given the importance of soil moisture to earth system processes, the quantification of its spatial and temporal behaviour is receiving increased attention from the hydrological scientific community from the hillslope and small watershed scale to the global scale (Grayson et.al., 1997). This task is not trival, since soil moisture exhibits a high degree of variability in time and space. Unfortunately, in-situ observations are rarely available as area representative measurements are expensive and tedious to collect (Hollinger and Isard, 1994). The difficulty of measuring soil moisture on the ground has motivated considerable research in the field of remote sensing to retrieve soil moisture of use for hydrological models (Engman and Chauhan, 1995). Remote sensing is capable of determining an effective water content of approximately 10cms of the top soil (Choudhury et al,1995).

1.6 OBJECTIVES OF THE STUDY

- Assessment of surface soil moisture using ASTER, MODIS and ENVISAT-ASAR
- To create a spatial database of watershed as per the requirement of MIKE SHE model.
- To generate soil moisture profiles in the watershed using MIKE SHE and comparison with the ground observed data.

1.7. RESEARCH QUESTIONS

- How the soil moisture in the watershed varying with respect to space and time?
- Is it possible to map soil moisture maps using different bands of electromagnetic spectrum?

1.8 OUTLINE OF THE THESIS

The thesis comprises of 7 chapters starting with the present one which describes its intent and usefulness. Chapter 2 gives a detailed review of the previous work done. The Chapter 3 gives a detailed description of the study area and Chapter 4 gives a description of the hydrological model MIKE SHE. Chapter 5 explains the data used and methodology adopted to achieve the objectives. The results and discussions are presented in chapter 6 followed by conclusion of the research in Chapter 7.

2. LITERATURE REVIEW

The condition of moisture in the soil can be assessed in three broadways: ground measurements, estimation from remotely sensed data and simulation from hydrological models. Each has its own advantages and disadvantages, none being perfect. So there is a continued demand for new and innovative ideas in this field. Many such methods are briefly reviewed to give a broad idea.

2.1. SOIL MOISTURE AND THE HYDROLOGIC CYCLE

Soil moisture is defined simply as the amount of water in a unit volume of soil. As water can only exist in the void space of a soil sample, the measured soil moisture can theoretically range from a minimum value of 0 (dry soil) to a maximum value of the porosity (all void space filled with water) for the given soil sample. In actual field conditions, this range is less as soils do not often dry completely but can reach full saturation. Soil moisture is commonly expressed as volumetric water content (?):

$$\mathbf{? = V_w / V_s}$$

where V_w = volume of water and V_s = volume of soil (Dingman 1994).

Another similar expression for soil moisture is degree of saturation (S) , which is the proportion of pore space that contains water:

$$S = V_w/(V_a + V_w) = ? / f$$

where V_a = volume of air and f = porosity (Dingman 1994). By knowing the porosity of the sample, conversions can easily be made between S and ?. Soil moisture is a key variable in the hydrologic cycle as it is directly related to infiltration and evapotranspiration. Thus, both the amount and variation of soil moisture play important roles in the amount of runoff and evaporation during a precipitation event.

The land surface exerts its influence on climate through two major mechanisms: on the one hand through modification of the surface radiation balance and surface energy partitioning (evaporation). Soil moisture controls the partitioning of energy and water related to

evapotranspiration and runoff and thereby influences the hydrological response of an area.(Hujtjes et.al., 1998)

The contributions of precipitation and evaporation and in turn soil moisture to the water budget demonstrate that the precipitation- evaporation- soil moisture mechanism is the dominant process in the water cycle, at both local and regional scales (Zhang et.al., 2003).

2.2. SOIL MOISTURE AND INFILTRATION

Soil moisture is directly related to hydraulic conductivity (K_h) and soil water pressure head (?). As the moisture content increases, K_h increases non-linearly from 0 at low to moderate soil moistures up to the saturated hydraulic conductivity (K_{hsat}) at ? = saturation (Figure 2.1). Although Figure 2.1 shows a typical curve, values of K_h at different soil moistures can vary by several orders of magnitude depending on the soil type and texture, and for a given soil, can increase by several orders of magnitude over the range of S values (Figure 2.2) (Dingman 1994).

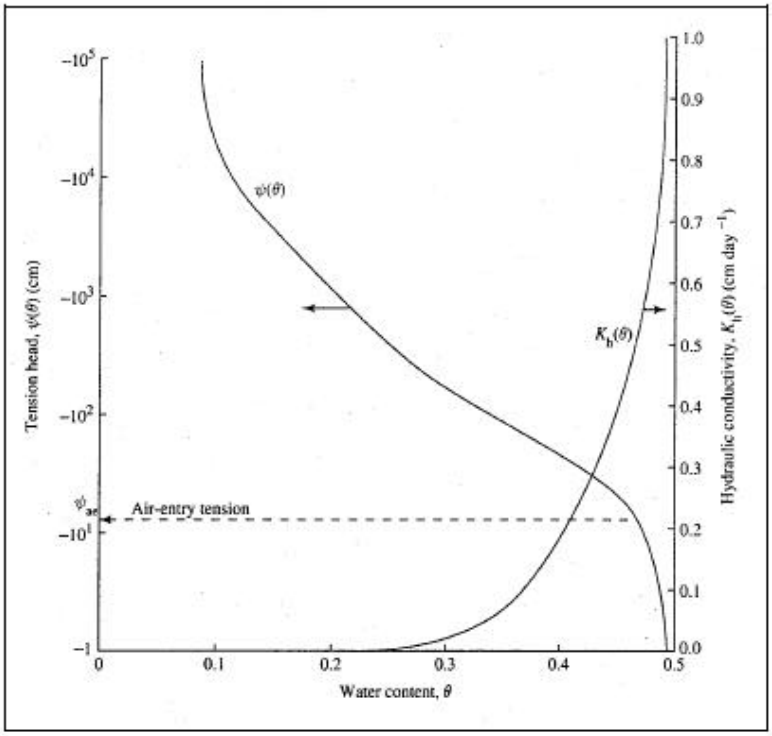

Figure 2.1: Typical forms of hydraulic relations ? (?) - ? and K_h(?) - ? for unsaturated soils (Dingman 1994)

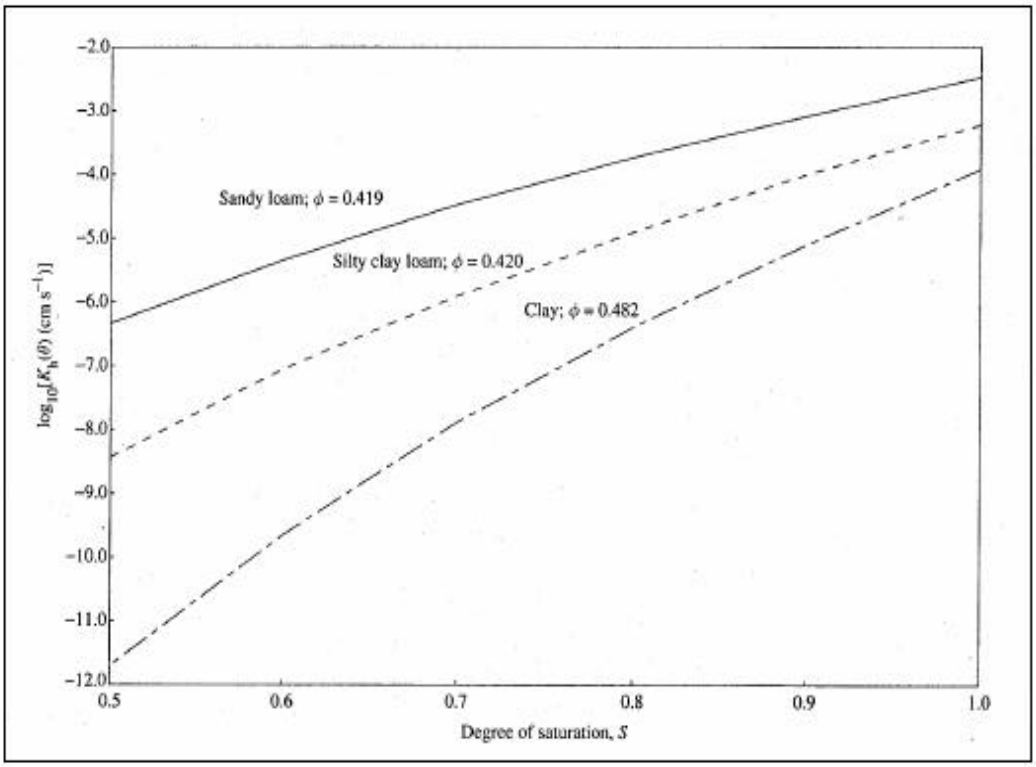

Figure 2.2: Hydraulic conductivity (K_h) vs. degree of saturation (S) for three different soil types (Dingman 1994)

Permanent wilting point corresponds to the soil moisture value at which transpiration ceases and plants wilt. Similar to field capacity, $?_{pwp}$ ranges from 0.05 for sands up to 0.25 for clays, but $?_{pwp}$ are approximately –15 000 cm for all soils, as plants cannot generate suctions greater than this value (Dingman 1994). Figure 2.3 shows the permanent wilting point, and the amount of soil moisture between this value and field capacity is called the available water content ($?_a$):

$$?_a = ?_{fc} - ?_{pwp}$$

where $?_{fc}$ is the soil moisture at field capacity and $?_{pwp}$ is the soil moisture at permanent wilting point. Because these values depend on soil type, $?_a$ will be different for various soils.

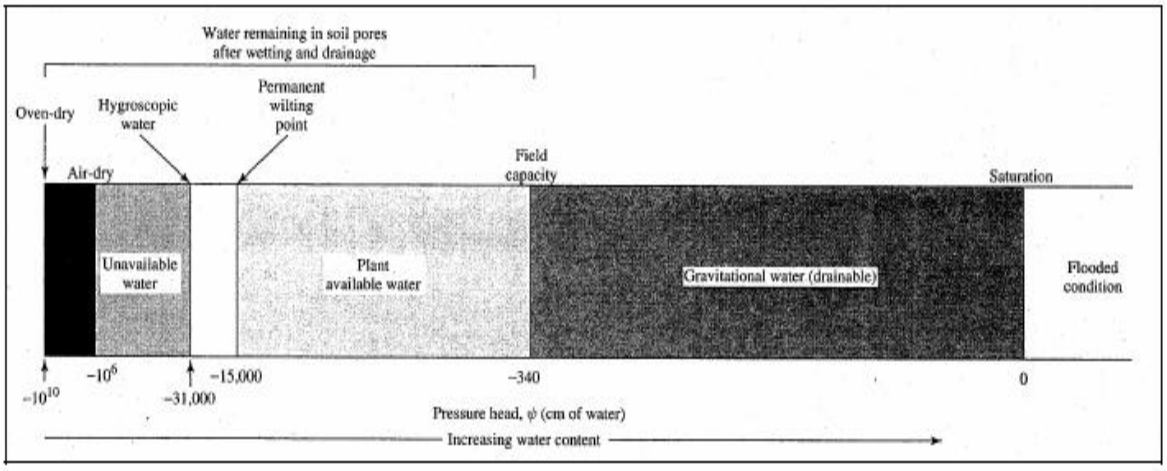

Figure 2.3 : Hydrologic soil-profile horizons (Dingman 1994)

Infiltration rates vary with time for any precipitation event, and depend on a number of factors including precipitation rate, saturated hydraulic conductivity of the soil, initial soil moisture, surface roughness, and physical and chemical properties of the soil and the water (Dingman, 1994). In general, rates are highest at the beginning of a precipitation event and decrease exponentially once surface ponding has begun, due to the steadily decreasing capillary gradient as the wetting front descends through the soil column (Dingman, 1994).

2.3. GROUND MEASUREMENT OF SOIL MOISTURE

2.3.1. GRAVIMETRIC (LAB) METHOD

The Gravimetric Method is the standard method for calculating soil moisture to which all other methods are compared (Maidment 1993). Samples of 100 g to 200 g of soil are taken from the field and placed in a container of a known weight. The samples and containers are weighed, placed in a drying oven, and dried at 105 ºC to 110 ºC until all water has evaporated. A drying period of 24 hr is normally adequate for most soils (Craig 1992). After drying, the samples are weighed again and the moisture content (?) is determined by:

$$q = \frac{M_{wet} - M_{dry}}{r_w V_s}$$

where M_{wet} and M_{dry} are the weights before and after drying, $?_w$ is the density of water, and V_s is the volume of the soil. The denominator $?_w V_s$ is equivalent to M_{dry} (Maidment 1993, Craig 1992).

The Gravimetric Method uses simple equipment and is indispensable for calibration of instruments (Roth et al. 1990). However, it is a time consuming procedure, and not suitable for monitoring field conditions (Maidment 1993, Dingman 1994).

2.3.2. GYPSUM BLOCKS

Soil moisture sensors (also called gypsum blocks or resistance blocks) are not a new invention but recent advances have improved their accuracy and ease-of-use. These moisture blocks measures soil moisture by measuring the electrical resistance between two electrodes imbedded in the sensor (Figure2.4). The blocks take up and release moisture as the soil wets and dries. The higher the water content of the block, the lower the electrical resistance. Several other types of soil moisture monitoring equipment are available but resistance blocks are perhaps the most common because they are one of the least expensive, easy to use, and they are reasonably accurate. The values can be interpreted by drawing a graph of pressure versus water content (Orloff and Hanson,1998).

One of the most common methods of estimating matric potential is with gypsum or porous blocks. The device consists of a porous block containing two electrodes connected to a wire lead. The porous block is made of gypsum or fiberglass (Zazueta and Xin, 1994).

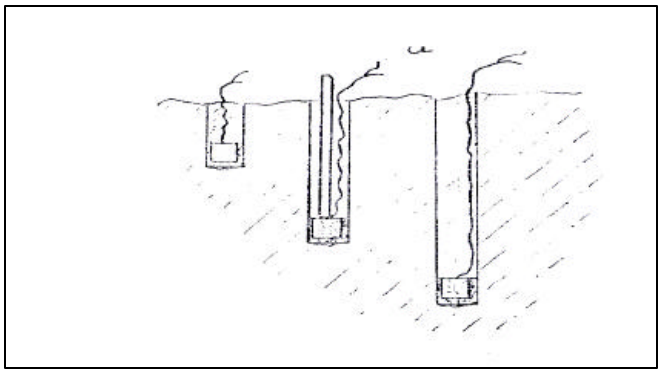

Figure 2.4: Different installs of gypsum blocks in the soil profile(European Soil Bureau, 2005)

While the soil is wet, the pores in the gypsum are filled with water which dissolves some of the gypsum - enough to make a saturated solution of calcium sulphate, and the water conducts electrical current (Richards and Campbell, 1950). The electrical conductivity of the block is then read with an alternating current bridge. A calibration curve is made to relate electrical conductivity to the matric potential for any particular soil.

Using a porous electrical resistance block system offers the advantage of low cost and the possibility of measuring the same location in the field throughout the season (Figure 2.5). The blocks function over the entire range of soil water availability. The disadvantage of the porous block system is that each block has somewhat different characteristics and must be individually calibrated (Zazueta and Xin, 1994). The main disadvantage of the gypsum block is that the calibration changes gradually with time, limiting the life of the block (Phene, 1988).

Figure 2.5: Gypsum Blocks .(Skinner et.al., 1997)

The depth of the crop roots will determine the depths at which the blocks should be installed. The most active portion is above 3 to 4 feet. Water at depths greater than this may be lost to deep percolation. Management of this active root zone can be accomplished using two blocks; the upper block placed at about one-fourth to one third depth of the root zone, while the lower block will be at two-thirds to three-fourths of the active root zone (Figure 2.6). This means block depth would be 12 to 18 inches for the shallow block and 30 to 36 inches for the deep block (Alam & Rogers, 2001)

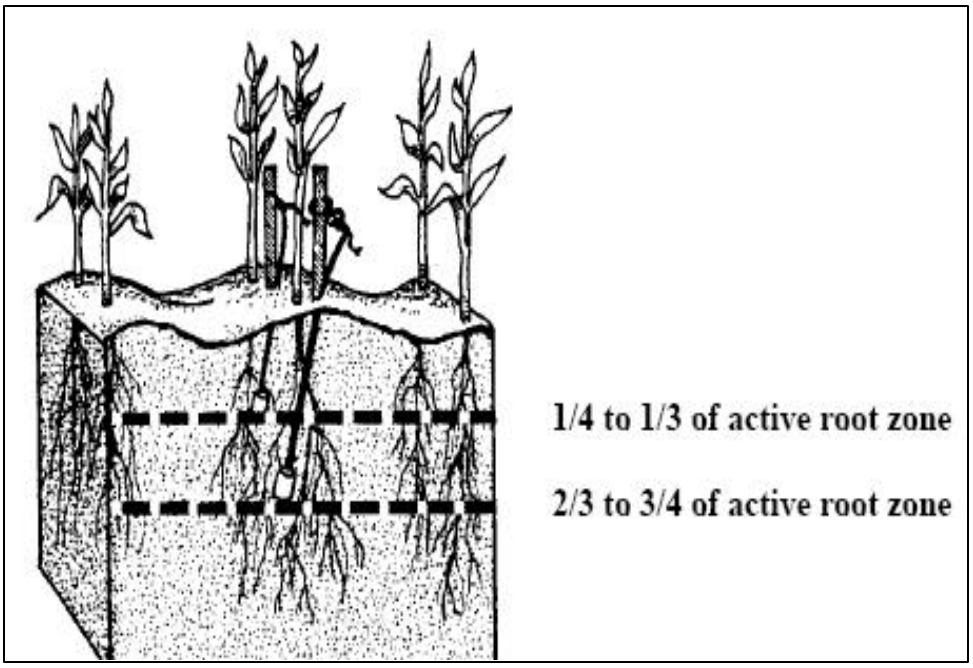

Figure 2. 6: Location of electrical resistance blocks in relation to the active root zone (Source: Alam and Roger, 2001)

The temporal variation in a soil moisture profile can be studied using resistivity sounding data acquired at different times (Goyal et.al., 1998).

Kirda & Reichardt (1992) compared different techniques available for the estimation of soil moisture in relation to stability. The variance of field water content measurements with neutron moisture gauges was lower than that of the gravimetric sampling, which therefore requires 2 to 6 times as many samples as the number of measuring sites of the gauges to attain the same level of significance. The space dependence of the measurements made with the subsurface gauge varied depending on the average field soil water content. Measurements with the tensiometers and resistance blocks manifested no spatial dependence and therefore randomly selected measuring sites can be adapted.

2.4. SOIL MOISTURE THROUGH REMOTE SENSING

Remote sensing can be defined as any non-contact method of determining information regarding an objects nature, properties or state. In this thesis it may be defined as the acquisition of digital data, either reflected or emitted by the Earth's surface, in the different channels of electromagnetic spectrum (McVicar and Jupp,1998).

Numerous researchers have shown that near-surface soil moisture content can be measured by visible and thermal infra-red remote sensing, as well as active and passive microwave remote sensing techniques (Bindlish et.al, 2000; Haider et.al., 2004). The main difference between these techniques is the wavelength region of the electromagnetic spectrum that is used by the sensor, and the source of the electromagnetic energy. A summary of the relative merits of the different remote sensing techniques are provided in the Table 2.1.

Table 0.1: Summary of spectral measurements for *ms* estimation

Physics	Advantages	Limitations
Visible, NIR, SWIR reflectance Spectral information in visible, NIR and SWIR wavelengths is related to volumetric soil moisture content(m_s) , as a function of spectral absorption features; for bare soils, increase in m_s generally leads to a decrease in soil reflectance.	Fine spatial resolution Broad coverage Multiple satellite sensors available Hyper spectral sensors show promise	Weak relation to water content Minimal surface penetration Limited ability to penetrate clouds and vegetation
TIR emittance Soil moisture directly influences soil temperatures by increasing both specific heat and thermal conductivity, thus thermal inertia of soils; for bare soil, variations in surface T_R primarily due to varying m_s	Fine spatial resolution Broad coverage Strong relation to m_s T_R/VI approaches show promise	Minimal surface penetration(~1mm) Limited ability to penetrate clouds and vegetation
Microwave T_R Intensity of microwave emission (at s^0- 1-30cm) from soil is related to m_s because of large differences in dielectric constant of dry soil(~3.5) and water(~-80); for bare soils, increase in m_s generally leads to increase in T_B	Broad coverage Strong relation to m_s Surface penetration up to ~5cm Insensitive to clouds and earth's atmosphere	Perturbed primarily by surface roughness and vegetation biomass Coarse resolution

Source: (Moran et.al,2004)

As remote sensors do not measure soil moisture content directly, mathematical models that relate the measured response of a particular remote sensing system to the soil moisture content must be derived (Troch et.al, 1996).

2.4.1. SOIL MOISTURE THROUGH OPTICAL REMOTE SENSING (Visible Region)

Remote sensing of near-surface soil moisture content using the visible region of the electromagnetic spectrum measures the reflected radiation of the sun from the earth's surface, known as albedo (Sadeghi et.al., 1984). Soil albedo is defined as the ratio of reflected to incoming radiation (Idso et.al., 1975), and has long been recognized as having a dependence up on the moisture status of the soil surface, soil texture, surface roughness, angle of incidence, plant cover and colour (Engman, 1991) causing wide variations. Vegetation indices developed from optical remote sensing have been continuously used for water stress detection and vegetation vigor monitoring. Rao et. al.(1993) did a study on vegetated fields and found that NDVI and root zone soil moisture share a linear relationship. Farrar et.al. (1994) found that NDVI was controlled by the surface soil moisture of the concurrent month and not the present.

In past, spectral optical estimations were well performed in the ability to be correlated with crop and soil properties but were not consistent within the whole production season. At the wavelength of 850nm soil reflectance ranged between 10%(peat) to 74%(sand). The reflectance of top soils varied from 21% to 32%. Increase in soil water content from 0% to 25% decreased signatures of soil reflectance at 850nm. The interrelation of soil reflectance and soil moisture revealed a non-linear exponential function (Behrens et.al., 2005)

2.4.2. SHORTWAVE INFRA-RED REGION

Soils have an increasing reflectance from the visible to the shortwave infra-red, with absorption bands around 1.4µm and 1.9µm related to soil moisture (Figure 2.7) (Leblon, 2000).

Lobell and Asner (2002) quantified the reflectance in shortwave region (400-2500nm)of the electromagnetic spectrum. The observed changes in soil reflectance revealed a non linear dependence on moisture that was well described by an exponential mode, and was found similar for different types of soil when moisture was expressed as degree of saturation. Reflectance saturated at much lower moisture contents in the visible and near infra-red (VNIR) spectral region than in the shortwave infra-red (SWIR) spectral region, suggesting that longer wavelengths are better suited for measuring volumetric moisture contents above ~20%.

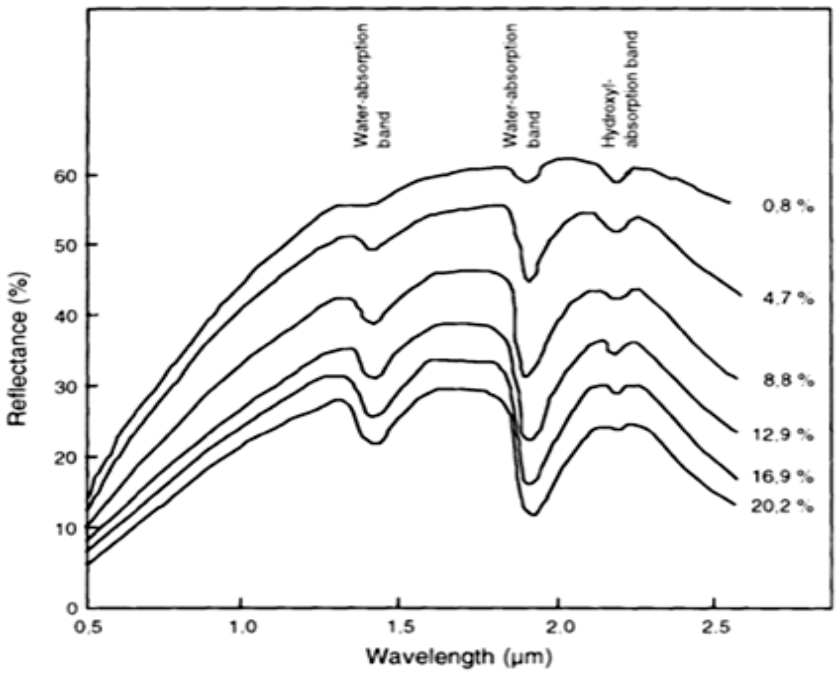

Figure 2. 7:Spectral reflectance curves for soils at various moisture contents (Bowers and Hanks, 1965)

Soil moisture condition was assessed using mid infra-red data in eastern part of India. Four qualitative surface soil moisture conditions very wet, wet, moist and dry was assessed. MIR response was inversely related to the qualitative surface soil moisture conditions (Hariprasad et.al ,1997). Fensholt and Sandholt(2003) derived a shortwave infrared water stress index (SIWSI) on a daily basis from MODIS data. They used the information of channel 6(1.628-1.652μm) and channel 2(0.841-0.876μm) (SIWSI=Ch6-Ch2/Ch6+Ch2). The indices were compared with the top layer soil moisture measurements from semi-arid Senegal 2001-2003. Results showed a strong correlation between SIWSI and soil moisture. The result indicated that the combined information from the MODIS near and shortwave infrared wavelengths can be used to know the soil moisture status.

2.4.3. THERMAL INFRA RED REMOTE SENSING

Thermal infra-red remote sensing operates in a slightly longer wavelength region of the electromagnetic spectrum (3-14mm) than visible remote sensing, and measures the thermal emission of the earth.

As soil moisture content has a strong influence on the thermal properties(heat capacity, thermal conductivity and latent heat of vaporization of water) of the earth's surface, relatively minor changes in moisture content have a large effect on the bulk thermal properties of the ground (Ellyett and Pratt, 1975). Thus, areas having higher soil moisture content are cooler during the day and warmer at night. The amplitude of diurnal cycle of surface skin temperature, T_s, is related to internal factors the combined effect of which is termed as thermal inertia and external factors which are metrological conditions like relative humidity, wind speed, solar radiation, air temperature and cloudiness. When the surface is drier, the effect of the internal factors or the thermal inertia becomes dominant so that the amplitude of diurnal cycle of T_s is related to the surface soil moisture. So it is in the midday that T_s is found to be most sensitive to soil moisture(Wetzel et.al.,1984).

The scaling approach for land surface temperature was proposed over flat relief area based on Stefan-Boltzmann law to explore the combined uncertainties in scaling using satellite retrieved data (Liu et.al., 2006). ASTER and MODIS data were examined. The satellite derived ASTER land surface temperature products over the relief area was examined using the statistical analysis. The analysis showed that the ASTER and all the scaled images followed a normal distribution, as did the MODIS LST images. The scaling generally reduced the variation in LST. Comparison of surface emmisivity and radiometric temperature retrievals derived from data collected with the MODIS and ASTER sensors was carried out (Frederic Jacob et.al.,2004). The MODIS estimates were computed using a designed Temperature Independent Spectral Indices of Emissivity (TISIE) method and ASTER estimates were derived using Temperature Emissivity Separation Algorithm (TES). The radiometric temperature retrievals were in good agreement and emissivity estimates were similar for MODIS/ASTER matching bands at 8-11 micrometer.

They suggests a simplified land surface dryness index (Temperature-Vegetation Dryness Index, TVDI) based on an empirical parameterization of the relationship between surface temperature(Ts) and vegetation index (NDVI). The index is conceptually and computationally straight forward and was related to soil moisture. The spatial pattern and temporal evolution in TVDI was analyzed for NOAA-AVHRR images. The spatial pattern in TVDI was compared with simulations of soil moisture from a distributed hydrological model MIKE-SHE (R^2 =0.70). They concluded that the spatial variation in TVDI reflects the variation in moisture on a finer scale than that can be derived from the hydrological modeling (Sandholt et.al., 2002).

Van Trung and Minch (2001) present the experimental results in applying two methods: Reference Channel method (RCF) and Emissivity normalization method (NOR) for Landsat ETM+ imageries to create the land surface temperature map. The results were compared to monitored data of the meteorological stations and accuracy was evaluated. LST maps derived from the two methods were little different and LST values were higher at the city centre than that in the surrounding areas.

Moran, (1994) developed the water deficit index (WDI) that uses both surface minus air temperature and a vegetation index to estimate the relative water status of a field. The distribution of surface minus air temperature at a particular time was found to form a trapezoid when plotted against percent cover. Note that for many crops, there is a linear relationship between percent cover and a vegetation index (such as the normalized difference vegetation index (NDVI = [NIR-Red]/ [NIR+Red]), so the index can be used in place of a direct measure of percent cover. The upper left of the trapezoid corresponds to a well-watered crop at 100 percent cover and the upper right to a non - transpiring crop at 100 percent cover (points 1 and 2, respectively). These two points are the upper and lower limits of the trapezoid.

The lower portion of the trapezoid (bare soil) is bound by a wet and dry soil surface. These points can also be calculated using the energy balance concepts. The concept of the WDI is illustrated in the figure 2.8(a). In the other way WDI can be modified and represented as figure 2.8(b), by reversing x- axis and y-axis as NDVI and temperature difference respectively. ETR line is the actual evapotranspiration and this can be derive through the use of surface temperature and vegetation index scattergrams (Troofleau, 1998).

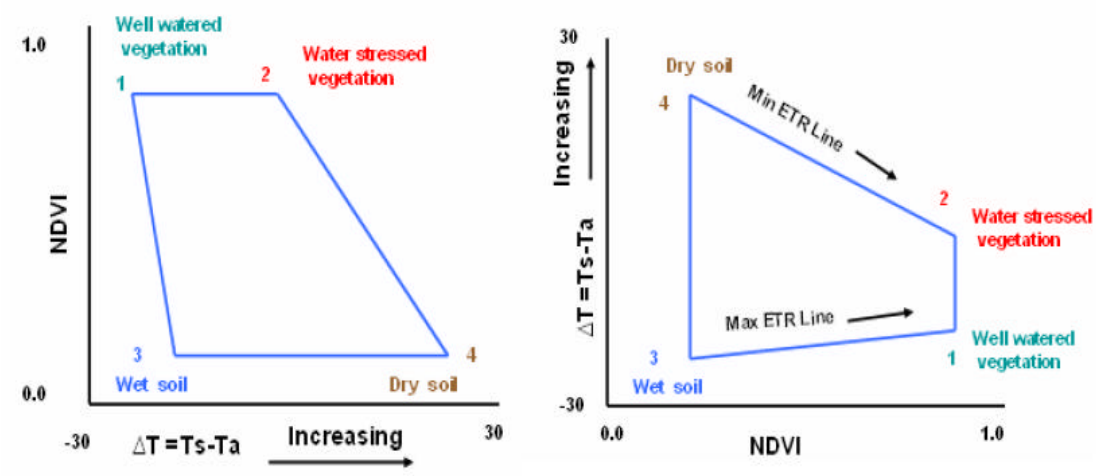

Figure 2.8: The Schematic plot for WDI (Moran, 1994) and modified schematic plot of WDI

2.4.4. MICROWAVE REMOTE SENSING

Microwave remote sensing measures the electromagnetic radiation in the microwave region of the electromagnetic spectrum, which has wavelengths between 0.5 and 100 cm. The fundamental basis of microwave remote sensing for soil moisture content is the contrast in dielectric properties of water and dry soil, and the relationship between the Fresnal reflection coefficient and dielectric constant (Jackson et.al., 1996).

The two types of microwave remote sensing differ in the source of electromagnetic energy. Passive microwave sensors measure the naturally emitted signals from earth surfaces and active microwave remote sensors or radars send out a pulse of electromagnetic radiation and measure the amount that is scattered back in the direction of the sensor (Jackson et.al., 1996). The two types are different because of their advantages also. One main difference is in the spatial resolution of data given. The amount of radiation emitted by the earth surface in the microwave region is relatively small. So it is difficult to obtain data with high spatial resolution using passive microwave remote sensing which currently provides data at tens of kilometers. On the other hand, active sensors can provide data on the order of tens of meters, though their sensitivity to surface roughness, topographic features and vegetation make their processing relatively complex (Oevelen, 2000).

The most common type of imaging radar used today is the synthetic aperture radar (SAR), which transmits electromagnetic pulses as the radar antenna flies across the image scene (Ulaby et al. 1996). A set of backscatter coefficients (s°) can be calculated for each pixel of the radar image by comparing the phase and amplitude of both the transmitted and reflected pulses (horizontal-vertical / vertical-horizontal, horizontal-horizontal, and vertical-vertical), and these coefficients are used in determining soil water content. Various operational frequency bands and wavelengths exist for SAR systems (Table 2.2), however, research has shown the optimal specification of an SAR system for maximum soil moisture sensitivity is a C-band system operating at an incidence angle of 10° to 20° (Ulaby et al. 1996, Tansey et al. 1999).

Table 0.2: Various operational frequency and wavelength bands for SAR systems

Letter Designation	Frequency (GHz)	Wavelength (cm)
P- Band	0.44	68
L-Band	1.28	23
S- Band	3.0	20
C-Band	5.3	5.7
X- Band	9.6	3.1

The potential of Advanced Synthetic Aperture Radar(ASAR) for the retrieval of surface soil moisture over bare soils was evaluated for several ASAR acquisition configuration. The best estimates of soil moisture can be made if the ASAR data is acquired at both low and high incidence angles. ASAR proves to be a good remote sensing tool for measuring surface soil moisture, with accuracy for the retrieved soil moisture that can reach 3.5% RMSE (Baghdadi et.al, 2006).

Zribi et.al (2006) presented a methodology for mapping and monitoring surface soil moisture over the Kori Dantiandou region in Niger, using data provided by the ASAR/ENVISAT radar instrument. Soil moisture was estimated only for fields with bare soil or low-density vegetation, using low incidence angle radar data. A high correlation was observed between in-situ and processed radar data.

Holah, et.al. (2005) highlights the potential of ENVISAT/ASAR for the characterization of soil surface parameters over bare agricultural fields. Soil surface parameters

(surface roughness and soil moisture) can be analyzed using ASAR data at various polarizations (HH, HV and VV) and incidence angles (20°-43°). The study showed that the radar signal is more sensitive to surface roughness at high incidence angles than at low incidence angles and HH polarization is slightly more sensitive than VV polarization to soil roughness. When the soil becomes very wet (soil moisture>35%) the back scattering co-efficient becomes independent of surface roughness for both HH and VV evaluated the roughness description in terms of several characterizations through a correlation function using a numerical back scattering model. A relationship was developed between the rms height of soil surface and the shape of the correlation function (Zribi, et.al., 2005).

An original methodology to retrieve surface soil moisture based on the use of the ENVISAT-ASAR multi-incidence angle sensor was presented. They developed a linear approach to estimate mean soil surface moisture of a small watershed. The proposed a new methodology to normalize multi-incidence angle radar signals to one angle and to correct it for roughness. The approach was developed for HH polarization (Zribi, et.al., 2005).

The major difficulties in retrieving soil moisture with SAR measurements are due to the effects of surface roughness and vegetation cover. A technique was demonstrated (Yang et.al., 2006) to estimate the relative soil moisture change by using multi-temporal C-band HH polarized Radarsat Scan SAR data. The vegetation correction was performed based on a semi-empirical backscattering. Vegetation model with the vegetation water content information obtained from the optical sensors as the input. Comparison with the ground soil moisture measurements showed a good agreement for prediction of the relative soil moisture change with a RMSE of 1.14.

Providing the vegetation cover is less than 15cm, active microwave remote sensing can measure the volumetric moisture content of the near-surface soil layer with an rms error of 3.5% at low microwave frequencies (Ulaby et.al.,1996). However, grass covered sites often have a large volume of litter on the surface, which can hold a significant amount of water,

masking the relationship between SAR data and the underlying soil moisture content (Sano et.al, 1998).

2.5. MIKE SHE HYDROLOGICAL MODEL

Recent developments in hydrologic models for estimating soil moisture profiles provide an alternative to directly or indirectly measuring soil moisture content in the field. A variety of hydrological models have been published. They differ in the level of detail they use in representing the physical system and temporal variation of the driving forces. Computation of evapotranspiration, partitioning between infiltration and runoff, computation of vertical and lateral redistribution and number of soil layers used are some of the main differences in these models (Schmugge et.al, 1980). The advantage of hydrologic models is that they can provide timely information on the spatial soil moisture distribution without the necessity of field visits. The error associated with their estimates is a general disadvantage of hydrological models. They are mainly related to the fact that soil moisture exhibits large spatial and temporal variations (Wigneron et.al, 1998) , as a result of heterogeneity of soil properties, vegetation, precipitation and evaporation (Ottle and Vidal-Madjar, 1994).

The MIKE SHE model is a fully integrated watershed model that simulates all the major processes occurring in the land phase of the hydrologic cycle. Developed by three European organizations (Danish Hydraulic Institute, British Institute of Hydrology and the French consulting company SOGREAH) and sponsored by the Commission of the European Communities, it was originally named SHE (Système Hydrologique Européen) model. This deterministic, fully distributed, and physically-based model is used mostly at the watershed scale and from a single soil profile to several sub-watersheds with different soil types (DHI, 2004; Refsgaard and Storm, 1995). The model's distributed nature allows a spatial distribution of watershed parameters, climate variables, and hydrological response through an orthogonal grid network and column of horizontal layers at each grid square in the horizontal and vertical, respectively (Abbott et al., 1986b). Being physically-based, the topography along with watershed characteristics (vegetation and soil properties) is included into the model. The MIKE SHE model has a modular structure, enabling data exchange between components as well as addition of new components. The flexible operating structure of MIKE SHE allows the use of as many or as few components of the model, based on availability of data (Abbott et al.,

1986a). Since the MIKE SHE model was selected to be evaluated in this study, more detailed explanation of the model is provided in the next chapter.

Bathurst (1986) used MIKE SHE for an upland catchment in mid-Wales. Basic parameter values used in the application were derived from field measurements. Good agreements between observed and simulated responses in all parts of the catchments were observed. The use of catchment parameters based firmly on field measurements and the ability to improve the simulations by physical reasoning indicate the considerable power of this modeling system.

Many investigators have evaluated the MIKE SHE model for various catchments in India. Kumar (1991) implemented for Hemavati basin in Karnataka which is about 600Km^2. There were good agreements between observed and simulated responses. SHE has been successful used for hydrological modeling of the Kolar catchment in Madhya Pradesh (Jain et.al., 1992). The hypothetical plot of simulations to study the effect of different landuse scenarios represented by changes in soil type, soil depth and vegetation type, have shown that SHE model has the capability to provide an assessment of the effect of landuse changes in real catchments.

Sensitivity analysis of the SHE model for a typical grid of Ganjal sub-basin of river Narmada was done by Kumar (1992). It was observed that simulated runoff and actual evapotranspiration are some what sensitive to the choice of the various pan evaporation measurement station. Increase in the value of conductivity of unsaturated zone leads to increase in actual evapotranspiration and decrease in runoff. Reduction in the values of water content of soil also reduces runoff and significantly increases actual evapotranspiration.

Mertens et.al (2004) proposed a methodology to include prior information in the estimation of effective soil parameters for modeling the soil moisture content in the unsaturated zone. A two-horizon single column 1D MIKE SHE model based on Richard's equation was

setup for nine soil moisture measurement locations along the middle transect of the hill slope. The goal of the model was to simulate the soil moisture profiles at each location. The results indicated the importance of prior soil parameter information.

Vazquez et.al. (2004) studied the application of the physically based distributed MIKE SHE code to a medium size catchment (585 km^2) using different grid sizes to investigate scale effects on the model results. First a 600m grid-square model was calibrated. This was then subjected to a multi-resolution validation test by using the effective parameters of the calibrated model in a 300m and a 1200m grid square model. The test indicated that the model for the resolutions analysed only differed marginally. The investigation indicated that the best validation results, in terms of river discharge, were obtained with a 600m grid resolution.

In this research project, the applicability and predictive capacity of the MIKE SHE model is tested for simulating spatial and temporal soil moisture profiles. MIKE SHE is applicable for different objects- from simple soil profile to the large areas containing basins of several rivers (Manukyan and Karpenko,2001). One dimensional Richard's equation is used for computing water content in the unsaturated zone. Several soil layers with different characteristics can be incorporated and allowance is made for the disappearance of the unsaturated layer as the phreatic surface rises to the ground surface. Also, this model simulates all the processes in the hydrologic cycle by fully integrating the surface, subsurface and groundwater flow. Overall, the unique feature of MIKE SHE hydrology component is the integration of various hydrological processes in the model, at different time scales.

3. MIKE SHE

The chapter describes the features of MIKE SHE and the input parameters required. The soil moisture assessment using MIKE SHE is explained in methodology. The Systeme Hydrologique European or European Hydrological System (SHE) is an advanced, physically-based, distributed, modeling system developed by the Danish Hydraulic Institute of Hydrology. The scientific concepts represented by the system are as follows:

- Representation of spatial variations in hydrological quantities, both across the catchment and through the soil column;
- Representation of the major land phases of the hydrological cycle in a manner that is both physically and computationally acceptable;
- Allowing for interactions between the different hydrological processes, each having its own characteristic space and time scale.

The SHE is physically based in the sense that the hydrological processes of water movement are modeled, either by finite difference representations, or the partial differential equations of mass, momentum and energy conservation, or by empirical equations derived from independent experimental research. Spatial distribution of catchment parameters, rainfall input and hydrological response is achieved in the horizontal through the representation of the catchment by an orthogonal grid network and in the vertical by a column of horizontal boundaries of the grid squares. Grid spacing in the horizontal can vary across the network but must be the same for a given row or column within the network array. Node spacing in the vertical is a function of the vegetation type which characterizes a given grid squares and can vary between the root zone and the soil layer below the root zone.

Only the primary components of the land phase of the hydrological cycle are modeled-snowmelt, canopy interception, evapotranspiration, overland and channel flow and unsaturated and saturated subsurface flow. MIKE SHE is applicable to a wide range of water resources and environmental problems related to surface water and groundwater systems and the dynamic interactions between them. MIKE SHE is applicable on spatial scales ranging from a single soil profile to large regions.

3.1. Integrated Modular Structure

The basic MIKE SHE module is MIKE SHE (WM) water movement for the description of water movement in the area under study. The WM module has a modular structure with one component dedicated to each hydrological process. Several components include alternative options for describing certain processes.

3.2. Water Movement Module (MIKE SHE WM)

The overall model structure is illustrated in figure 3.1. MIKESHE WM has been designed with a modular program structure comprising six process oriented components, each describing the major physical processes in individual parts of the hydrological cycle and in combination describing the entire hydrological cycle:

- Interception and Evapotranspiration (ET)
- Overland and Channel Flow (OC)
- Unsaturated Zone (UZ)
- Saturated Zone (SZ)
- Snow Melt (SM)
- Exchange between aquifer and rivers (EX)

The modular form of system structure, or architecture, ensures a great flexibility in the description of the individual physical processes. The governing partial differential equations for the flow processes are solved numerically by efficient and stable finite methods in separate process components. All process descriptions operate at time steps consistent with their own most temporal scales. Hence the processes may be simulated using different time steps which may be updated during simulation and coupled with the adjoining processes as and when their time step coincides. The facility allows for a very efficient operation, making it possible to carry out simulations extending over long periods of time. The ability to provide an integrated description of the various processes, despite different time scales, is the most important feature of MIKE SHE WM. This integration has probably been the largest problem encountered during its development and provides a unique feature.

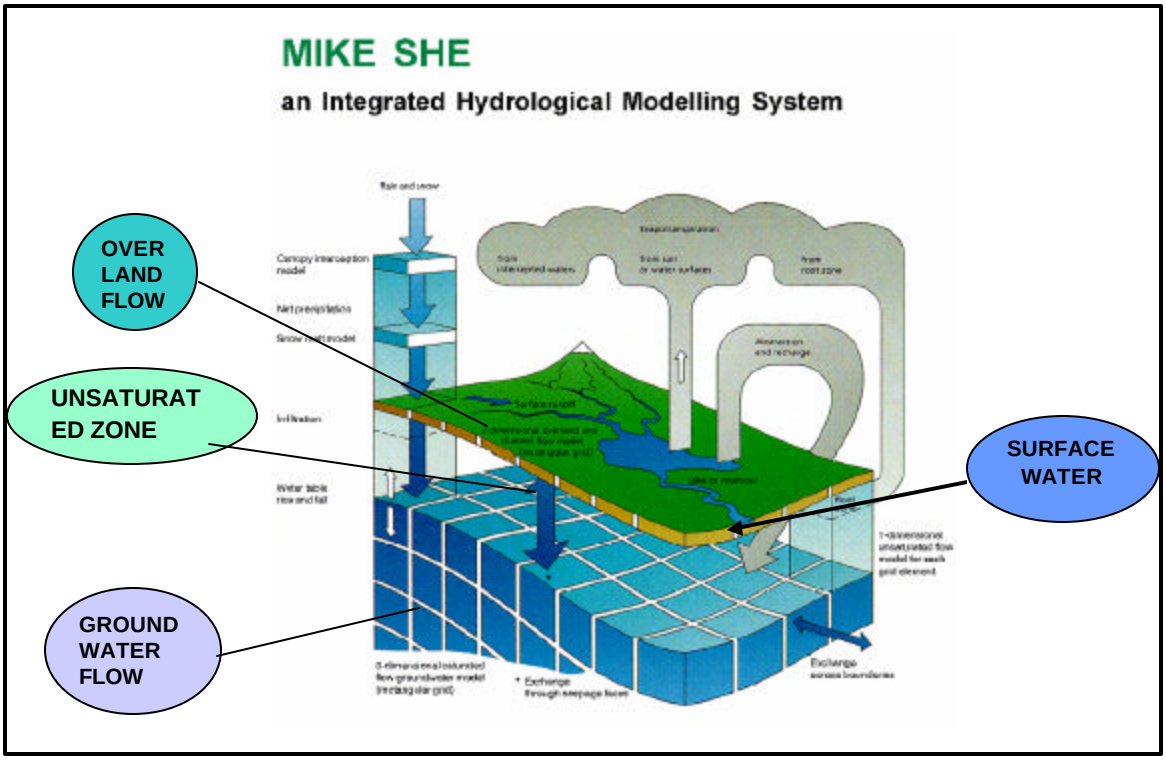

Figure 3.1: Schematic presentation of the WM module of MIKE SHE (Refsgaard and Storm,1995)

3.3. TYPICAL APPROACHES OF MODELLING OF DIFFERENT PROCESSES

2. Frame Component
2. Interception and evapotranspiration component
2. Overland and channel flow component
2. Unsaturated component
2. Saturated zone component
2. Snowmelt component

3.3.1. FRAME(CENTARL CONTROL) COMPONENT

The FRAME component coordinates the parallel running of the other component by selecting their different time scales and organizing their data interchanges. Its functions include the following:

- Controlling the reading of the parameter sets and the initialization of all computations variables. The FRAME marshals the organizational data required for each square in the

grid network. Such data include topographic levels, soil and vegetation type and rainfall and metrological station codes. The specific parameter values, such as soil conductivity or channel flow resistance, are called later by the relevant process component.

- Controlling the sequence in which each component is called to perform its computations. For each component there may be different time steps as well as changes in the time steps during a simulation, depending on the rate of hydrological response. It is often necessary, therefore, to accumulate calculated values over a period before they are transferred from one component to another.
- Controlling the exchange of data between components. The results provided by one component will in some cases need to be processed in to a different form for input to another component. This transfer is handled in such a way as to minimize inaccuracies in the overall water mass balance for the simulation.
- Controlling the mass balances between all components and within each component separately. This is carried out for the grid as a whole and not for individual squares.

3.3.2. INTERCEPTION AND EVAPOTRANSPIRATION COMPONENT

This component uses ***metrological input data and vegetation parameters*** to simulate the total evapotranspiration and net rainfall amounts resulting from the processes of:

- Interception of rainfall by the vegetation canopy;
- Drainage from the canopy;
- Evaporation from the canopy surface;
- Evaporation from the soil surface;
- Uptake of water by plant roots and its transpiration.

Net rainfall, transpiration and soil evaporation rates are supplied to the unsaturated zone component, which in return provides information on soil moisture conditions in the root zone.

3.3.2.1. Canopy Interception

The interception component calculates net rainfall reaching the ground through the canopy, the amount of water stored on the canopy and evaporation from the canopy. Interception is modelled by Kristensen and Jensen model. In this method interception storage is calculated based on the actual leaf area index and an interception capacity co-efficient.

$$I_{max} = C_{int}.LAI$$

The size of the interception storage capacity, I_{max}, depends on the vegetation type and its stage of development, which is characterised by the leaf area index, *LAI*. The coefficient C_{int} defines the interception storage capacity of the vegetation.

3.3.2.2. Evapotranspiration

The primary ET model is based on empirically derived equations that follow the work of Kristensen and Jensen (1975). In this model, the ET processes are split up and modelled in the folowing order:

1) A proportion of the rainfall is intercepted by the vegetation canopy, from which part of the water evaporates.
2) The remaining water reaches the soil surface, producing either surface water runoff or percolating to the unsaturated zone.
3) Part of the infiltrating water is evaporated from the upper part of the root zone or transpired by the plant roots.
4) The remainder of the infiltrating water recharges the groundwater in the saturated zone.

3.3.2.3. Evaporation from the Canopy

The evaporation from the canopy storage is equal to the potential evapotranspiration, if sufficient water has been intercepted on the leaves, that is

$$E_{can} = min(I_{max}, Ep\Delta t)$$

where E_{can} is the canopy evaporation, E_p is the potential evapotranspiration rate and Δt is the time step length for the simulation.

3.3.2.4. Plant Transpiration

The transpiration from the vegetation, E_{at}, depends on the density of the crop green material, (i.e. the leaf area index, LAI) the soil moisture content in the root zone and the root density. Thus,

$$E_{at} = f_1(LAI).f_2(\theta).RDF.E_p$$

where E_{at} is the actual transpiration, $f_1(LAI)$ is a function based on the leaf area index, $f_2(\theta)$ is a function based on the soil moisture content in the root zone, and *RDF* is a root distribution function.

3.3.2.5. Soil Evaporation

Soil evaporation is calculated by Kristensen and Jensen method in MIKESHE based on the following function

$$\mathbf{E_s = E_p.f(}\theta\mathbf{)+\{(E_p-E_{at}-E_p.f3(}\theta\mathbf{)\}.f_4(}\theta\mathbf{).(\{1-f_1(LAI)\}}$$

where E_s is the soil evaporation, E_p is the potential evapotranspiration, E_{at} is the actual transpiration.

In addition to the Kristensen and Jensen method, there is a TWO –Layer Water Balance Method for describing the evapotranspiration. This method divides the unsaturated zone into a root zone,from which evapotranspiration can occur and a zone below the root zone,from where evapotranspiration does not occur.This method is primarily suited for areas where the water table is shallow, such as wetlands.

3.3.3. OVERLAND AND CHANNEL FLOW

This component uses ***topographic, channel shape and flow resistance parameters*** to route surface water as overland and channel flow. The depth of surface water available as runoff is determined from the net rainfall and evaporation rates supplied by the interception/evapotranspiration component and from the soil infiltration rate determined by the unsaturated zone component.

When the net rainfall rate exceeds the infiltration capacity of the soil, water is ponded on the ground surface. This water is available as the surface runoff, to be routed down gradient towards the river system. The exact route and quantity is determined by the topography and flow resistance as well as the losses due to evaporation and infiltration along the flow path.

The water flow on the ground surface is calculated by overland flow module, using the diffusive wave approximation of the Saint Venant equation.

$$\frac{\partial h}{\partial t}+\frac{\partial (uh)}{\partial x}+\frac{\partial (vh)}{\partial y}=q$$

$$\frac{\partial h}{\partial x}=S_{ox}-S_{fx}$$

$$\frac{\partial h}{\partial y}=S_{oy}-S_{fy}$$

where,

h(x,y) = water depth

t= time

x,y horizontal cartesian coordinates

u(x,y), v(x,y) = flow velocities in the x and y directions

q(x,y,t) = net precipitation minus infiltration

S_{ox} & S_{oy} = ground slopes in the x and y directions

S_{fx} & S_{fy} = friction slopes in the x and y direction

Channel flow is modeled in one dimension as

$$\frac{\partial A}{\partial t} + \frac{\partial (Au)}{\partial x} = q_L$$

$$\frac{\partial h}{\partial x} = S_{ox} - S_{fx}$$

where,

A(x) = flow cross-sectional area

S_{ox} = Channel bed slope

q_L = source /sink term for evaporation, rainfall, lateral inflow and outflow.

3.3.4. UNSATURATED ZONE

This component determines the soil moisture content and tension, or pressure, distributions in the unsaturated zone. The zone extends from the ground surface to the phreatic surface. It is mostly nonuniform in its physical properties and the upper part, the root zone, exhibits considerable fluctuations in moisture content as a result of evapotranspiration and rainfall infiltration. Its lower boundary also varies through time, as the phreatic surface elevation changes.

There are three options in MIKE SHE for calculating vertical flow in the unsaturated zone:

- the full Richards equation, which requires a tabular or functional relationship for both the moisture-retention curve and the effective conductivity,
- a simplified gravity flow procedure, which assumes a uniform vertical gradient and ignores capillary forces, and
- a simple two-layer water balance method for shallow water tables.

The full Richards equation is the most computationally intensive, but also the most accurate when the unsaturated flow is dynamic. The simplified gravity flow procedure provides

a suitable solution when you are primarily interested in the time varying recharge to the groundwater table based on actual precipitation and evapotranspiration and not the dynamics in the unsaturated zone. The simple two-layer water balance method is suitable when the water table is shallow and groundwater recharge is primarily influenced by evapotranspiration in the root zone.

Each cell in the model is assigned to a soil zone, for which a soil profile is defined. In this way, the unsaturated zone can be nominally 'lumped', in so far as the soil profile that is defined for each soil zone represents some sort of average soil profile in the zone. If the depth to the water table is also divided into zones of equal depth, then the unsaturated flow needs only be calculated once for each area with the same soil profile and water table depth. Such lumping can decrease the computational burden considerably. However, when the water table is very dynamic and spatially variable, there may be no choice but to solve the unsaturated flow equations for each cell in the model using the full Richards solution.

Richards Equation

In its most comprehensive mode, MIKESHE WM solves Richards equation for one dimensional vertical flow, which includes the effects of gravity, soil suction, soil evaporation and transpiration .

$$C\frac{\partial j}{\partial t} = \frac{\partial}{\partial z}(K\frac{\partial j}{\partial z}) + \frac{\partial K}{\partial z} - S$$

where,

j = Soil moisture tension

t = time

z = vertical space coordinate (positive upwards)

C = soil water capacity

S = source/sink term for root extraction and soil evaporation

K = hydraulic conductivity

In order to solve Richard's equation ***unsaturated hydraulic conductivity and the soil moisture retention curve*** are required.Both functions should be known for any soil type included in any soil profile within the model area.

3.3.5. SATURATED ZONE FLOW

The saturated zone flow determines the phreatic surface level and the flows in the saturated zone of an unconfined aquifer, stream/aquifer interactions, groundwater seepage at the ground surface, and artificial groundwater extraction. The variation of the phreatic surface level with respect to time at each square grid is modeled by the nonlinear Boussinesq equation. This combines Darcy's law and the mass conservation of two dimensional laminar flow in an anisotropic , heterogeneous aquifer, to give

$$S\frac{\partial h}{\partial t} = \frac{\partial}{\partial x}(KxH\frac{\partial h}{\partial y}) + \frac{\partial}{\partial y}(KyH\frac{\partial h}{\partial y}) + R$$

where,

S(x,y) = specific yield

H(x,y,t) = phreatic surface level

(Kx(x,y), Ky(x,y) = saturated hydraulic conductivities in the x and y directions

H(x,y,t) = saturated thickness

T = time

x,y = horizontal cartesian coordinates

R(x,y,t) = instantaneous vertical recharge into the saturated zone.

Table 3.1: Data and parameter requirements for each grid square in the SHE model

Model components	Model input	Model parameters
Frame component	Map of rainfall stations	Ground surface elevation, Distribution codes for rainfall and metrological source stations.
MIKE SHE SZ Saturated zone flow	Geological model, Boundary conditions, Drainage depth(drain maps), Wells and withdrawal rate.	K_h, Horizontal hydraulic conductivity, K_v, Vertical hydraulic conductivity, S, confined storage co-efficient, Drainage time constant.
MIKE SHE UZ Unsaturated zone flow	Map of characteristic soil types, Hydraulic conductivity curves, Retention curves.	K_s, saturated hydraulic conductivity ?s, Saturated water content, ?res, residual water content, ?eff, Effective saturation water content, pFc, Capillary pressure at field capacity, pFw, Capillary pressure at wilting point n, Exponent of hydraulic conductivity curve
MIKE SHE ET Evapotranspiration	Time series of vegetation Leaf Area Index Time series of vegetation root depth	C1, C2, C3 : Empirical parameters, C_{int} : Interception parameter, Aroot :Root mass parameter, K_c : Crop coefficient.
MIKE SHE OC Overland	Topographical Map, Boundary conditions	M, Overland Manning no, D , Detention storage,

4. STUDY AREA

4.1 WATERSHED

Generally a watershed can be defined as a land area that contributes runoff (drains) to a given point in a stream or river. It is synonymous with catchment and drainage or river basin.

4.2 LOCATION AND EXTENT OF SOLANI WATERSHED

The present study area was taken in parts of Saharanpur district of Uttar Pradesh and Haridwar district of Uttarakhand state of India. The study area defined as *"**Solani watershed**"* lies between latitude 29°52'45" to 30°16'00'' N and longitude 77°44'00'' to 78°00'00'' E covering an area of 529.35 sq km. The study area comprises of Siwalik hills, piedmont plains and alluvial plains. The mean annual rainfall is 900 mm and mean annual temperature is about 24.26°C. The study area is as shown in the Figure 4.1.

The Solani river originates from the Northeast part of Siwalik hills (787 meter) of Saharanpur district near the Kaluwala pass (30°15'59.36" N latitude and 78°53'16.83" E longitude). Solani river is a moderate size right bank tributary of the river Ganga. The river flow essentially SW to SE for 60.177km to join the Ganga river near Jansath tehsil of Muzaffarnagar district (U.P.). It traverses over Roorkee District of Uttranchal and Saharanpur and Muzaffarnagar districts of Uttar Pradesh.

It is at first a mere torrent but gradually becomes a river of considerable magnitude and importance. The stream is formed by the union of the Chilawala, Kania, Sukh and Mohand Raus, which drain the sub-mountain tract immediately to the east of the Mohand road. Near Thapal Ismailpur, it is joined by the Rajwa and Khandus Raus, the former being of little importance while the latter is of considerable size, carrying the combined water of the Khujnawar and Shahjahanpur Raus as also of the Hatni Sot and other streams. The whole is then known as the Solani, which flows in a south – easterly direction under the high bank that marks the eastern limits of the upland plain. Just above the town of Roorkee the Solani receives on its left bank the Sipia, a water course of considerable length that rises in the ravines of

Sakrauda plateau and is fed by several affluent streams such as the Haljaura, the Jakni and Dhandora, all of which are seasonal streams in character.

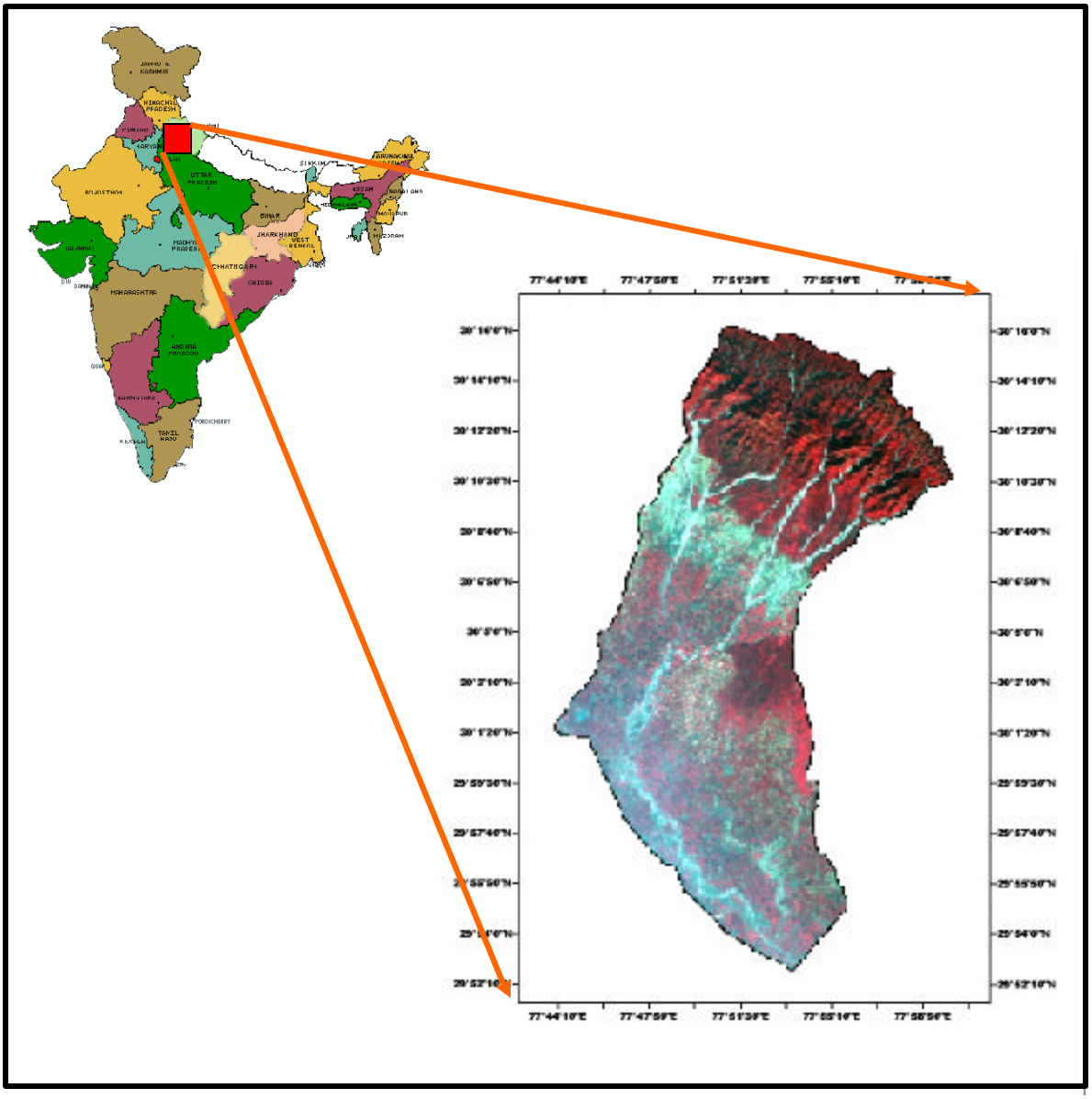

Figure 4.1: Location of Solani Watershed

At Roorkee the Solani passes under the great canal aqueduct and flows in a south-easterly direction to the northern border of pargana Mamglaur where it receives the Ratmau on its left bank. From these points onwards the river flows southward through the Khadir tract keeping close to the high bank till it finally passes into district Muzaffarnagar.

The position of the watershed on FCC of LISS III is as shown in the figure 4.2.

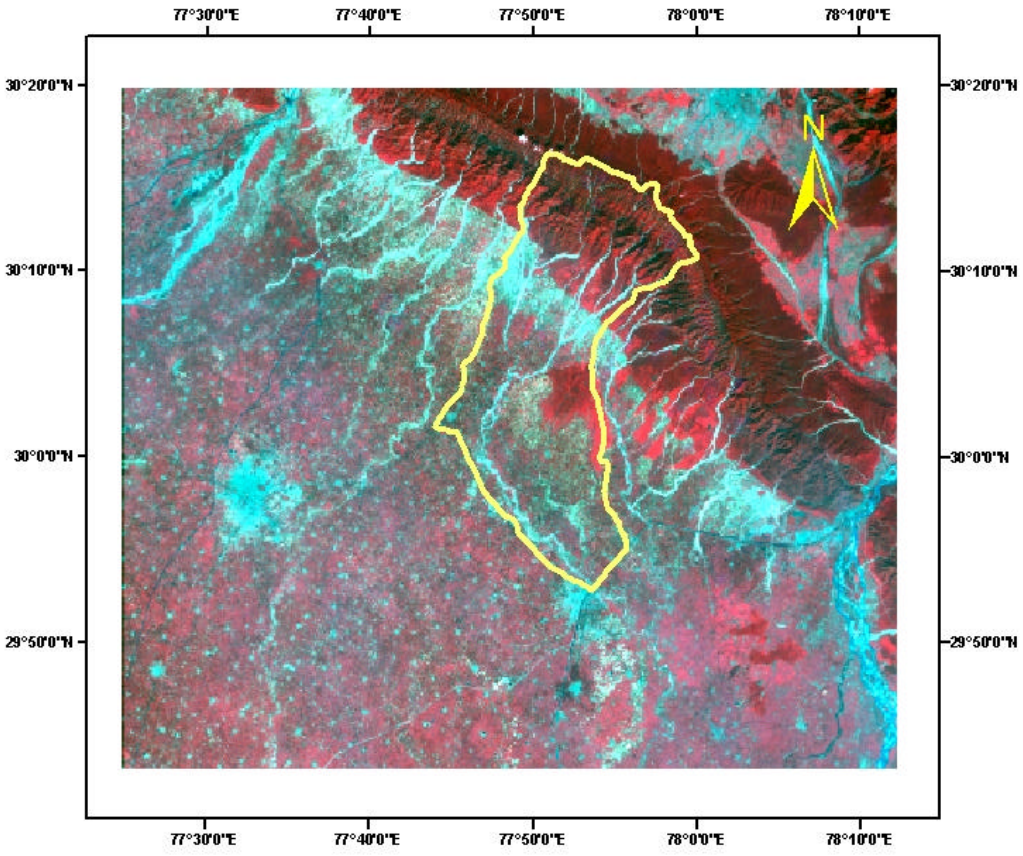

Figure 4.2: IRS P6 LISS III 10th October 2006 FCC showing the study area

4.3 CLIMATE

The climate of the Solani watershed resembles the average climate of Uttar Pradesh and Uttrakhand in general but its northern position and its proximity to the hills give its own peculiarity. Though the region lies well outside the tropics yet its climate is like rest of the north India essentially because of Himalayan chain. It is a sub- humid region. Like other parts of north India the Solani watershed also experiences four seasons in a year.

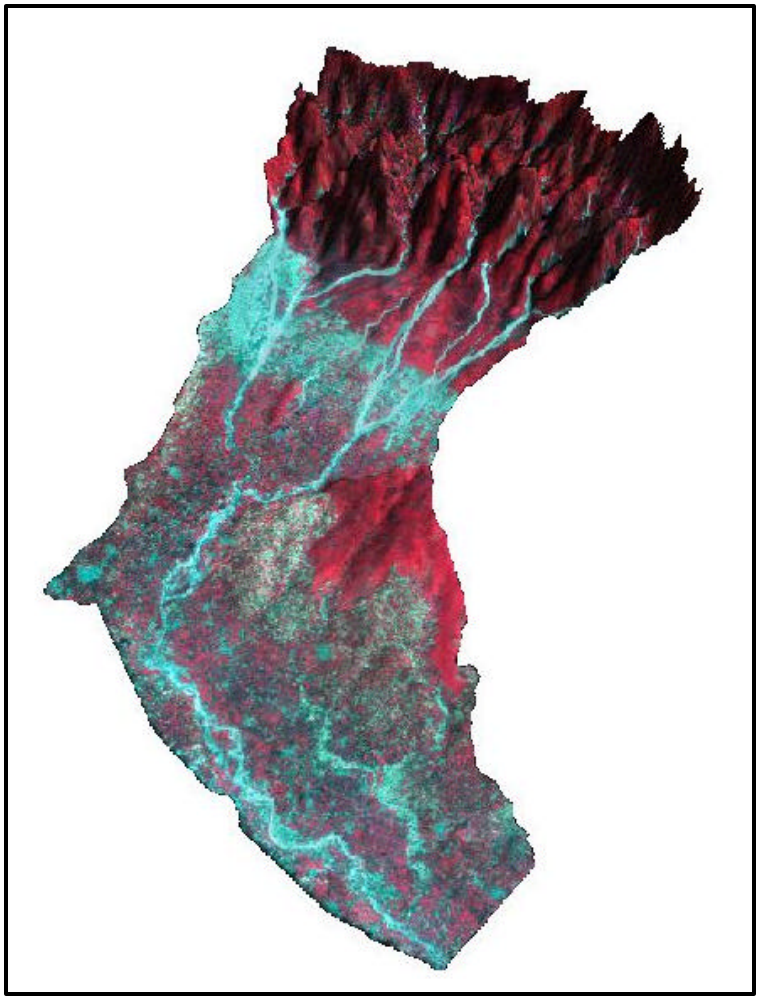

Figure 4.3: FCC Draped over the CARTOSAT DEM

4.4. TOPOGRAPHY

It can be seen from Figure 4.3 that upper part of the watershed is hilly having an average elevation of 650 m. The lower part of the watershed is plain having an average elevation of 250 m.

4.5 RAINFALL

The average annual rainfall in the watershed (National Institute of Hydrology, Roorkee Station) is 900 mm. The rainfall generally increases from the south-west, towards the north-east. About 83% of the annual rainfall in the watershed is received from June to August. The rainfall and potential evapotranspiration for the area in the hydrologic year (June 2006-May 2007) is as shown in the Figure 4.4.

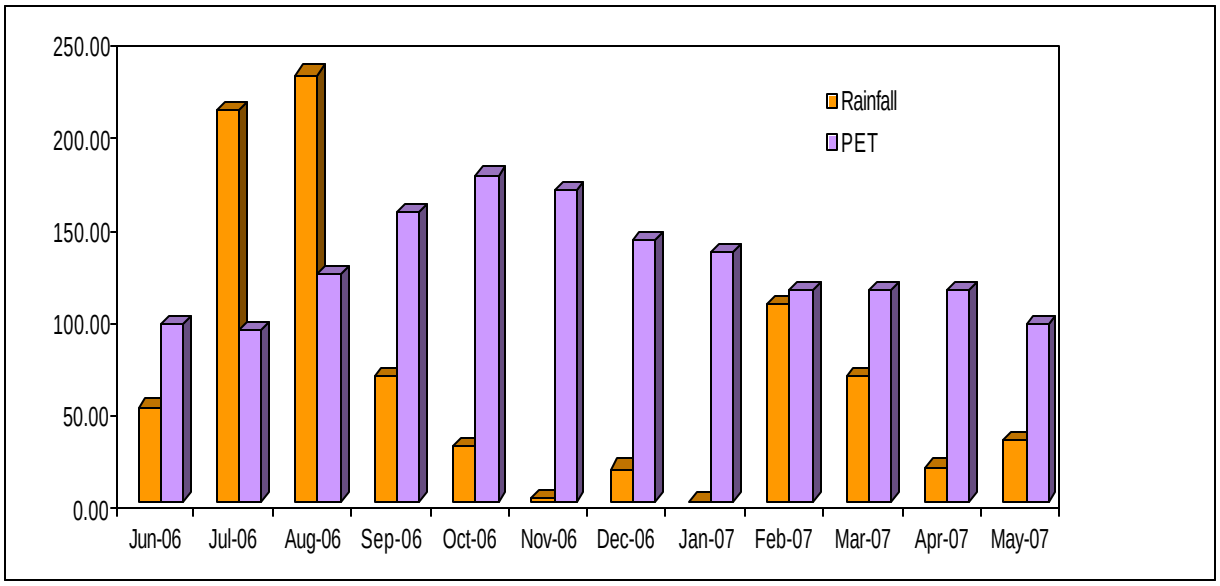

Figure 4.4: Graph showing rainfall and PET in Solani watershed

4.6 TEMPERATURE AND HUMIDITY

There are three meteorological observatories in the watershed, the records of which may be taken as representative of the meteorological conditions prevailing in the watershed. From end of February, temperature begins to increase rapidly. May and June are the hottest months with the mean daily maximum and minimum temperature around 39ºC and 25ºC respectively. With the onset of monsoon by beginning of July there is appreciable drop in the day temperature. But nights continue to be as warm as during the later part of summer. There is a slight increase in the day temperature in September but the night temperature begins to decrease. After October temperature decreases, and night starts getting cooler. January is generally the coldest month with the mean daily maximum at 20.1ºC and the mean daily minimum at 6.6ºC. During the cold season, under the influence of western disturbances, cold waves affect the climate of watershed.

The humidity is high during the south-west monsoon season. Thereafter, humidity starts decreasing. The driest part of the year is the summer season particularly April and May months when the relative humidity in the afternoons is usually less than 25 percent.

4.7 GEOLOGY

The watershed, forming a part of the Indo-Gangetic alluvial tract in the South and the Siwalik hills in the north comprises the following succession of rock groups arranged in order of increasing age from top to bottom:

The Siwalik mainly consist of sandstones, grits, conglomerates, pseudo-conglomerate, clays, and silts having the characters of fluviatile deposits of torrential streams and floods in shallow fresh-water basins. The sandstones show poor stratification and are generally upgraded as to grain size.

The Siwalik Hills on the southern side is fringed by talus fans. The upper portion of the talus fans is composed of rock fragments, gravel and soil, and supports good forests. This zone, known as the Bhabar, which has a vertical extent of less than 300m.

4.8 SOIL

The soil in the study area can be classified into five classes namely loam, loamy sand, sand, sandy clay and sandy loam. The major part of the watershed consists of sandy loam.

4.9 PHYSIOGRAPHY

Physiographic is the study of the factors and processes of the landform evolution. The factors involved in physiographic processes are mostly the same as those influencing soil formations. Soil is a three dimensional natural body of landscape. Different contributing features include vegetation, topography, soil, color etc. Based on the variation in the physiographic characteristics, the study area is divided into four major lands forms namely

1. Siwalik Hills (S)
2. Piedmont (P)
3. Residual Hills (RH)
4. Alluvial Plain (AP)

4.10 NATURAL VEGETATION:

The forest types of study area are mostly moderate to open type and in the upper ridge of Siwalik it is degraded to great extent. The natural vegetation consists of trees, shrubs, and grasses. Taking into consideration the difference in altitude and the climatic conditions the

flora of the watershed may be divided into three main botanical divisions: the moist tropical forests, the tropical dry mixed deciduous forests, and the Siwalik chir forest.

The field photographs are shown in Figure 4.5. For this study the outlet of Solani river is taken near Roorkee.

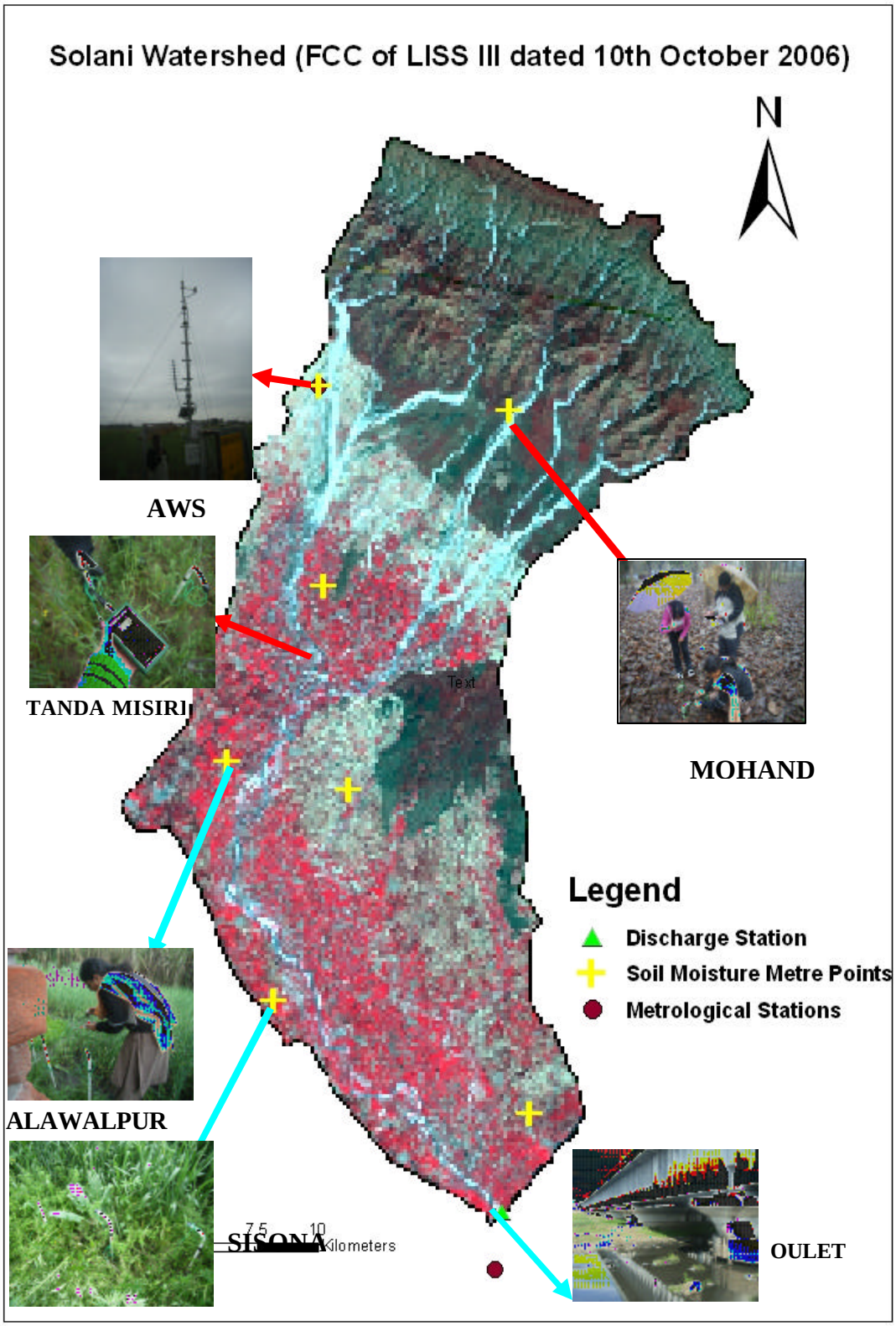

Figure 4.5: LISS III FCC showing soil moisture observation points and the outlet of Solani River at Roorkee

5. MATERIALS AND METHODOLOGY

The main objective of the study is to map soil moisture in the watershed spatially and temporally for the year 2006-2007 on a fortnight basis. The approaches used here are remote sensing and hydrologic modeling. Optical remote sensing data has been used to derive soil moisture index and water deficit index (WDI). A regression analysis has been done between the indices and volumetric soil moisture content obtained from gypsum block readings installed at seven locations in the watershed at a depth of 15cm ,45cm and 75cm. MIKE SHE a distributed hydrological model simulates soil moisture at various depths using Richard's equation. The model requires extensive data input and for this purpose metrological data, remote sensing data with ancillary data has been used. This chapter explains the data used to achieve the objectives of the study and adopted the methodology.

5.1. MATERIALS

5.1.1. REMOTE SENSING DATA and PRE-PROCESSING

The data used for this study is as given in Table 5.1. The digital analysis of the satellite data was carried out using ERDAS IMAGINE 8.7, ENVI 4.3, ARCGIS 9.1, and PCI GEOMATICA 10.0.

Table 5.1: Data used in the study

Satellite	Sensor	Acquisition date
TERRA	ASTER	1st November 2006
	MODIS	October 06 to May 07
IRS P6	LISS III	10th October 2006
IRS P5	CARTOSAT	2nd October 2005
ENVISAT	ASAR	5th August and 24th October 2006

Advanced Space born Thermal Emission and Reflection Radiometer (ASTER)

ASTER (Advanced Space borne Thermal Emission and Reflection Radiometer) is an imaging instrument that is flying on the NASA's Terra satellite launched in December 1999 as part of NASA's Earth Observing System (EOS). Terra carries five scientific instruments: ASTER, CERES, MISR, MODIS and MORPITT. ASTER is a co-operative effort between NASA, Japans Ministry of Economy and Japans Earth Remote Sensing Data Analysis center (ERSDAC). The specifications of the 14 ASTER spectral bands are mentioned below in the table (Table 5.2).

Table 5.2: Specifications of ASTER Spectral bands

Spectral channel	Spectral range	Spatial resolution	Dynamic range	Comment
1 (Visible Green)	0.52-0.6µm	15m	8 bit integer	The visible data has been used to derive NDVI and land use land cover.
2 (Visible Red)	0,63-0.69µm	15m	8 bit integer	
3 (Near Infrared)	0.76-0.86µm	15m	8 bit integer	
4 (SWIR)	1.6-1.7µm	30m	8 bit integer	The SWIR data has been used to develop a soil moisture index.
5 (SWIR)	2.145-2.185µm	30m	8 bit integer	
6 (SWIR)	2.185-2.225µm	30m	8 bit integer	
7 (SWIR)	2.235-2.285µm	30m	8 bit integer	
8 (SWIR)	2.295-2.365µm	30m	8 bit integer	
9 (SWIR)	2.36-2.43µm	30m	8 bit integer	
10 (TIR)	8.125-8.475µm	90m	12 bit integer	The TIR data has been used develop water deficit index (plot between T_s-T_a and NDVI)
11(TIR)	8.475-8.825µm	90m	12 bit integer	
12 (TIR)	8.925-9.275µm	90m	12 bit integer	
13 (TIR)	10.25-10.95µm	90m	12 bit integer	
14 (TIR)	10.95-11.65µm	90m	12 bit integer	

(Source: http://asterweb.jpl.nasa.gov/eos.asp)

ASTER acquires 14 spectral bands and can be used to obtain detailed maps of land surface temperature, emissivity, reflectance and elevation. The date of acquisition is on 1st November 2006.

MODIS Data Products

The **MOD**erate Resolution **I**maging **S**pectrometer (MODIS) is a key instrument for NASA's Earth Observing System(EOS). It was launched on board the Terra spacecraft in December 1999 and the Aqua spacecraft in May 2002. It has a viewing swath width of 23330km and views the entire surface of the Earth every one to two days. Its detectors measure 36 spectral bands between 0.405 and 14.385 µm wavelength, 20 reflective solar bands (0.405-2.2 µm) and 16 thermal emissive bands (3.5-14.385 µm) and 16 thermal emissive bands (3.5-14.385 µm). It acquires data at three spatial resolutions: 250m, 500m, and 1000m (http://edudaac.usgs.gov/modis/dataproduct.asp). A brief description about the MODIS Land products used in this study is given below.

MODIS/Terra Surface Reflectance 8-Day L3 Global 250m SIN Grid V004&V005

The MODIS Surface Reflectance products provide an estimate of the surface spectral reflectance as it would be measured at ground level in the absence of atmospheric scattering or absorption. Low-level data are corrected for atmospheric gases and aerosols, yielding a level-2 basis for several higher-order gridded level-2 (L2G) and level-3 products.MOD09Q1 provide Bands 1 and 2 at 250-meter resolution in an 8-day gridded level-3 product in the Sinusoidal projection. Each MOD09Q1 pixel contains the best possible L2G observation during an 8-day period as selected on the basis of high observation coverage, low view angle, the absence of clouds or cloud shadow, and aerosol loading.16 date images corresponding to the date of field observation were downloaded for the year October 2006- May 2007. The data has been used to estimate WDI.

MODIS/Terra Surface Reflectance 8-Day L2G Global 500m SIN Grid V004&V005

The MODIS Surface Reflectance products are computed from bands 1-7 to provide an estimate of the surface spectral reflectance for each band as it would be measured at ground

level in the absence of atmospheric scattering or absorption The MODIS/Terra Surface Reflectance Daily L2G Global 500m SIN Grid product, MOD09GHK, contains data for each of the seven land bands, two at 250m resolution (bands 1-2), and five at 500m resolution (bands 3-7).16 date images corresponding to the date of field observation were downloaded for the year October 2006- May 2007. The data has been used to estimate Short Wave Infrared Water Stress Index (SIWSI).

MODIS/Terra Land Surface Temperature/Emissivity 8-Day L3 Global 1km SIN Grid V004& V005

The level-3 MODIS global Land Surface Temperature (LST) and Emissivity 8-day data are composed from the daily 1-kilometer LST product (MOD11A1) and stored on a 1-km Sinusoidal grid as the average values of clear-sky LST's during an 8-day period. MOD11A2 is comprised of daytime and nighttime LST's, quality assessment, observation times, view angles, bits of clear sky days and nights, and emissivities estimated in Bands 31 and 32 from land cover types. The data has been used to develop WDI.

MODIS/Terra Leaf Area Index/FPAR 8-Day L3 Global 1km SIN Grid V004&V005

The MODIS global Leaf Area Index (LAI)/ FPAR product is composites every 8 days at 1-kilometer resolution on a Sinusoidal grid. Both variables are used as satellite-derived parameters for calculating surface photosynthesis, evapotranspiration, and net primary production, which in turn are used to calculate terrestrial energy, carbon, water cycle processes, and biogeochemistry of vegetation. Weekly data starting from June 2006-May 2007 has been downloaded and is used as an input to MIKE SHE.

Preprocessing

Steps of preprocessing before the MODIS data were used for analysis:

- Conversion of file format
- Layer Stacking
- Re-projection
- Scaling with a multiplication factor
- Sub-setting

MODIS products are available to the users in HDF (Hierarchical Data Format) which is a multi object file format for sharing scientific data in a multi platform distributed environment. It is imported to .img format using ERDAS IMAGINE 8.7. The bands imported are stacked and re-projected from Sinusoidal projection to Albers Equal Area Projection. The projection parameters for India are given below:

Projection: Albers Equal Area Projection
Spheroid Name: WGS-84
Datum Name: WGS-84
Latitude of 1st standard parallel: 12:00:00:00N
Latitude of 2nd standard parallel: 28:00:00:00N
Longitude of central meridian: 78:00:00:00E
Latitude of origin of projection: 20:00:00:00N
False easting at central meridian: 2000000m
False northing at origin: 2000000m

After re-projection, the MODIS data products were scaled with their respective multiplication factors, which is 0.0001 for the surface reflectance, 0.002 for LST images and 0.01 for LAI images.

ENVISAT-ASAR (Advanced Synthetic Aperture Radar)

ENVISAT is the first permanent space born radar to incorporate dual-polarization capabilities- it can transmit and receive in either horizontal or vertical polarizations. This Alternating Polarization (AP) mode can improve the capability of a SAR instrument to classify different types of terrain. ASAR uses an active phased-array antenna, with incidence angles between 15° and 45°. The ASAR is a high resolution imaging radar that can be operated in distinct measurement modes:

- Image mode
- Alternating Polarization mode
- Wide Swath mode
- Global Monitoring mode
- Wave mode

Wide swath mode covers 400km wide with 150m resolution, Global monitoring mode can cover 400km width by 1km resolution, and high resolution mode can have 10m resolution. The

nominal spatial resolution (30m) and swath coverage of ASAR image mode (100Km) and 35 days repeat orbit. It is operating at C-band (wavelength 4 to 8cm, frequency). The cross polarization combinations offer better discrimination between terrain types. The AP mode can help better identify the boundaries between sea ice and open water. In dual polarization, data can be acquired in three polarization modes viz. horizontal (HH) and vertical (VV) or cross polarization (HH & HV or VV&VH). The ENVISAT data was acquired for two dates 5th August 2006 and 24th October 2006. The standard specification is given in Table 5.3.

Table 5.3: Standard Specification for ENVISAT ASAR data products

Product ID	Product Name	Nominal Resolution(m) (range x azimuth)	Nominal Pixel Spacing (m) (range x azimuth)	Appx. Coverage (Km) (range x azimuth)
APP	Alternating Polarization Precision image	30 x 30	12.5 x 12.5	100 x 100
APS	Alternating Polarization Single-look Complex	9 x 12	natural	100 x 100

(Source: http://envisat.esa.int)

IRS P6 LISS III and IRS P5 CARTOSAT 1

IRS-P6 Resourcesat-1 was successfully launched on October 17, 2003. It carries three sensors namely LISS IV at 5.8m spatial resolution, LISS III at 23.5m spatial resolution and AWiFS at 56m spatial resolution. LISS III data acquired on 10th October 2006 has been used to derive a soil moisture index based on the reflectance of the surface. The specification of LISS III is given in Table 5.4.

Table 5.4: Specification of IRS P6 LISS III Sensor

Spatial Resolution	23.5m
Spectral resolution	Band 2 (520-590nm) Band 3 (620-680nm) Band 4 (770-860nm) Band 5 (1550-1700nm)
Radiometric resolution	7 bit

IRS-P5 Cartosat-1 was successfully launched on May 5, 2005. The spatial resolution of the image is 2.5m. Thus this high-resolution data has been used for the field work carried out to validate MODIS LAI. It is also used to generate a high resolution DEM of 5 m which is an input to the hydrological model MIKE SHE.

Preprocessing

LISS III data was imported using ERDAS IMAGINE 8.7 and was geo-referenced. CARTOSAT data was also imported to img format was used for the field work.

5.1.2. METROLOGICAL DATA

Daily metrological data such as rainfall, minimum and maximum temperature, pan evaporation data were obtained from Automatic Weather Station (AWS), Muzzafarabad and National Institute of Hydrology (Roorkee). The daily rainfall was used as an input to the MIKE SHE model. Maximum and minimum temperature was used to calculate potential evapotranspiration by Hargreave's method which was also an input to the MIKE SHE model.

5.1.3. ANCILLARY DATA

The other ancillary data used are as follows:

- Soil texture obtained from NIH, Roorkee.
- Soil map obtained from Agriculture and Soils Division, IIRS.
- Pressure curves for converting soil meter readings to volumetric soil moisture content were obtained from NIH, Roorkee.
- Digital Elevation Model obtained from Photogrammetry division, IIRS.
- Land use Land cover map of March 2001 obtained from Agriculture and Soils Division, IIRS.

5.2. METHODOLOGY

5.2.1. MEASUREMENT OF SOIL WATER CONTENT

Soil sampling over various locations in the watershed

The soil moisture samples in order to analyze the spatial distribution of surface soil moisture were collected. The soil samples were taken from different fields having variable crop

type and variable soil texture at the time of satellite pass. GPS readings were taken at each sample location to allow accurate identification of the soil sample location on the image. The various soil samples were collected as per the sampling strategy and were collected at 5cm and 10cm depth respectively in containers. The wet soil samples were weighed and were dried in oven at 100°C for 24hrs. The gravimetric moisture content was estimated from the weight of the dry soil and the weight of wet soil. The moisture content is expressed as a percentage of dry soil weight.

$$M_s = \frac{W_w}{W_d}$$

Where
M_s= soil moisture content (%)
W_w= weight of wet soil (g)
W_d= weight of dry soil (g)

The volumetric soil moisture obtained at 5cm depth were used to develop a regression equation with the backscattering co-efficient obtained from ENVISAT ASAR data dated 5th August 2006. Its also has been used for correcting the co-efficient for vegetation effects.

Measurement of soil moisture using Gypsum Blocks

Gypsum blocks installed at six locations in the watershed monitors the soil moisture content by measuring soil water suction. Soil water suction is the pressure required to extract the water present in the soil. This pressure is measured as centibars (cB). Gypsum blocks are installed at three depths: 15cm, 45cm and 75cm. Gypsum blocks installed in the watershed is as shown in the Figure 5.1.

Figure 5.1: Gypsum blocks installed in the watershed and soil moisture meter used to take the readings

The details where the gypsum blocks have been installed in the watershed is as given in the Table5.5.

Table 5.5: Details of Gypsum blocks installed sites

S.No.	Location	Latitude	Longitude	Depth	Land use	Soil Type
1	Sisona	29°57'32.1"N	77°47'51"E	15	Agricultural field(bare)	Sandy loam
				40		Sandy loam
				75		Sandy loam
2	Alwalpur	30°02'45.5"N	77°46'41.2"E	15	Agricultural field(cultivated)	Sandy loam
				40		Sandy loam
				75		Silt
3	Tanda Misri	$30^0$06'36.2"N	$77^0$49'8.7"E	15	Agriculture (Cultivated and irrigated)	Sandy loam
				40		Sandy loam
				75		Sand
4	Mohand	$30^0$10' 25.8"N	$77^0$53'52"E	15	Forest	Sandy loam
				40		Sandy loam
				75		Silty loan
5	AWS	30°11'00"N	77°49'00"E	15	Agricultuaral field(rain fed)	Sandy loam
				40		Sandy loam
				75		Sandy loam
6	Nagal MK	29º55'05.6"N	77º54'24.5"E	15	Agriclutural field	Sandy loam
				40		Sandy loam
				75		Silty loam

A fortnightly field visit was carried out to collect the soil moisture meter readings. To covert the soil moisture meter readings (cB) to volumetric soil moisture content curves defining the relationship between soil water content and soil water tension were obtained by pressure plate apparatus from NIH, Roorkee. The curves and relationship are shown in appendix A. Using the relationship pressure readings were converted to volumetric soil moisture content.

5.2.2. OPTICAL REMOTE SENSING APPROACH

The methodology used for estimation of soil moisture using optical remote sensing from various sensors such as LISS III, ASTER and MODIS products are shown in the flowchart 5.1.

5.2.2.1. Soil moisture index from LISS III

LISS III data acquired on 10th October 2006 was imported and geo-referenced and the watershed was extracted. Reflectance is the ratio of the upwelling radiance from the surface to the equivalent solar radiance incident on the surface. Satellite sensors measure the upwelling radiance above the earth's atmosphere, and the received signals from various targets are represented on an image in terms of digital numbers. The digital numbers were converted to radiance using the formula:

$$L_{rad} = [(\frac{DN}{255}) * (L_{max} - L_{min})] - L_{min}$$

where

Lrad is the spectral radiance (mW /cm^2/sr/m)
DN is the digital number
L_{max} and L_{min} are the minimum and maximum radiance obtained from the header file. It's given in the Table 5.6.

Table 5.6: Values of Lmax and Lmin for LISS III Sensor

Band	Wavelength (µm)	L_{min} (mW /cm^2/sr/m)	L_{max} (mW /cm^2/sr/m)	$E_{sun?}$ (mW /cm^2 /m)
B2	0.52-0.59	0	18.471	185.216
B3	0.62-0.68	0	18.179	157.731
B4	0.77-0.86	0	20.695	109.666
B5	1.55-1.70	0	6.903	24.062

(Source:Srinivasuluet.al.,2004)

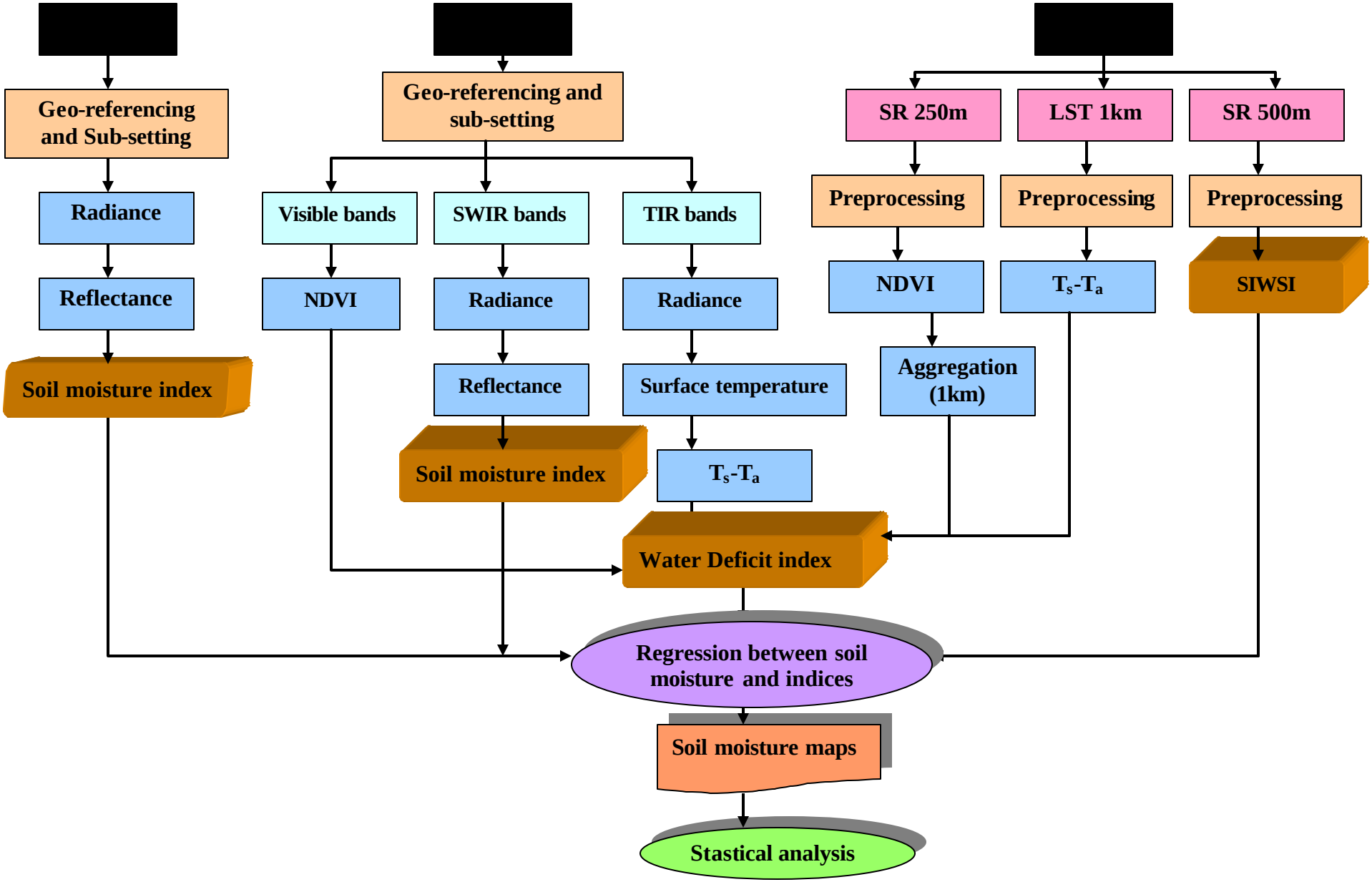

Flow Chart 5.1: Flow chart depicting methodology followed using Optical Remote Sensing Approach

The reflectance was found using the equation:

$$r = \frac{\Pi * L_{rad} * d^2}{E_{sunl} * \cos(q)}$$

where

? is the reflectance (a scale of 0-1)
p = 3.141
L_{rad} is the spectral radiance in mW /cm^2/sr/m
d is the Earth-sun distance in astronomical units
$E_{sun?}$ is the mean solar exoatmospheric spectral irradiance in mW /cm^2 /m
? is the sun zenith angle in degrees when the scene was recorded.

The soil moisture index was obtained using the near-infrared and short wave infrared bands. The index obtained was then compared at 6 locations with the volumetric soil moisture content obtained from gypsum blocks. The equation used to obtain this was:

$$SMI = \frac{(SWIR - NIR)}{(SWIR + NIR)}$$

5.2.2.2. Soil moisture index from ASTER

The ASTER data was acquired dated 1st November 2006. The data was imported and the study area was extracted.

Converting Digital numbers into Reflectance values

Following technique is used to rescale the digital numbers to the at-sensor spectral radiance L_i (W/m^2/sr/mm) for each pixel, using the gains listed in the ASTER metadata.

$$\mathbf{L_i = UCC\ (DN-1)}$$

where UCC is the Unit of Conversion. The co-efficients according to the gain of the bands which were used are given in the Table 5.7.with $E_{sun?}$ values. The spectral radiance (at-sensor) is converted to reflectance according to

$$r = \frac{\Pi * L_{rad} * d^2}{E_{sunl} * \cos(q)}$$

Where
? – Reflectance
E_{sun} – the in-band solar spectral irradiance in W/m2/nm
d - the distance between the Earth and sun in astronomical units
? – the sun zenith angle in degrees when the scene was recorded.

Table 5.7: Co-efficients used to convert DN in to reflectance values

Band No	Gains	UCC	$E_{sun?}$
1	Low	2.25	1845.99
2	Low	1.89	1555.74
3N	Low	1.15	1119.47
4	High	0.1087	231.25
5	High	0.0348	79.81
6	High	0.0313	74.99
7	High	0.0299	68.66
8	High	0.0209	59.74
9	high	0.0159	56.92

(Source: http://www.cnrhome.uidaho.edu/default.aspx?pid=85984)

Surface soil moisture index was developed by referring curves in the literature (Bowers and Hanks, 1965) which is shown in Figure 5.2. The band which gives maximum variation was chosen to derive a soil moisture index.

$$SMI = \frac{(Band\,5 - Band\,4)}{(Band\,5 + Band\,4)}$$

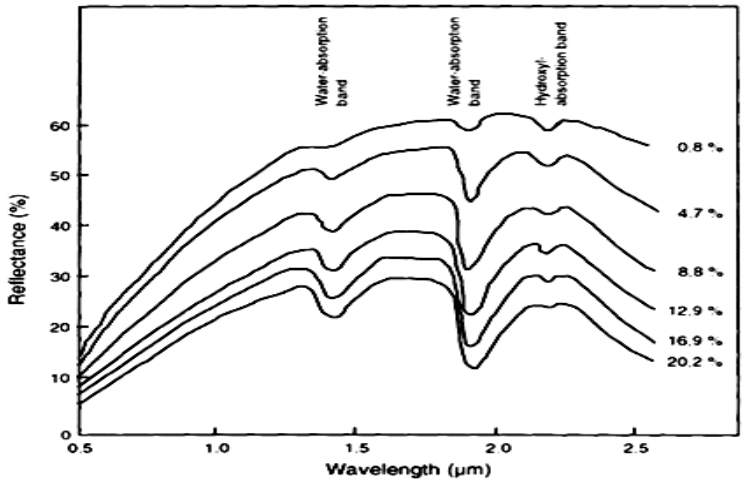

Figure 5.2Variation of surface soil reflectance with changing soil moisture (Bowers and Hanks,1965)

5.2.2.3. Water Deficit Index (WDI)

The WDI quantifies the relative rate of latent heat flux leaving a surface by evaporation and transpiration, where the surface is a mixture of vegetation and bare soil. The WDI is defined as 0.0 for well-watered conditions (i.e., a completely wet surface where latent heat flux is limited only by atmospheric demand) and 1.0 for no available water (i.e., a completely dry surface where there is no latent heat lost to the atmosphere). WDI as defined is not strictly related to crop water stress because it also accounts for evaporation from bare soil. Moran (1994) developed the water deficit index (WDI) that uses both surface minus air temperature and a vegetation index to estimate the relative water status of a field. The distribution of surface minus air temperature at a particular time was found to form a trapezoid when plotted against percent cover. Note that for many crops, there is a linear relationship between percent cover and a vegetation index (such as the normalized difference vegetation index (NDVI = [NIR-Red]/ [NIR+Red]), so the index can be used in place of a direct measure of percent cover. The concept of the WDI is illustrated in the Figure 5.3.

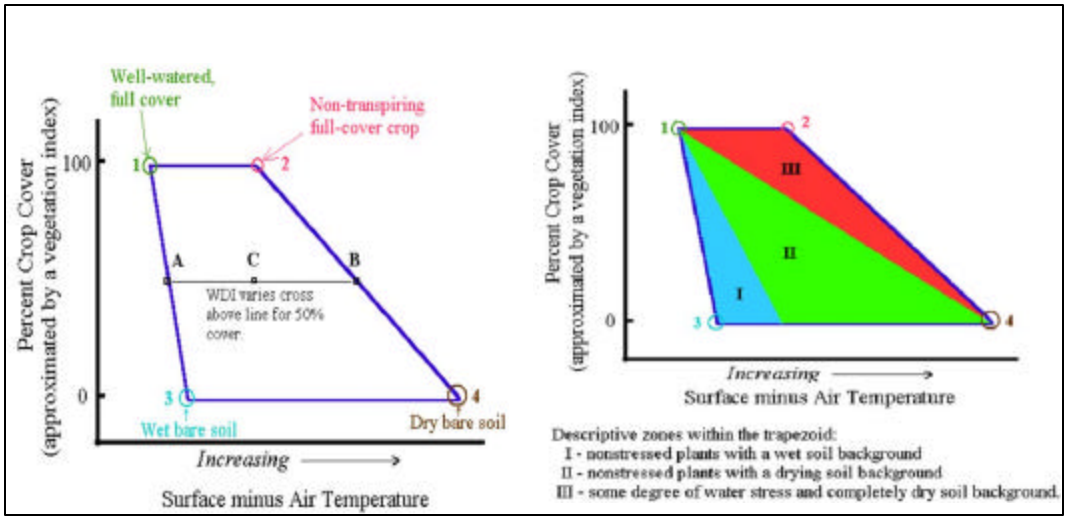

Figure 5.3Schematic scatter plot of physical interpretation of WDI based on NDVI-T_s-T_a space

The upper left of the trapezoid corresponds to a well-watered crop at 100 percent cover and the upper right to a non transpiring crop at 100 percent cover (points 1 and 2, respectively). These two points are the upper and lower limits of the trapezoid. The lower

portion of the trapezoid (bare soil) is bound by a wet and dry soil surface. Verstraeten, (2001) formulated the water deficit index (WDI) as

$$WDI = 1 - \frac{ET}{ET_m} \approx \frac{\Delta LST_{\min} - \Delta LST_0}{\Delta LST_{\min} - \Delta LST_{\max}} \approx \frac{a_{\min} NDVI + b_{\min} - \Delta LST_0}{(a_{\min} - a_{\max})NDVI + (b_{\min} - b_{\max})}$$

Where a_{min} , a_{max}, b_{min}, b_{max} are the coefficient of isoline drawn and $?LST_0$ denotes the difference between the LST and ambient air temperature. Further WDI can be represented as - Wet line or Max ETR line equal to $?LST_{NDVIimin} = a_{min}NDVI_i+b_{min}$ and dry line or Min ETR line equal to $?LST_{NDVIimax} = a_{max}NDVI_i+b_{max}$.

ASTER Land surface temperature

The data can be rescaled to at sensor radiance using the formula

$$\mathbf{L_i = UCC \times (DN-1)}$$

Where
UCC-Unit of conversion
DN- digital number.
The UCC required are given in the table 5.8.

Table 5.8: Unit of conversion for thermal bands

BAND	UCC
10	0.006882
11	0.006780
12	0.006590
13	0.005693
14	0.005225

(Source: Hideyuki et.al., 2004)

Various algorithms have been developed for converting the ASTER thermal bands measurements to land surface temperature maps as reported by the ASTER temperature/emissivity working group (1999). However, a universally accepted method is not available at this time for computing LST from multiple bands of TIR data such as those found in ASTER data. In this study 13 band (10.25-10.95µm) was selected to compute LST. It involves two steps: converting DN to spectral radiance and correcting spectral emmissivity. Correction for emissivity was done as follows:

Brightness temperature was found using the equation:

$$T_c = \frac{C_2}{l_c * In(\frac{C_1}{l_c \Pi L_l} + 1)}$$

where
T_c- brightness temperature in K from a central wavelength
$L_?$- spectral radiance in $W/m^3/sr/\mu m$
$?_c$- sensor's central wavelength
C_1- 1st radiance constant = $3.741x10^{-16}$ $W/m^2/sr/\mu m$
C_2- 2nd radiance constant = 0.0143879mK.
The temperature values were obtained from the equation below

$$LST = \frac{T_c}{1 + (l * T_c / r)}$$

where
LST- Land surface temperature in K
?- wavelength of emitted radiance (10.6μm in this case)
?- constant = 1.438×10^{-2} mK.

NDVI map was prepared from the visible band data using the formula

$$NDVI = \frac{(NIR - \mathrm{Re}\, d)}{(NIR + \mathrm{Re}\, d)}$$

$$\text{i.e. } NDVI = \frac{(band3 - band2)}{(band3 + band2)}$$

A plot between Ts-Ta and NDVI was drawn, WDI was computed using the equation(pg 63) and the isolines were drawn as shown in the Figure 5.4. Based on the interpretation of the NDVI-? T space, the dry and wet lines were estimated with the linear regression method. Using the equations of wet and dry lines (Isolines), WDI was computed for each pixel.

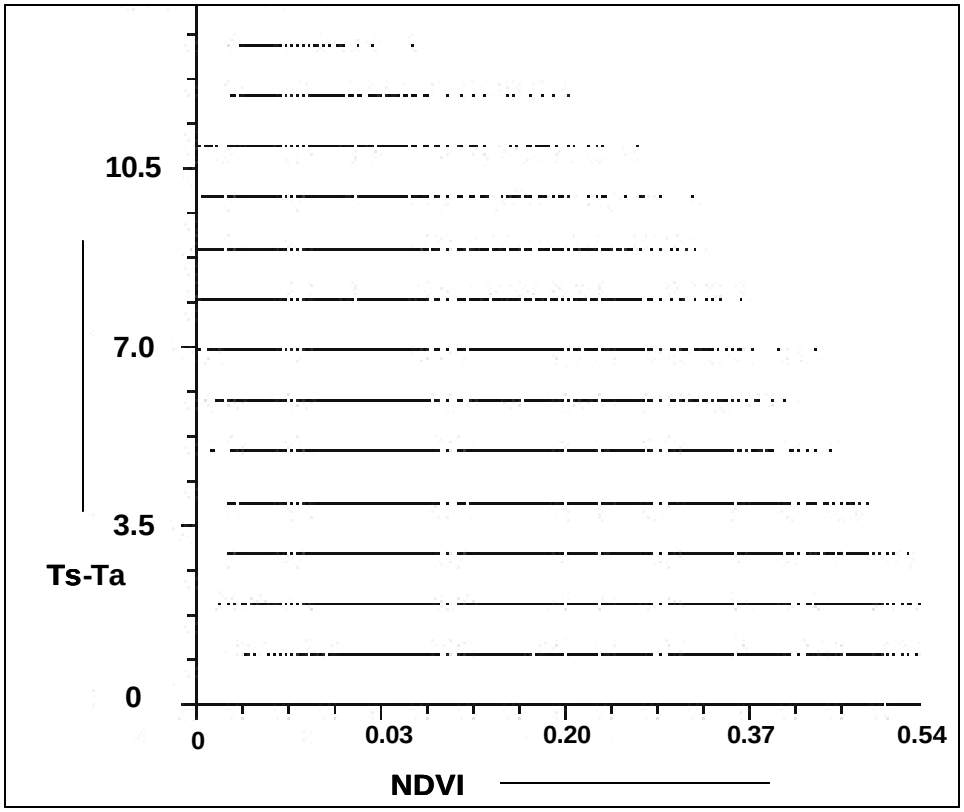

Figure 5.4: Scatter-plot between NDVI and (T_s-T_a)

MODIS

MODIS surface reflectance 250m and land surface temperature products were downloaded for 16 dates and was preprocessed using ERDAS. NDVI maps were obtained from the surface reflectance product. WDI was obtained by the method mentioned above. A regression analysis was carried out between this index and the volumetric soil moisture content obtained from gypsum blocks at different depths.

Short wave infrared water stress index from MODIS

MODIS level 2G 500m daily reflectance data was downloaded and was preprocessed. Combining the NIR reflectance information with the SWIR reflectance information, variations in the moisture content of the surface can be retrieved. SIWSI was found using the equation given by Fensholt et.al.(2003).

$$SIWSI = \frac{r_6 - r_2}{r_6 + r_2}$$

where ? is the reflectance and the spectral range of MODIS channel 2 is from 841 to 876nm and channel 6 is from 1628 to 1652nm. SIWSI thus obtained was compared with the in-situ soil moisture from gypsum blocks.

5.2.3. MICROWAVE REMOTE SENSING APPROACH

For assessment of soil moisture using active microwave remote sensing data, ENVISAT data was acquired on 5th August 2006 and 24th October 2006. The methodology adopted is as shown in the Flowchart 5.2.

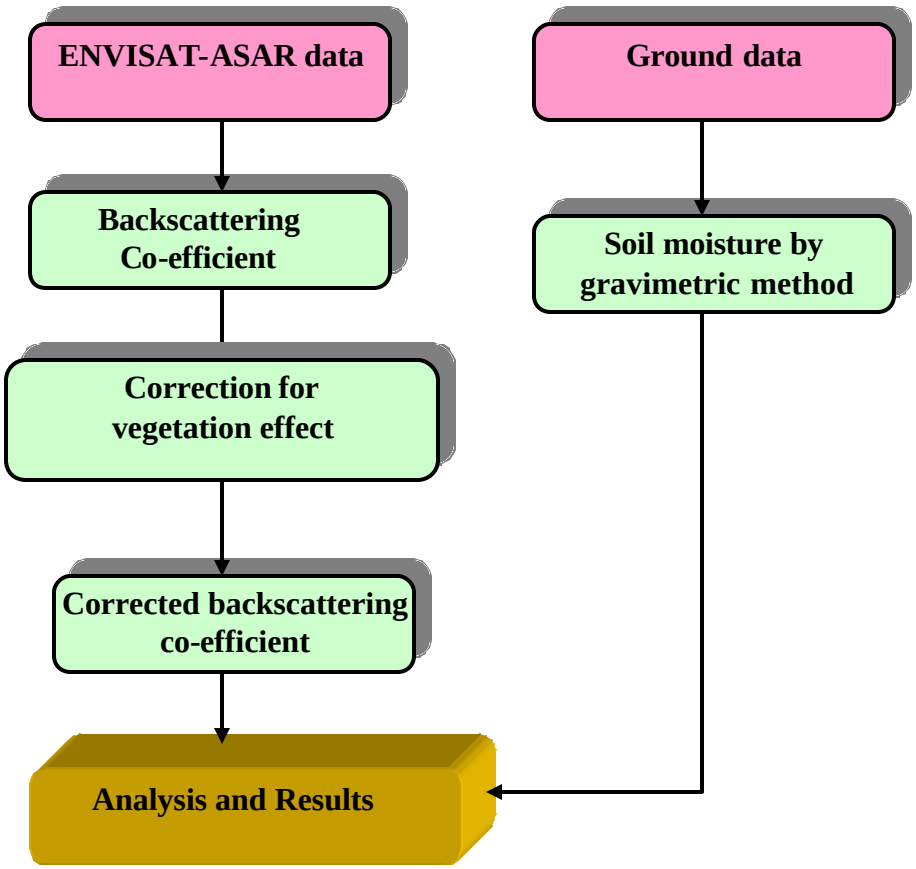

Flow Chart 5.2: Flowchart depicting the methodology used for microwave data

Derivation of backscattering co-efficient

The backscattering coefficients can be obtained using the formula:

$$s\,0 = \frac{A^2}{K} * \frac{1}{(G^2 q_d)} * (\frac{R_d}{R_{ref}})^2 * \sin(a_d)$$

K- absolute calibration constant
A^2- average pixel intensity
s °- distributed target sigma naught
$G^2(?_d)$- two-way antenna gain at the distributed target look angle
R_d- distributed target slant range distance
R_{ref}- reference slant range distance (800km for all beams and modes)
a_d- distributed target incidence angle

There is a group of PCI modules available to convert distributed RADARSAT and ASAR digital image data to radar brightness and calibrated radar backscatter. The following chart illustrates the sequence of module to calculate the backscatter coefficient.

CDASAR(read ASAR data)

|

SARSIGM (backscatter coefficient)

For backscatter coefficient the formula used in the software is

$$s_{ij} = 10\log_{10}(\frac{DN^2 + A_0}{A_j}) + 10 * \log_{10}(\sin I_j)$$

Where:
s_{ij} - output backscatter coefficient for scan line i, pixel j.
$\log_{10}$ ( ) - logarithm base 10 function.
DN - input image value for scan line i, pixel j.
A_0 - gain offset from the first member of A0SEG.
A_j - expanded gain scaling table value for column j.
sin ( ) - sine trigonometric function.
I_j - expanded incident angle table value for column j.

Thus the header information of ASAR data was read using CDASAR modeler. Thus we will be obtaining incidence angle file, orbital ephemeris file, offset and gain file. These files are used to obtain backscattering coefficient SARSIGM modeler. The backscatter image was obtained for both HH and HV polarization respectively for the study area. The image was re-projected to Albers equal area projection. Thus the

backscattering coefficients obtained and soil moisture content obtained by gravimetric method are used to establish a relationship.

Vegetation Correction

A simple water cloud model has been used to correct the backscattering coefficient for vegetation. Water-cloud model are commonly used to interpret radar data in terms of soil and vegetation variables (Attema and Ulaby, 1978,Mo et.al., 1984): they involve bulk variables such as surface soil moisture and vegetation biomass and the number of parameters to fit is low. Thus they can easily be inverted if several radar configurations are available. The radar cross-section of the canopy s^o is expressed as the incoherent sum of the contribution of the vegetation layer s^o_{veg} and the contribution of the soil layer s^o_{soil}, the latter being attenuated through the vegetation. For an incidence angle ?, we can write:

$$\textit{Whole canopy}: \mathbf{s^o = s^o_{veg} + t^2 s^o_{soil}}$$

$$\textit{Vegetation} : \mathbf{s^o_{veg} = Acos? (1-t^2)}$$

$$\mathbf{t^2 = exp(-2Bm_v/cos?)}$$

where s^o is the backscattering co-efficient, t^2 is the two-way attenuation through the vegetation, and m_v is the water content of the canopy(kg/m^2), which is equal to the product of the volumetric water content times the height of the canopy. For a given radar configuration, the soil contribution is usually expressed as a linear function of its surface soil moisture content m_s:

$$\mathbf{s^o_{soil} = C+Dm_s}$$

Only four parameters are needed, A and B for vegetation and C and D for soil. The parameter A corresponds to the albedo of the vegetation and B is an attenuation factor. The parameter D is the sensitivity of the signal to soil moisture and C can be considered as a calibration constant. These parameters have to be fitted for each radar configuration.

Due to the limitation in the availability of different configuration of ASAR data over the study area these parameters are taken from the literature. The constant C and D are taken as -13.92 and 0.195 from the literature for similar configuration (Zribi et.al, 2007;Taconet et.al, 1996; Prevot et.al, 1993; Bagdadi et.al., 2006).

5.2.4 MIKE SHE: Hydrological Modeling

Translating the entire physical system in to one that can be modeled numerically is very important part of the hydrologic modeling process. The conceptualization of an integrated hydrological model includes the main processes and storage components of the hydrologic cycle. This section outlines the MIKE SHE setup and discusses initial model parameter selection. The methodology followed is as shown in the flowchart 5.3.

Boundary

The boundary of the watershed was digitized and was given input as a shapefile to the model. The model itself converts shapefile in to grid format. Grid cells outside the model domain were assigned a value of 0. Grid cells inside the model domain were assigned a value of 1 and cells on the model boundary were assigned a value of 2. The pre-processed boundary is as shown in the Figure 5.5. A grid size of 200m was chosen for the simulation after several preliminary runs. The results obtained at larger grid size such as 1000m and 500m were not satisfactory.

Topography

Land elevation data of the study area was obtained from generating a digital elevation model using CARTOSAT 1 data (Source: PRSD,IIRS). Two scenes DEM were generated with an RMS error of 0.6787- 0.936 pixel. Accuracy of DEM was about 5-10m. The DEM is as shown in the Figure 5.6. The digital format was converted to ASCII format as an input to the model.

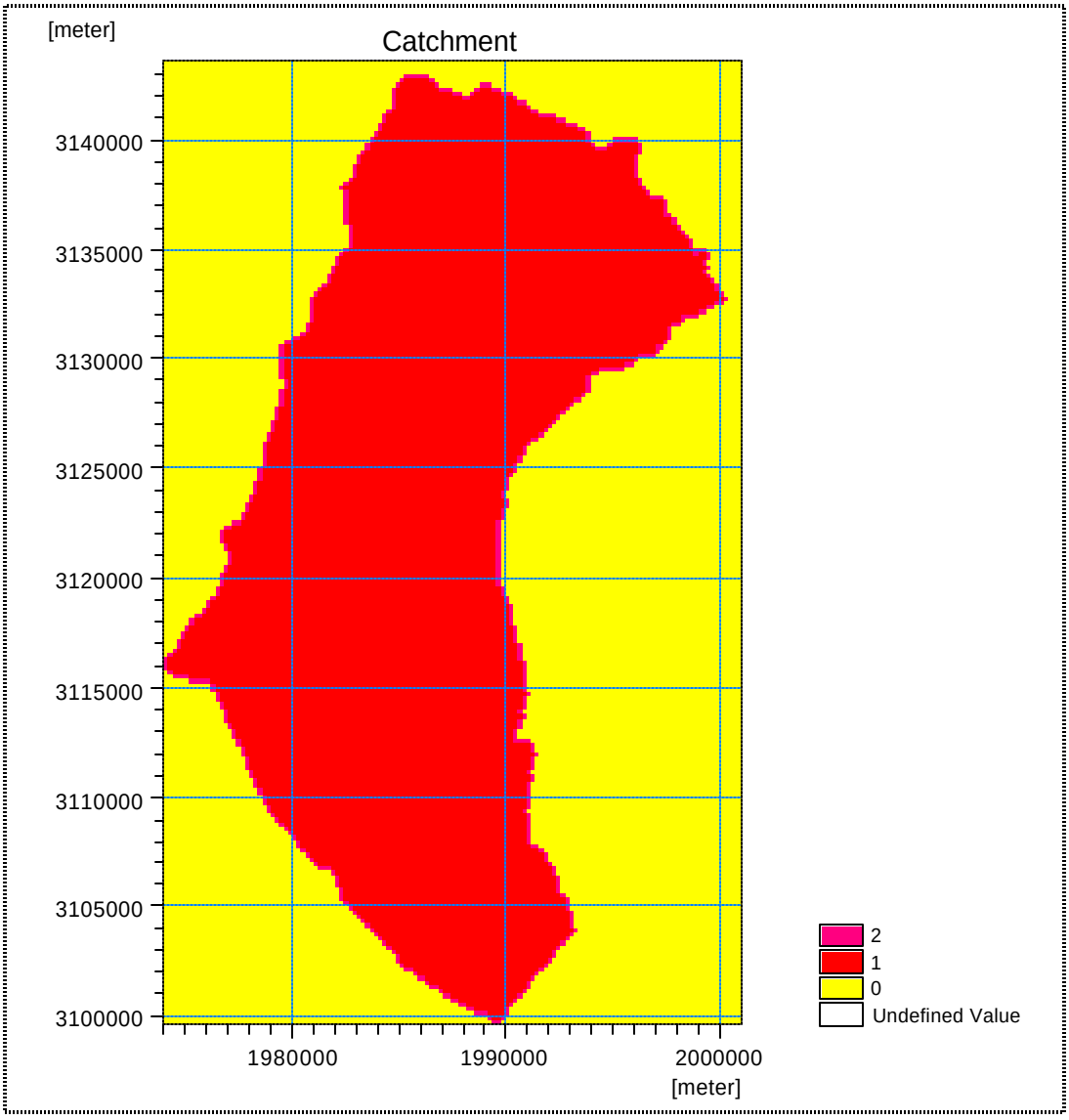

Figure 5.5: The MIKE SHE processed boundary of Solani Watershed

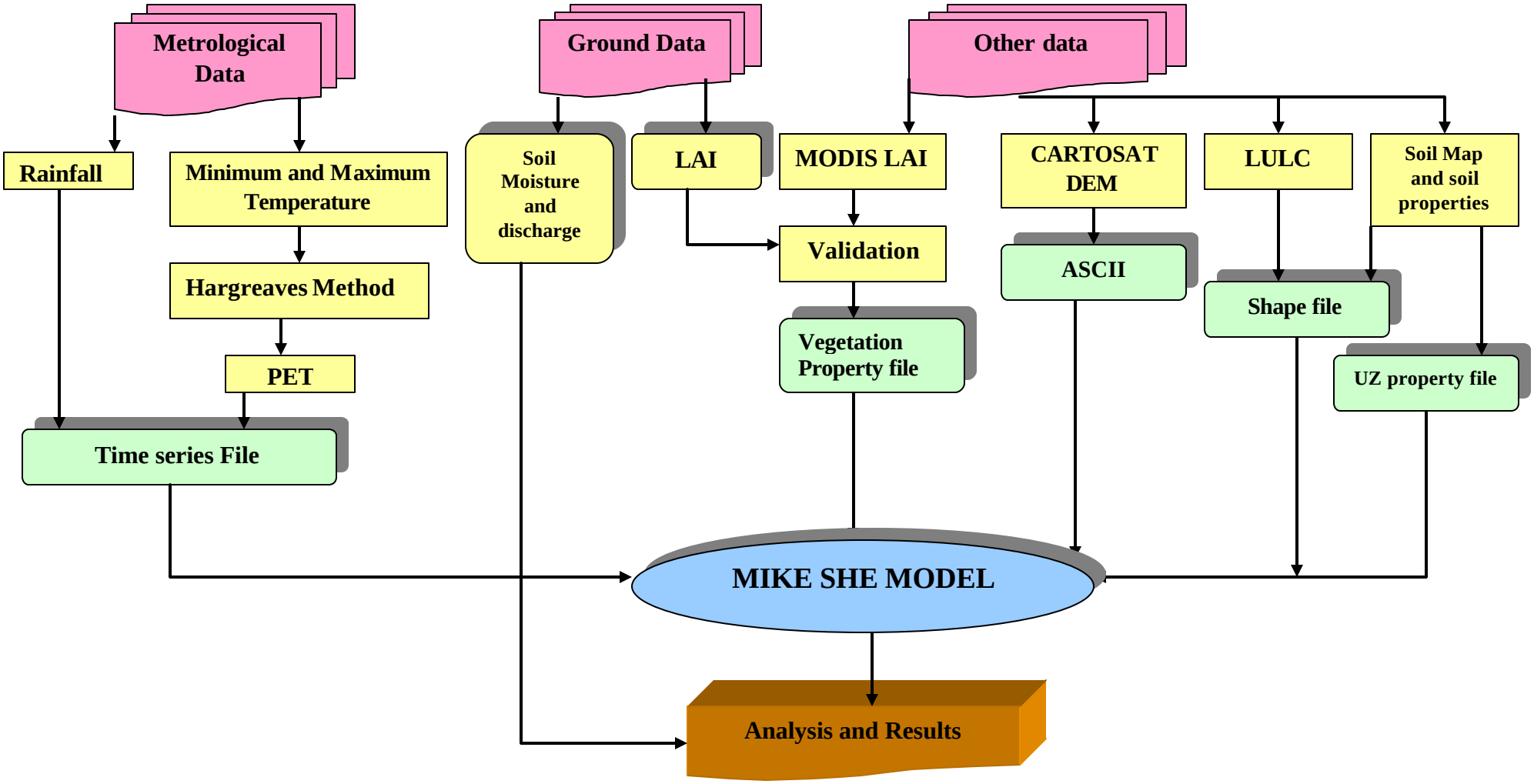

Flow Chart 5.3 Flow chart depicting methodology used for MIKE SHE

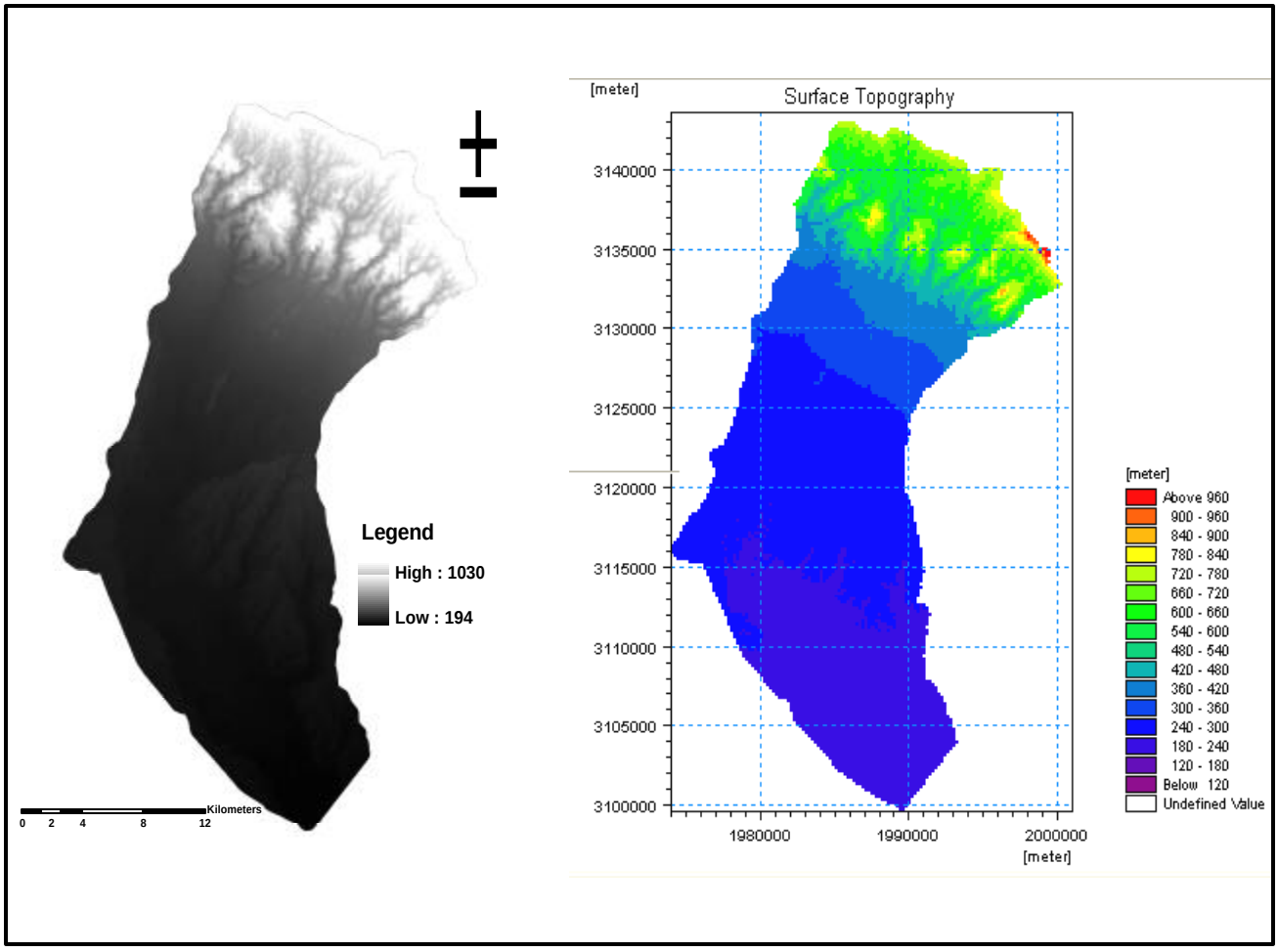

Figure 5.6 CARTOSAT DEM and DEM processed by MIKE SHE of Solani Watershed

Precipitation and Potential Evapotranspiration

Daily rainfall data were obtained from three stations present in the watershed. To account for the spatial distribution of rainfall, Thiessen polygons were delimitated for the watershed Figure 5.7. The weightage factors for different stations are as follows: AWS- 44%, Muzzafarabad- 15% and NIH- 41%. Time series file was used to define the temporal distribution in MIKE SHE for each station.

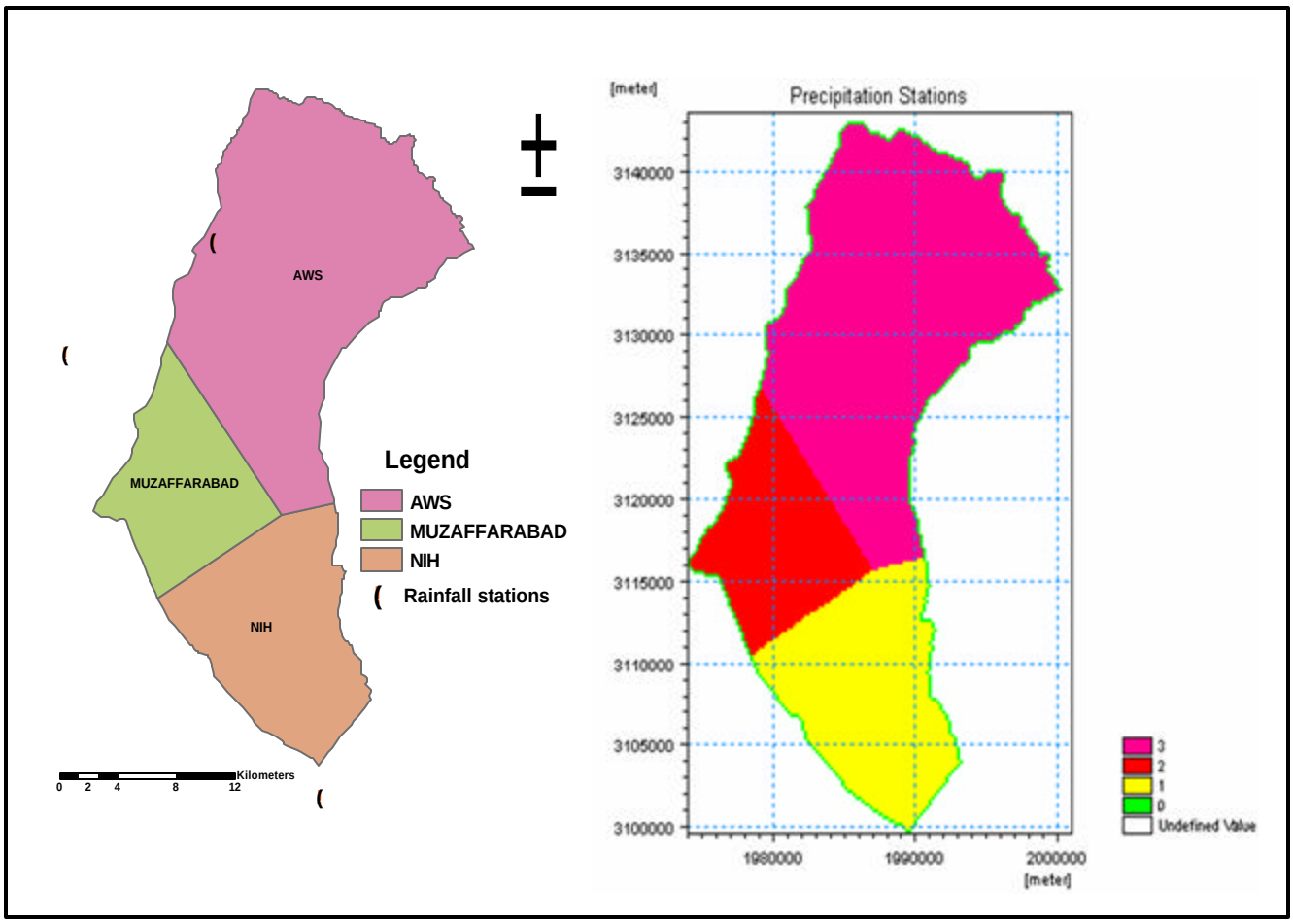

Figure 5.7Thiessen Polygons for the metrological stations in Solani Watershed

PET calculation

Estimates of potential evapotranspiration (ET_o) for the same locations of the rainfall stations were estimated using Hargreaves and Samani equation. Those estimates were implemented in the numerical model with the spatial distribution of the Thiessen polygons along with time series file for defining temporal distribution. Daily reference evapotranspiration ($_o ET$) was estimated using the method of Hargreaves and Samani (1985)

$$ET_0 = 0.0023 * R_a * (\Delta T + 17.8) * \sqrt{T_{\max} - T_{\min}}$$

ET0- daily reference potential evapotranspiration
Ra- extraterrestrial radiation (mm)
? T-average daily air temperature (°C)

Tmax- average daily maximum temperature (°C)
Tmin- average daily minimum temperature (°C)

Land use and Vegetation property

Land use / land cover map generated using FAO classified of ASTER data was obtained from Agriculture and soils division, IIRS(Figure 5.8). The shape file was used to give as an input to the MIKE SHE. The vegetation properties such as leaf area index, rooting depth and crop coefficients were defined in a vegetation property file in MIKE SHE for different land cover classes.

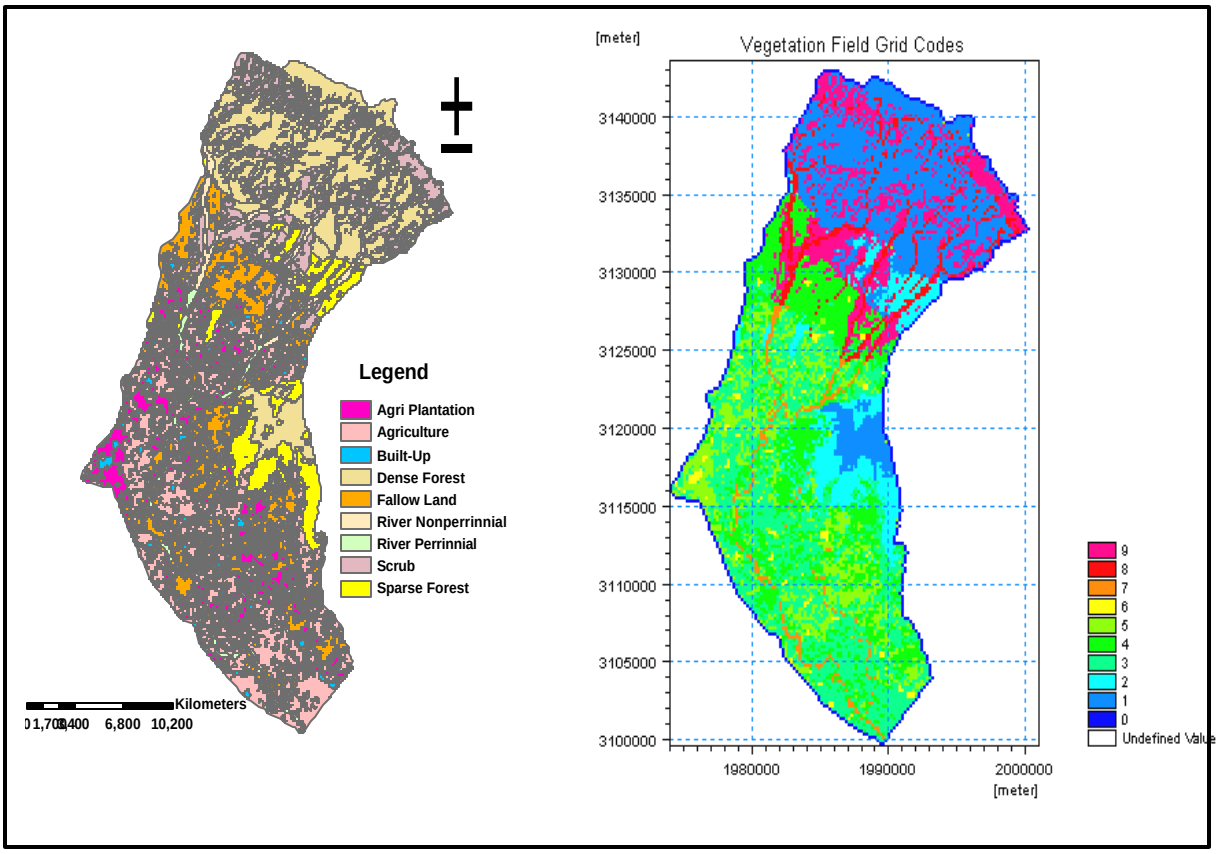

Figure 5.8 Land Use and Land Cover map of Solani Watershed (Source: ASD, IIRS)

LAI

MODIS LAI product at 1km resolution was downloaded and was preprocessed using ERDAS. MODIS LAI was validated for agricultural fields. Continuous field observations were made at various locations (Figure 5.9) using LAI 2000. To cover a 1 km pixel of MODIS

nearly an average of 10 field observations were taken. Eight observations were taken in each field to get an average LAI of the field. The validation period was in last week of August 2007. The relationship obtained was satisfactory and hence MODIS LAI data was used to give as an input to MIKE SHE. The relationship is as shown in the Figure 5.10. . LAI for agriculture taken from MODIS data as an input to MIKE SHE is as shown in the Figure 5.11.

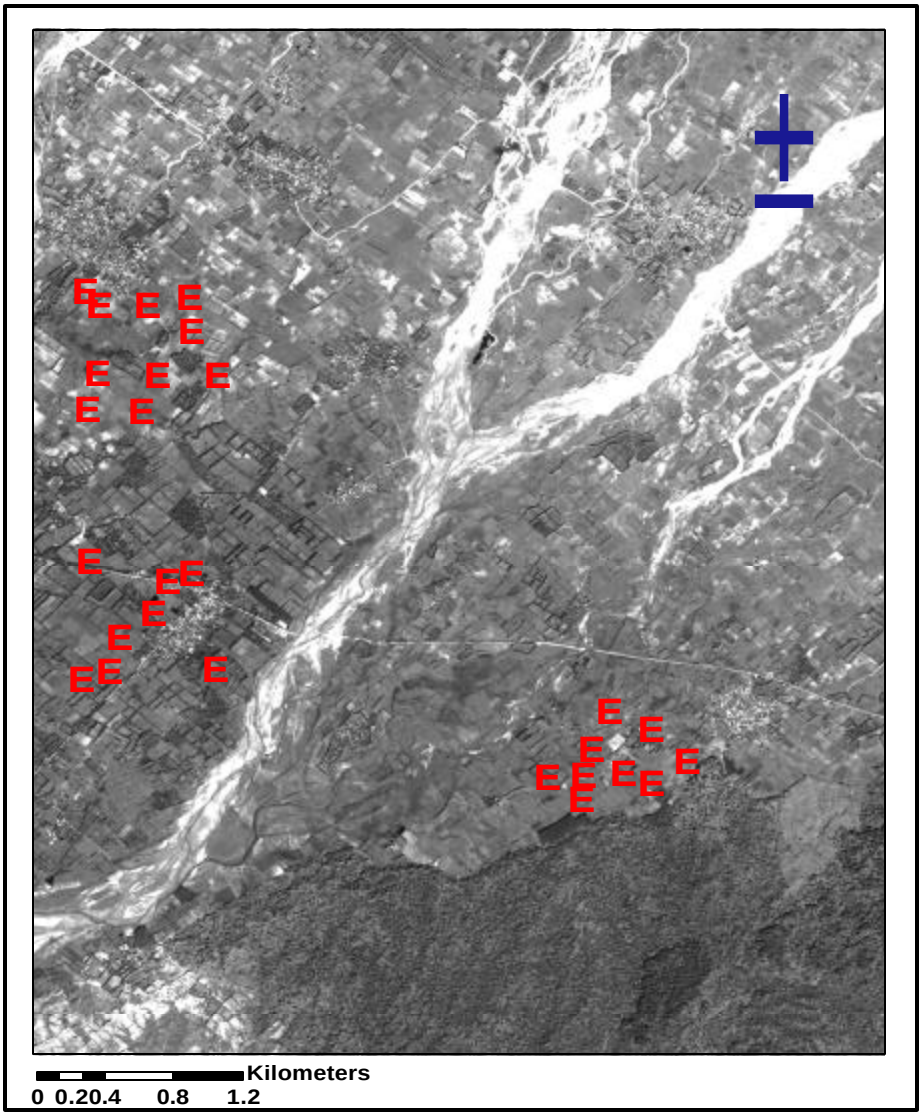

Figure 5.9LAI Field Observed Points on CARTOSAT 1 dated 2nd October 2006

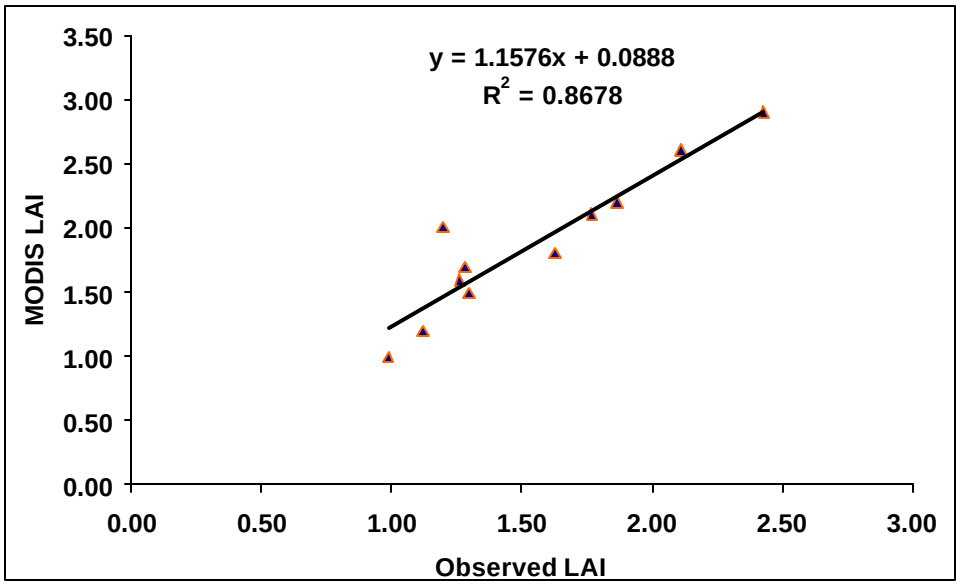

Figure 5.10Relationship between Observed LAI and MODIS LAI

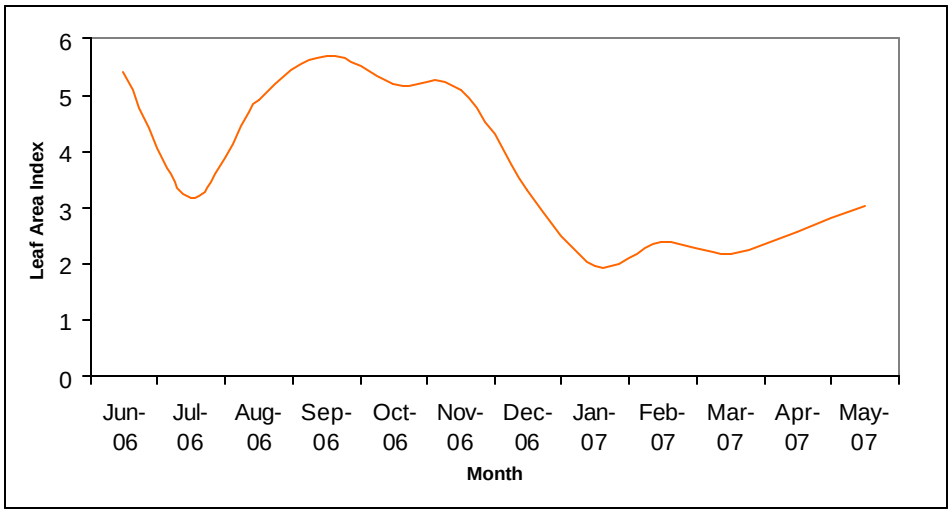

Figure 5.11LAI variation for Dense Forest in Solani Watershed

Manning's Number

The approach proposed for modeling overland flow in the study requires the specification of a roughness coefficient which represents the water flow resistance over different surfaces. Manning's M is defined as the reciprocal of Manning's n, commonly used in the literature. Manning's number for the whole coefficient was assumed to be same for the

whole watershed. It was taken as 5 m^(1/3)/s. The initial water depths and detention storage was taken as 0mm uniformly over the watershed as the watershed has high slope and thus it has been assumed that all the water in the upper catchment drains to the outlet.

Vadose Zone

Soil map for the watershed was obtained from agriculture and soils division, IIRS. The map was reclassified in to six classes as shown in the Figure 5.12. The texture information of the soils was obtained from National Institute of Hydrology, Roorkee. Texture information up to a depth of 1m was obtained. Based on this the vertical profile was defined. The infiltration rate equals the saturated hydraulic conductivity for the method used in the numerical model to account for the vadose zone (DHI, 2005, p.277). The values used are given in the Table 5.9.

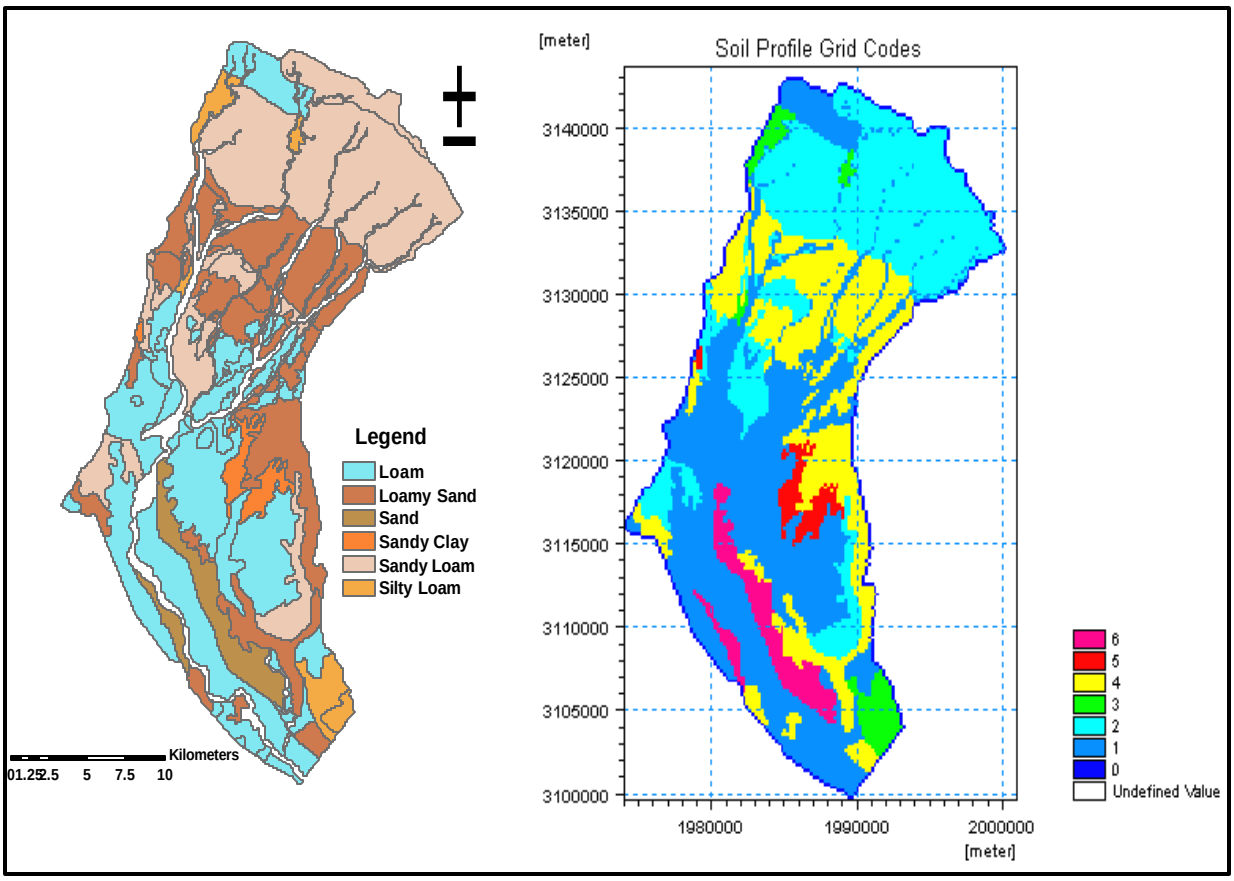

Figure 5.12 Soil Map of Solani Watershed

Table 5.9 Soil parameter before Calibration of MIKE SHE for soil moisture

Soil Texture	K_s (m/s)	$?_s$	$?_r$	a
Loamy Sand	5.98x10-6	0.437	0.035	0.067
Sand	6x10-5	0.337	0.02	0.067
Loam	1.32x10-6	0.463	0.027	0.067
Sandy Loam	2.18x10-5	0.453	0.041	0.067
Sandy Clay	1.2x10-7	0.480	0.109	0.067
Silty Loam	6.8x10-6	0.501	0.0150	0.067

Model Calibration

Model parameters represent the physical or hydrologic characteristic of a watershed (Singh, 1995). To adequately represent the system being modeled, during calibration, an iterative process, model parameters are set within an appropriate range. During this process, each model parameter is varied following a trial and error procedure, with all other parameters being constant. Formal sensitivity analysis was not performed during this study, due to the model's high computational time. Nevertheless, it was found during the calibration process that saturated hydraulic conductivity and Manning's M was the sensitive model input.

The model was calibrated for soil moisture in the vadose zone. As mentioned by Refsgaard and Storm (1995), ? the number of parameters subjected to adjustment during calibration process of a distributed hydrological model like MIKE SHE should be as small as possible. However, given the inability to fully characterize all hydrological processes and the possible difference in scale between the measurement and the model grid square, slight calibration is generally required. Consequently, the model was calibrated by adjusting the saturated hydraulic conductivity and saturated soil moisture content for one year (for hydrologic year 2006-2007).

Model Performance

In addition to qualitative assessment with graphical displays, the model simulation results were evaluated quantitatively using statistical measures. Statistical parameters such as mean deviation, root mean square error and Nash-Sutcliffe coefficient were used. The *root mean square error (RMSE)* measures the difference between predicted and observed values. It is sensitive to the extreme values and deals with both systematic and random errors.

$$RMSE = \sqrt{\frac{\sum_{i=1}^{n} (Q_i - P_i)^2}{n}}$$

where Q_i is the observed reading and P_i is the predicted reading.

The *Nash-Sutcliffe model efficiency coefficient* is used to assess the predictive power of hydrological models. It is defined as:

$$E = 1 - \frac{\sum_{t=1}^{T} (Q_o^t - Q_m^t)^2}{\sum_{t=1}^{T} \left(Q_o^t - \overline{Q_o}\right)^2}$$

where Q_o is observed discharge, and Q_m is modeled discharge. Q_t is discharge at time t.

Nash-Sutcliffe efficiencies can range from -8 to 1. An efficiency of 1 (E=1) corresponds to a perfect match of modeled discharge to the observed data. An efficiency of 0 (E=0) indicates that the model predictions are as accurate as the mean of the observed data, whereas an efficiency less than zero (-8<E<0) occurs when the observed mean is a better predictor than the model.

The MIKE SHE model was used to evaluate soil moisture profiles spatially and temporally. The discharge at the outlet was also evaluated. Main emphasis is given for soil moisture simulated.

5.2.5. STASTICAL ANALYSIS OF THE SPATIAL DISTRIBUTION MAP OF SOIL MOISTURE

Association refers to coefficients which gauge the strength of s relationship. Stastical analysis was done to know the accuracy of the map obtained. The ground observed data was interpolated to get the spatial distribution map using spline method of interpolation. The

observed map thus obtained was also divided in to four classes as well watered vegetated areas, wet areas, sparsely watered vegetated areas and dry areas. The spatial maps were crossed and the number of image. pixels in each combination were tabulated and output along with a stastcal measure of association between the images, namely Cramer's V, a correlation coefficient indicating the strength of the association was found. Cramer's V may be defined as follows:

Suppose X and Yare two categorical variables that are to be analyzed in a some experimental or observational data with the following information:

- X has M distinct categories or classes, labeled X_1,…….X_M,
- Y has N distinct categories, labeled Y_1,……., Y_N,
- n pairs of observations (x_k, y_k) are taken, where x_i belongs to one of the M categories in X and y_i belongs to one of the N categories in Y.

Form a M X N contingency table such that Cell (i, j) contains the count n_{ij} of occurrences of Category X_i in X and Category Y_j in Y :

$X\backslash Y$	Y_1	Y_2	...	Y_N
X_1	n_{11}	n_{12}	...	n_{1N}
X_2	n_{21}	n_{22}	...	n_{2N}
⋮	⋮	⋮	⋱	⋮
X_M	n_{M1}	n_{M2}	...	n_{MN}

Note that $n = \sum nij$.

Definition. Suppose that the null hypothesis is that X and Y are independent random variables. Based on the table and the null hypothesis, the chi-squared statistic X^2 can be computed. Then, *Cramer's V* is defined to be

$$V = V(X,Y) = \sqrt{\frac{\chi^2}{n \min(M-1, N-1)}}.$$

The closer V is to 0, the smaller the association between the categorical variables X and Y. On the other hand, V being close to 1 is an indication of a strong association between X and Y. If X=Y, then V(X,Y)=1.

Kappa Statistic

The k$\hat{k}$ (KHAT) statistic is a measure of the difference between the actual agreement between reference data and an automated classifier and the chance agreement between the reference data and a random classifier. It can be defined as

$$\hat{k} = \frac{observedaccuracy - chanceagrrement}{1 - chanceagreement}$$

This statistic serves as an indicator of the extent to which the percentage correct values of an error matrix are due to true agreement versus chance agreement. In reality, $\hat{k}$ usually ranges between 0 and 1.

6. RESULTS AND DISCUSSIONS

The present study attempted to assess the soil moisture in a watershed of 539 km^2 using different approaches: Remote sensing and Hydrologic modeling (MIKE SHE). The knowledge of soil moisture variation spatially and temporally is useful for managing the watershed efficiently. Due to difficulty involved in obtaining in-situ soil moisture observations, effort are made to investigate sensitivity of optical, microwave and hydrologic model to assess soil moisture temporally and spatially. This chapter summarizes the results obtained in accordance with the objectives intended. The database creation and processing was done for the whole watershed and the analysis was done on specific sites where gypsum block observation was available. The sites used for the study with MIKE SHE grid is as given in the Table 6.1.

Table 6.1: Soil moisture observation points in the watershed with MIKE SHE grid numbers

Name	Latitude	Longitude	MIKE SHE GRID No.	
			x	y
Sisona	29º57'32.1"N	77º47'51"E	33	45
Alawalpur	30^{0}02'45.5"N	77^{0}57'32.1"E	21	91
Tanda Misri	30^{0}02'45.5"N	77^{0}57'32.1"E	45	128
Mohand	30^{0}10' 25.8"N	77^{0}53'52"E	81	165
AWS	30º11'00"N	77º49'00"E	42	168
Nagal MK	29º55'05.6"N	77º54'24.5"E	73	44

6.1. SOIL MOISTURE DATA FROM GYPSUM BLOCK

The pressure readings of gypsum block obtained at various observatory stations were converted to volumetric soil moisture values using curves defining the relationship between soil water content and soil water tension obtained by pressure plate apparatus from NIH, Roorkee (Appendix A). The readings thus obtained are presented below.

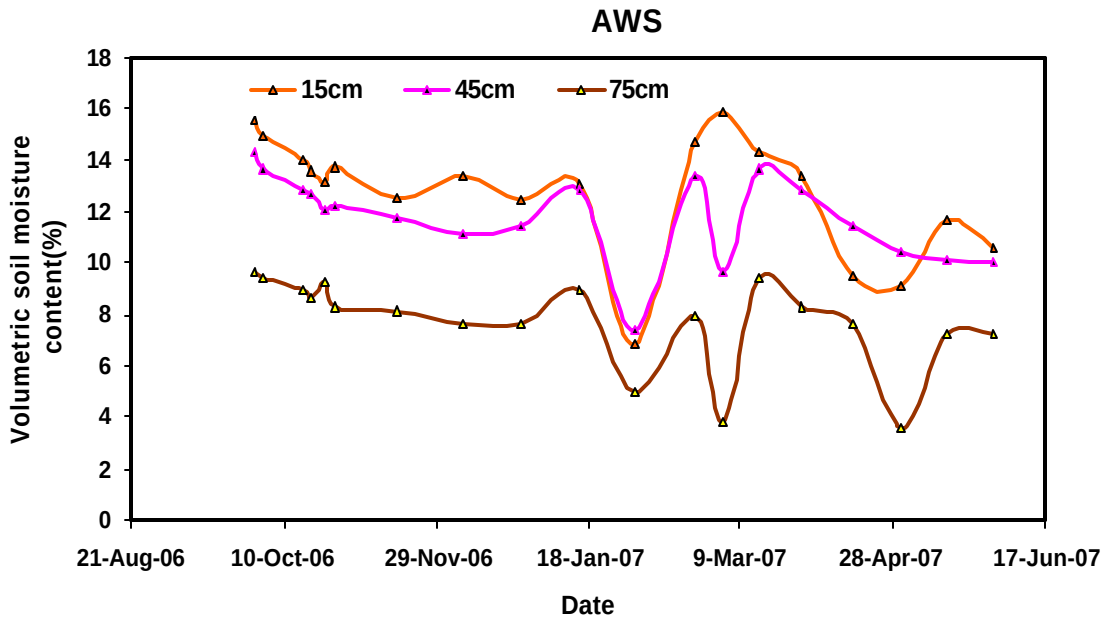

Figure 6.1 Variation of Soil moisture for 15, 45, 75 cm depths at AWS

It can be seen from the Figure 6.1 that the variation of soil moisture at depths 15cm and 45 cm are almost same as compared with the curve obtained at 75 cm depth. The trends of the curves are almost same in the months of October to December irrespective of the depths. There is fall in soil moisture in the month of February as the dry season begins. The land cover here is agriculture and the cultivation is mainly wheat, sugarcane, maize and groundnuts. The fields are rain fed and hence the soil moisture content decreases in dry season of the year. Also soil moisture at a depth of 75 cm has little variation.

The trend of soil moisture at Alawalpur (Figure 6.2) for depths 15 and 45 cm are almost same. As such there is no abrupt change in the moisture at these depths. Agriculture pre-dominates this area. Soil moisture content is more at a depth of 75 cm. There is a drop in the month of April as water is used by the crop to meet their demand since the period is dry.

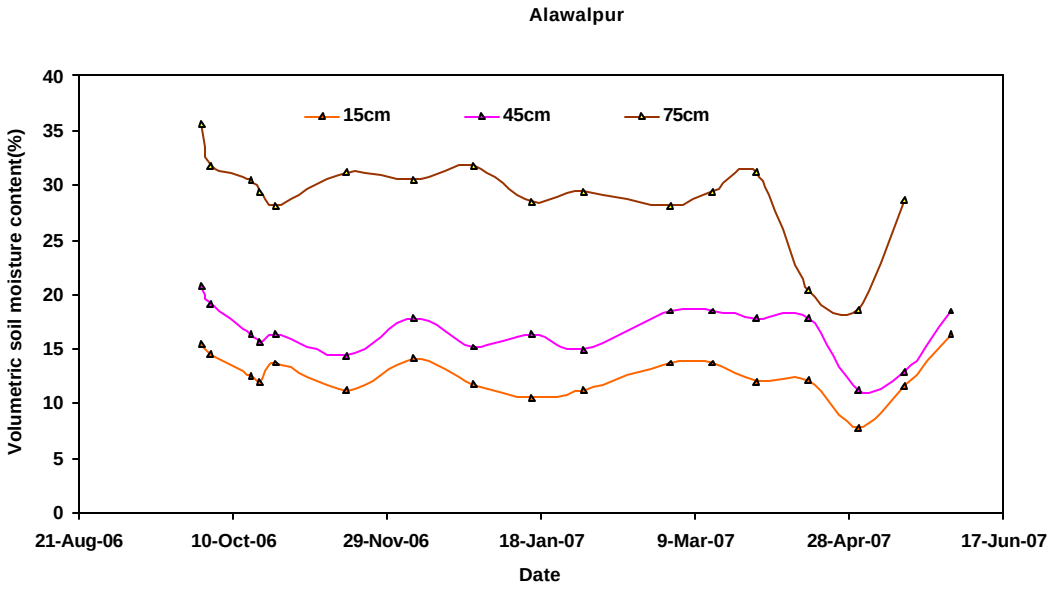

Figure 6.2 Variation of soil moisture for 15, 45, 75 cm depths at Alawalpur

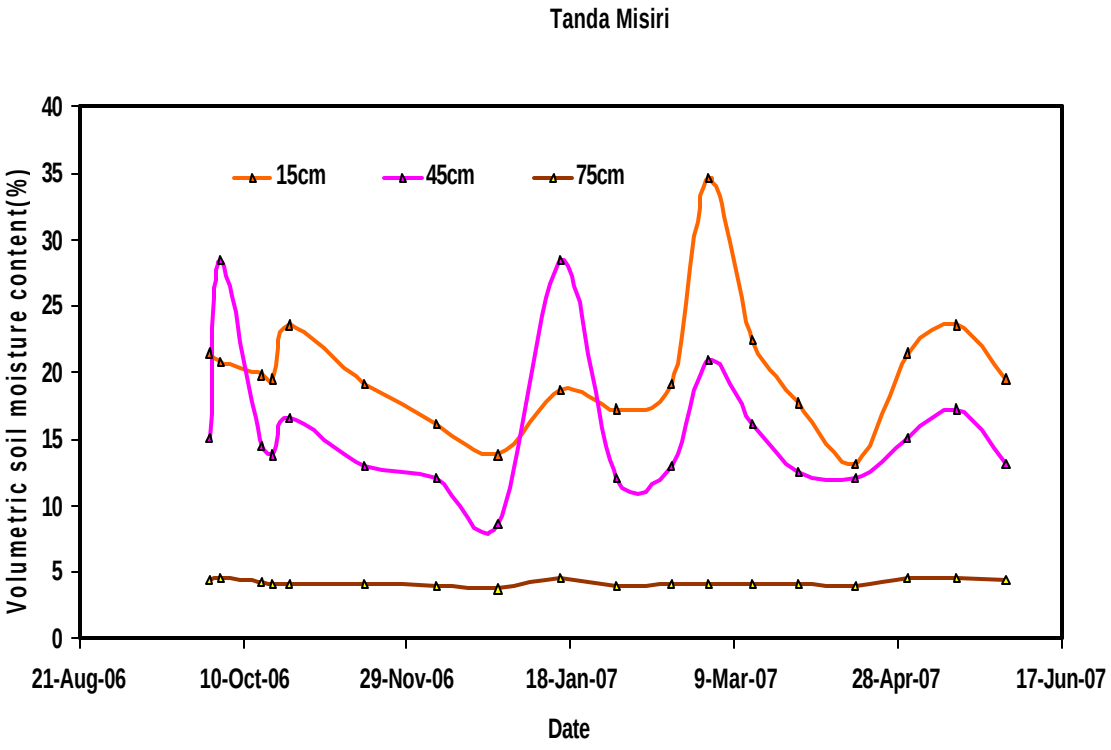

Figure 6.3 Variation of soil moisture for 15, 45, 75cm depths at Tanda Misiri

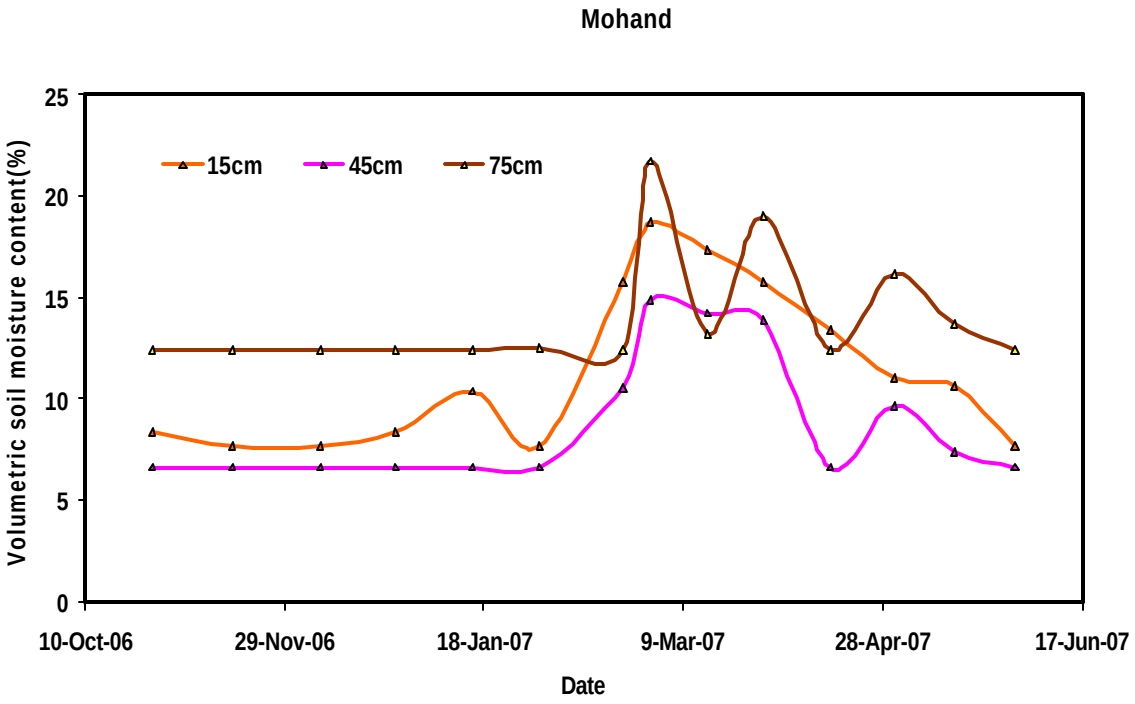

Figure 6.4Variation of soil moisture for 15, 45, 75 cm at Mohand

The trend of soil moisture variation at 15, 45 and 75 cm for Tandamisiri station is as shown in figure 6.3. Soil moisture significantly varies at 15 and 45cm depths but the variation is insignificant for a depth of 75cm. It remains almost same irrespective of the throughout the study period. The land use type at this station is agriculture and mainly cultivated by vegetables, sugarcane and maize.

Soil moisture trend at Mohand (Figure 6.4) remains same in the dry months (October to January). The variation of moisture is significant at the three depths. There is a change in the trend of soil moisture from February onwards. It increases drastically in the month of March for all the stations as observed in the graph. The reason for this increase was the hail storm that occurred on March 13th 2007 over the area.

Soil moisture at Sisona (Figure 6.6) for depths 45 and 75 cm vary insignificantly throughout the observation period. Soil moisture for a depth of 15cm decreases constantly and there is a sudden increase in the value in march. The area is quite dry throughout the year. The variation of soil moisture at Nagal MK is as shown in Figure 6.5. The moisture trend for the

depths does not vary significantly but in the month of april moisture value shoots up drastically.

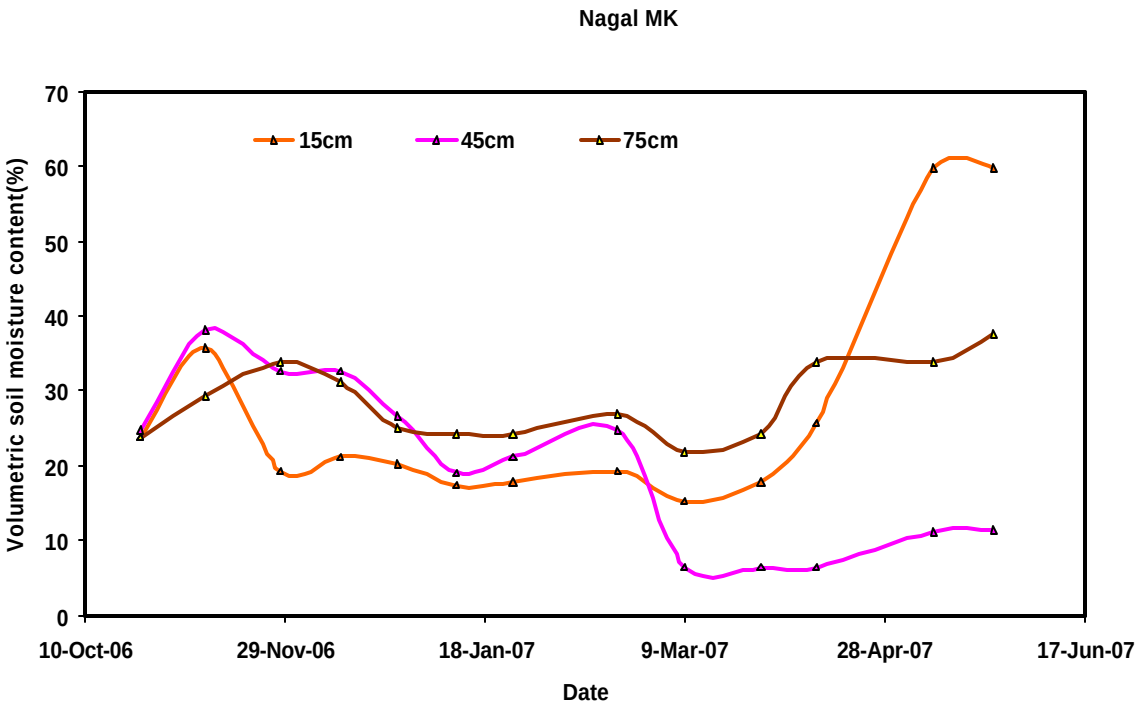

Figure 6.5 Variation of soil moisture for 15, 45, and 75cm depth at Nagal MK

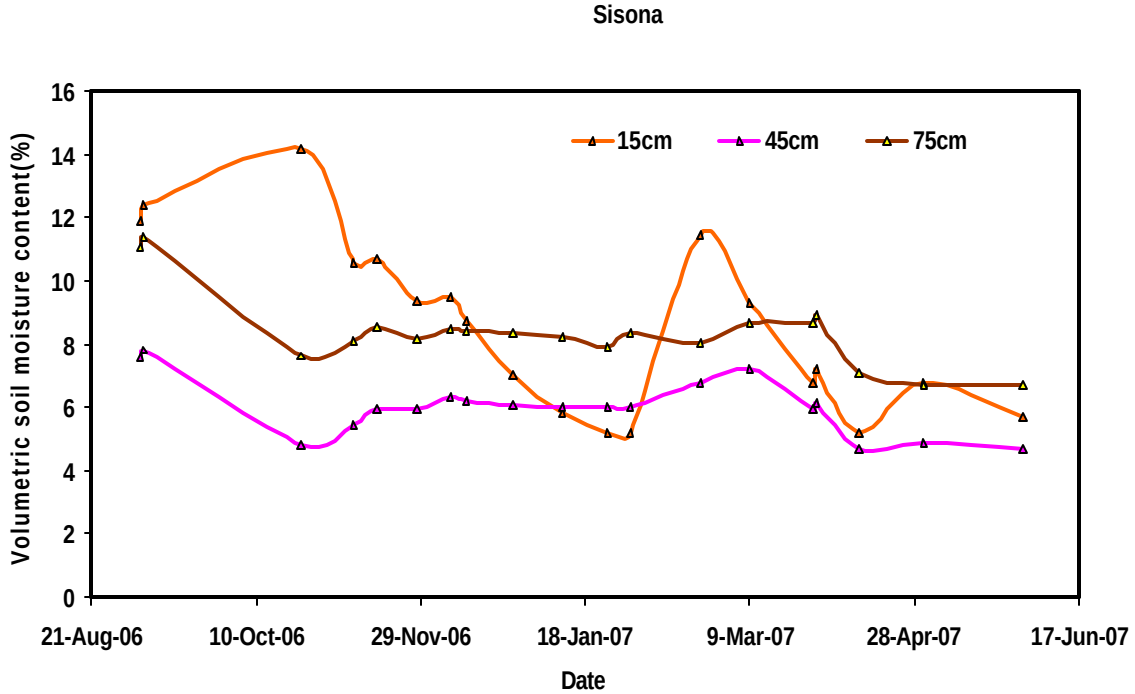

Figure 6.6Soil moisture variation for 15, 45 and 75cm depths at Sisona

6.2. THE OPTICAL REMOTE SENSING APPROACH

6.2.1. Soil Moisture Index

In the optical remote sensing approach, soil moisture index developed using shortwave infra-red data of LISS III (10th October 2006) and ASTER (1st November 2006) was used to estimate the distribution of soil moisture spatially for a depth of 15cm. Regression analysis was done between the index and the volumetric soil moisture content obtained from gypsum blocks. The graph obtained is as shown in the Figure 6.7 and 6.8. The co-efficient of correlation obtained was satisfactory for both the datasets. The value of the index obtained varied from -1 to 1. Higher the index higher is the soil moisture. The index map was divided in to four classes as well watered vegetated areas, wet areas, dry areas and sparsely watered vegetated areas. The division of the index map thus provided the spatial distribution of soil moisture in the watershed.

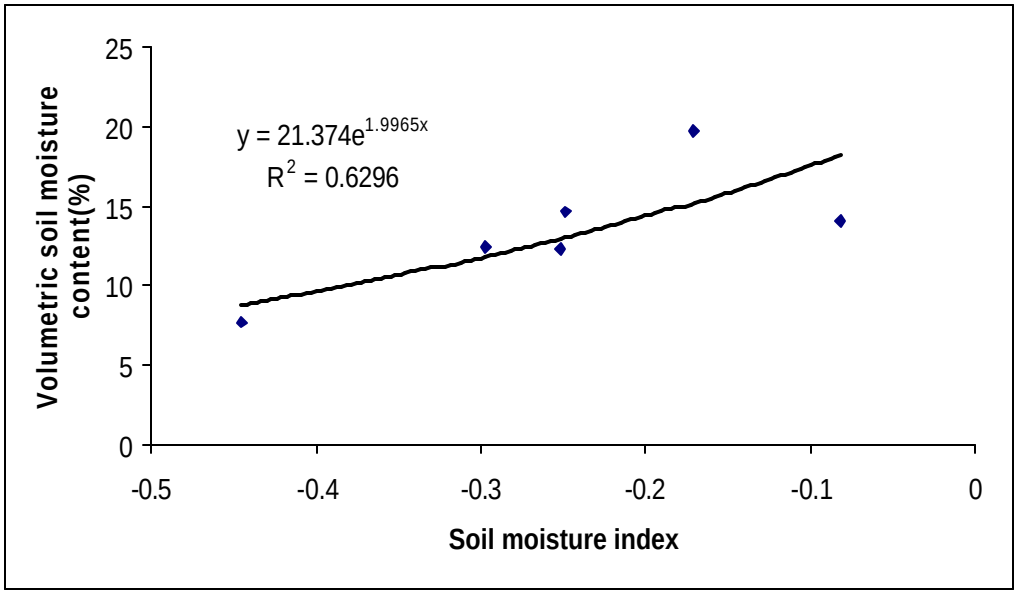

Figure 6.7Graph showing relationship between soil moisture index (LISSIII) and volumetric soil moisture content

The index and the spatial distribution map of the watershed are as shown in the figures 6.9 and 6.10. It can be seen from the map that upper part of the water has sufficient amount of soil moisture whereas lower part has dry areas also. The river bed is also depicted as a dry area. Some parts in the watershed are depicted as sparsely watered areas (lower part) as irrigation does not exist in all parts of watershed. Some areas are rain fed.

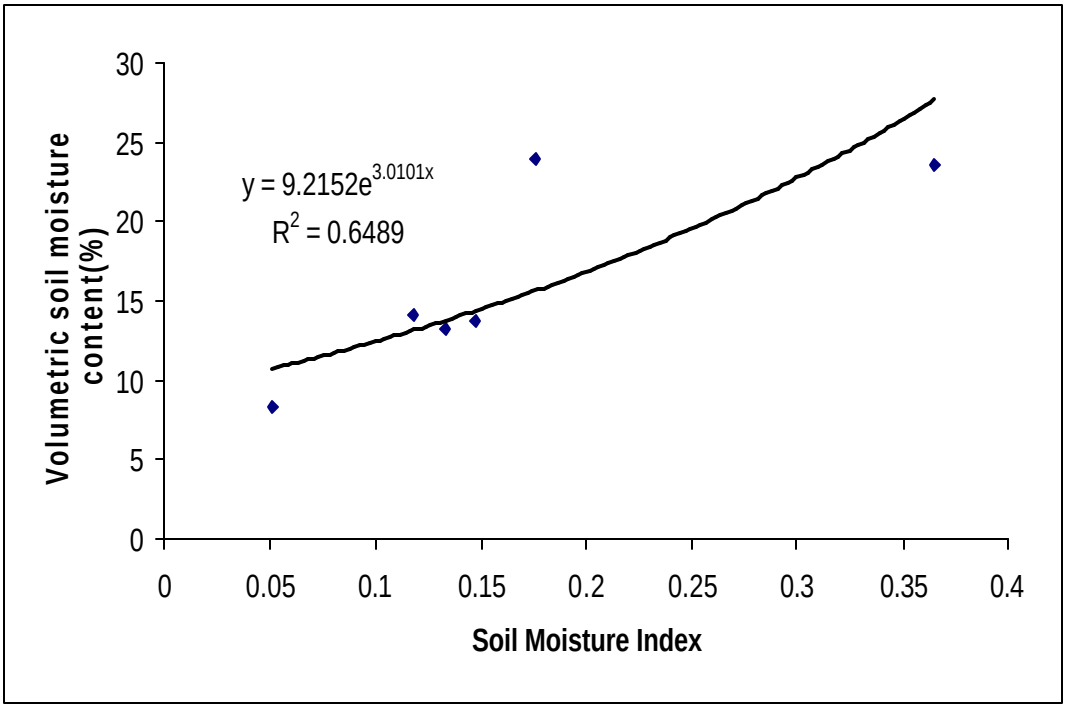

Figure 6.8Graph showing relationship between soil moisture index(ASTER) and volumetric soil moisture content

The index values were divided in to four classes based on the range of index values given in the table 6.2. The values of wet pixels such as river and dense forest cover were noted during the wet months and hence the range of values was decided.

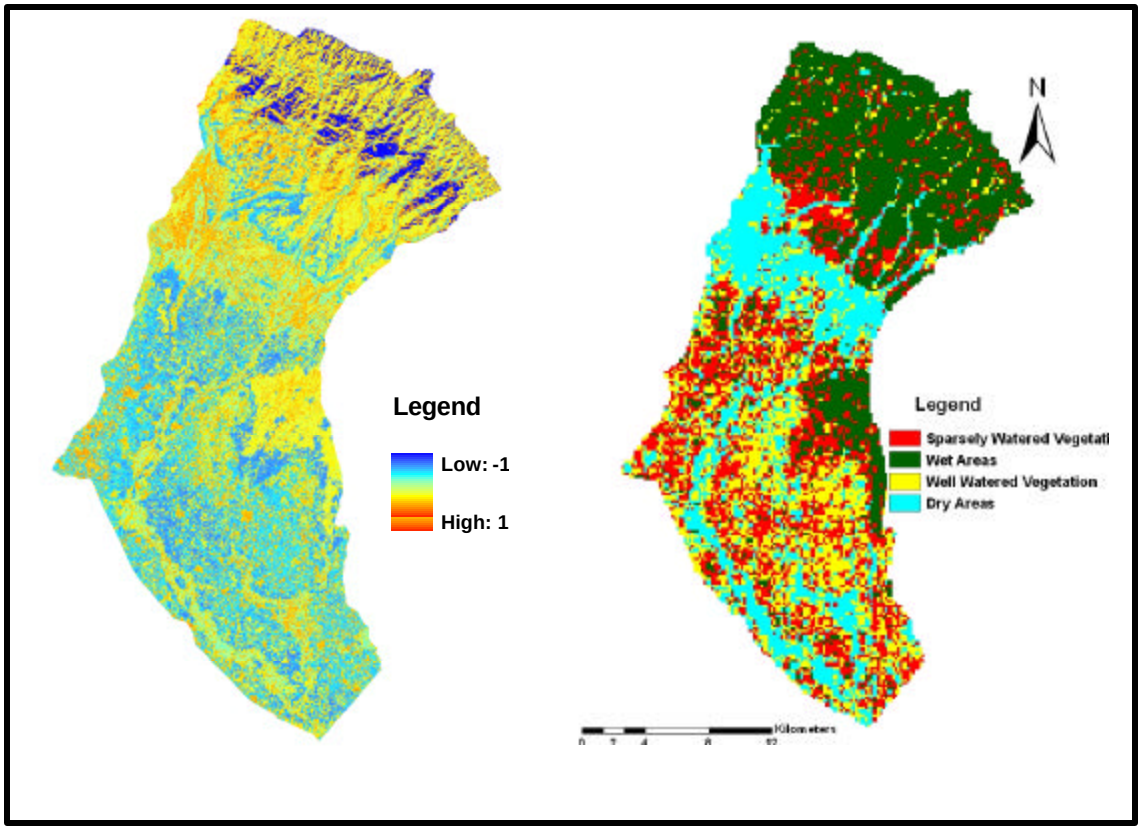

Figure 6.9Soil Moisture Index developed from LISS III dated 10th October 2006 and Spatial distribution map of soil moisture in the watershed

Table 6.2: Range of values of soil moisture index

Range of values	Classes
-1 to -0.32	Dry areas
-0.32 to 0.22	Sparsely watered vegetation
0.22 to 0.69	Well watered vegetation
0.69 to 1.0	Wet areas

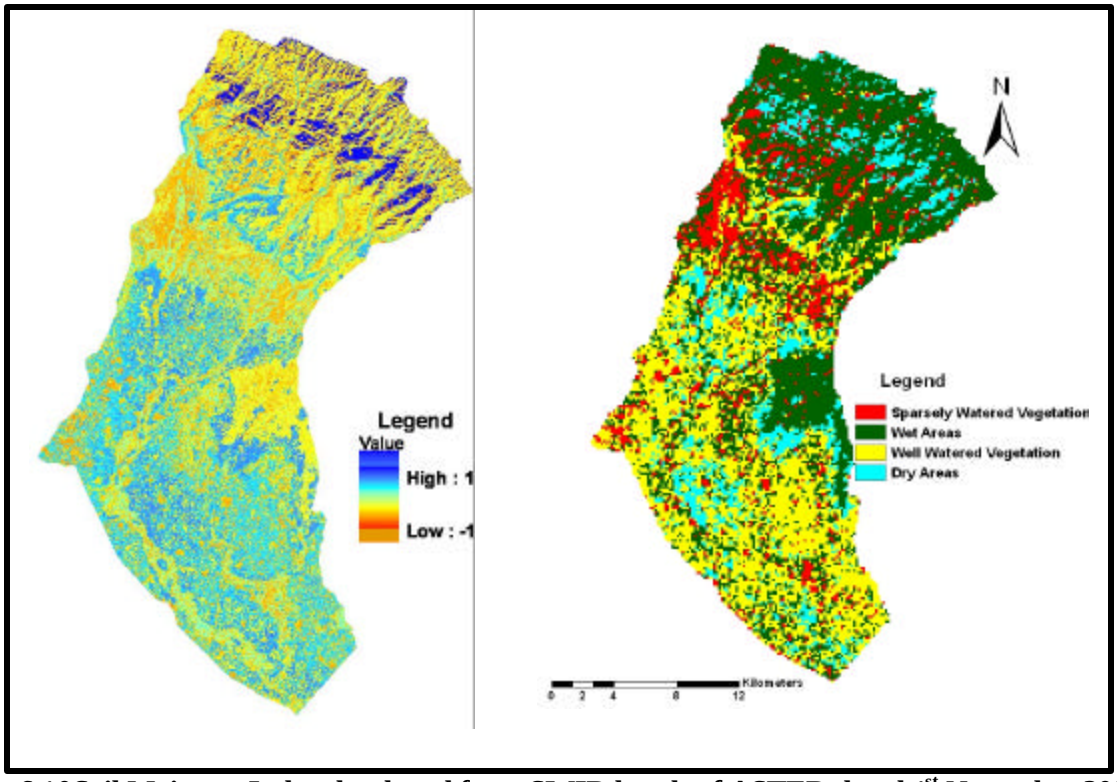

Figure 6.10 Soil Moisture Index developed from SWIR bands of ASTER dated 1st November 2006 and Spatial Distribution Map of Soil Moisture

Mapping of soil moisture is difficult as near-surface soil moisture changes more quickly than soil moisture at greater depths. The spatial distribution map as seen may contain some discrepancies or mixing because inferring general soil wetness is difficult from surface observations alone.

6.2.2. Water Deficit Index from NDVI - ? T_s relationships

An indirect approach for measuring the water status in soil is to measure the thermal infra-red energy emitted by the overlying canopy. Water deficit index (WDI) has been computed based on the NDVI - ? T_s space, 2D scatter plot relation for each pixel. The wet line and dry line pixels are subjected to linear regression equation and the derived equations are used for computation of WDI. Temperature difference (T_s-T_a) is the difference between land surface temperature and stations air temperature and NDVI images are used as an input parameter for WDI equations. WDI was computed on a fortnight basis from October 2006 to May 2007 using MODIS data and for ASTER data on 1st November 2006.

WDI from ASTER dated 1st November 2006

WDI from ASTER was calculated at a resolution 90m since the thermal bands are available at 90m spatial resolution. The plot between ?T and NDVI is as shown the Figure 6.11. The slope obtained from ?T-NDVI space relation for dry line is negative where as the slope obtained for wet line is positive. The negative slope implies that $?T_{max}$ decreases with increasing NDVI and positive slope implies that the $?T_{min}$ increases with increasing NDVI.

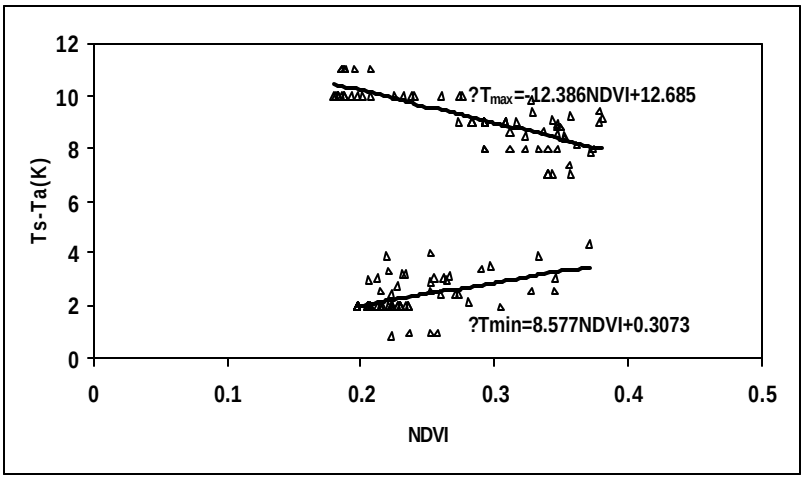

Figure 6.11The wet line and dry line from NDVI-?Ts space on 1st November 2006 using ASTER data

The equation obtained for dry line is $?T_{max}$=-12.386NDVI+12.685 with a R^2 of 0.60 and for wet line is $?T_{min}$=8.577NDVI+0.3073 with a R^2 of 0.341. The spatial distribution of soil moisture obtained after classifying the WDI is as shown in the figure 6.12.

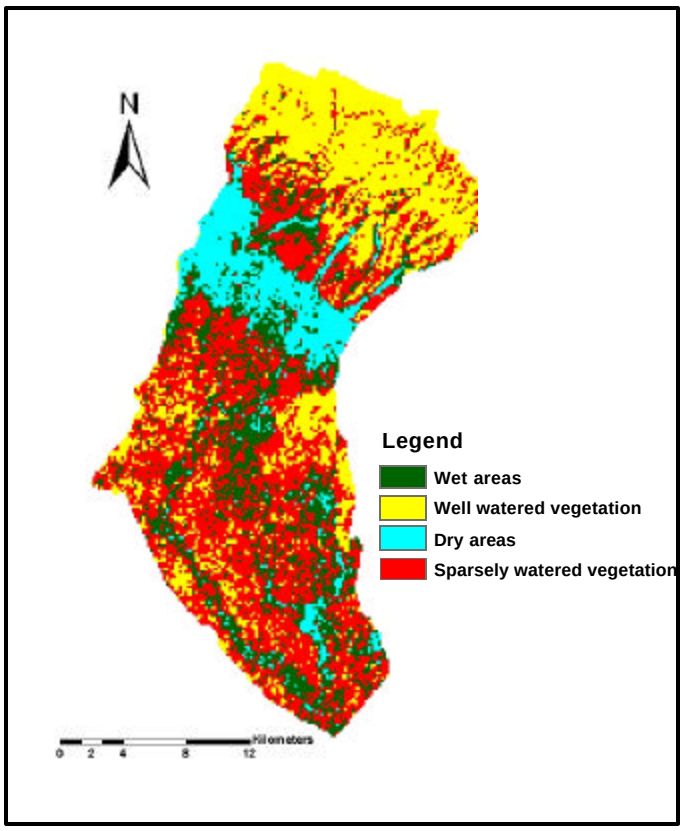

Figure 6.12Spatial pattern of soil moisture on 1st November 2006 derived from ASTER

WDI from MODIS temporal and spatial distribution

Similar methodology was followed to get the WDI using MODIS reflectance data and LST data. WDI has been obtained for those days for which in-situ soil moisture observations were available. The equations for dry and wet lines obtained are as given Table 6.3. Similar to ASTER, WDI from MODIS had 14 scatter plot based on NDVI - ?T_s space. The slope obtained for dry line is negative where as the slope obtained for wet line is positive.

Table 6.3:The wet line and dry line in NDVI-?T space estimated by linear regression on a fortnight basis from October 2006 to May 2007 for WDI

Date	Dry Line or Min ETR line	R^2	Wet Line or Max ETR line	R^2
16th Oct2006	-13.127NDVI+11.803	0.68	5.85NDVI+6.295	0.59
24th Oct 2006	-1.066NDVI+9.269	0.35	1.45NDVI+8.055	0.28
16th Nov 2006	-1.0323NDVI+1.277	0.32	0.947NDVI+1.25	0.21
8th Dec 2006	-14.695NDVI+13.393	0.73	4.44NDVI+3.635	0.43
1st Jan 2007	-20.109NDVI+10.476	0.67	9.379NDVI+20.24	0.33
15th Jan 2007	-12.25NDVI+21.398	0.58	15.945NDVI+15.09	0.55
1st Feb 2007	-0.746NDVI+3.145	0.25	0.864NDVI+0.605	0.14
18th Feb 2007	-3.748NDVI+14.51	0.49	8.963NDVI+10.599	0.46
1st Mar 2007	-4.892NDVI+4.258	0.67	0.243NDVI+0.268	0.70
15th Mar 2007	-10.259NDVI+16.40	0.58	11.039NDVI+12.97	0.62
29th Mar 2007	-6.721NDVI+10.86	0.36	13.215NDVI+10.773	0.54
15th Apr 2007	-17.105NDVI+2.19	0.73	8.756NDVI+2.341	0.54
1st May 2007	-15.832NDVI+3.28	0.68	11.741NDVI+15.69	0.45
16th May 2007	-17.151NDVI+19.60	0.62	9.557NDVI+15.509	0.58

The plots between ?T-NDVI for some of the days are as shown in the Figure 6.13. Similar plots were obtained for other days also. Thus WDI was computed for all fourteen days to get spatial pattern of soil moisture on those respective days.

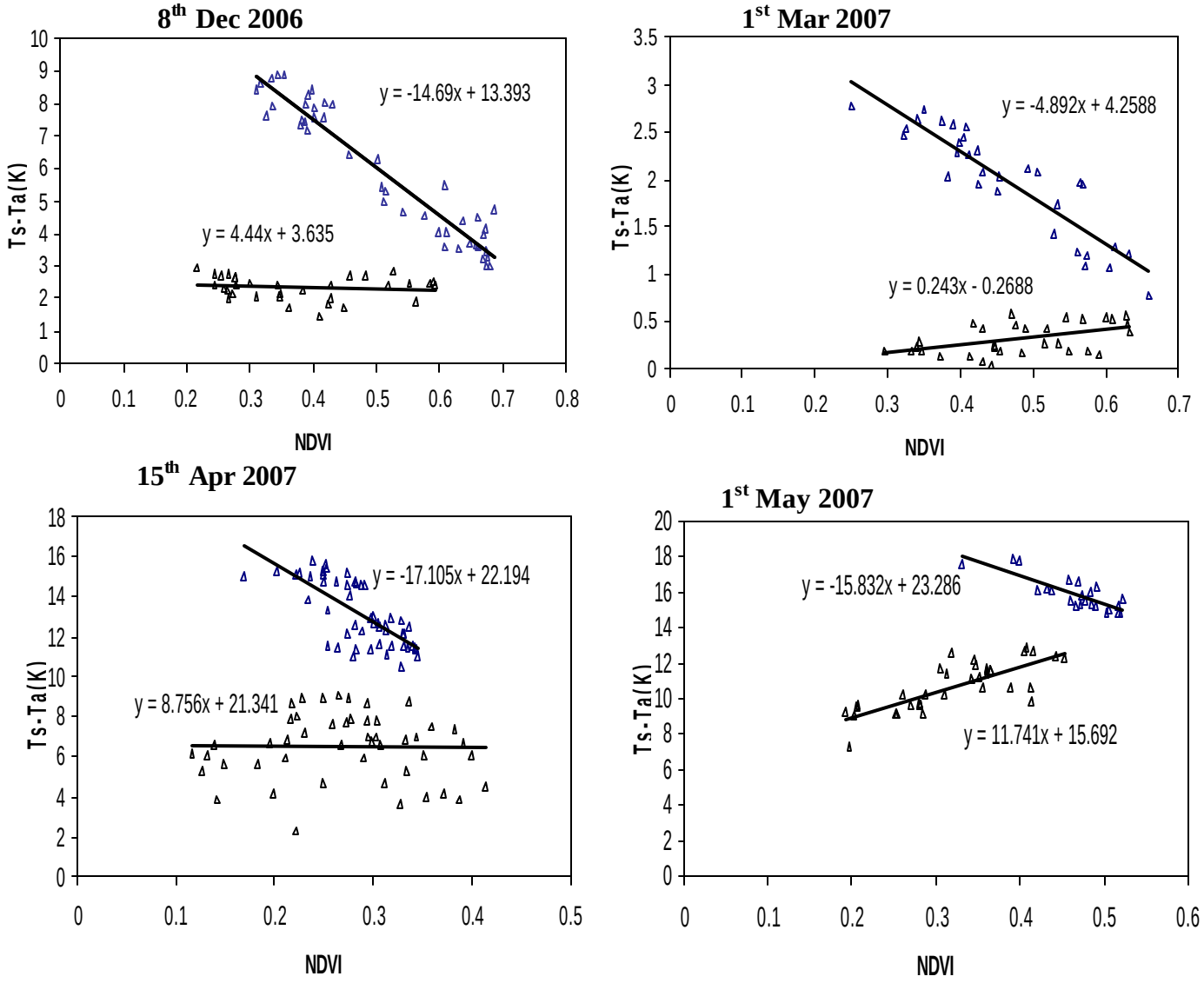

Figure 6.13The wet and dry lines from NDVI-?T space for MODIS data

Spatial pattern of WDI

The spatial pattern of WDI has been discussed in the watershed for some particular dates. The value of WDI varied from 0-1. The lower WDI value denotes the favourable condition i.e good condition of soil moisture. The WDI maps for the watershed are as shown in the figure 6.14. The WDI maps were divided in to four classes as given in the table 6.4 as per the range of WDI values. The values of wet pixels such as river and dense forest cover were noted during the wet months and hence the range of values was decided.

Table 6.4: Range of values of WDI for spatial distribution map

Range of WDI values	**Classes**
0-0.39	Wet areas
0.39-0.51	Well watered vegetation
0.51-0.61	Sparsely watered vegetation
0.61-1.0	Dry areas

Lower the WDI values higher are the moisture content. Thus from the maps obtained we can observe that upper part i.e. Shiwalik contain good amount of soil moisture while lower parts has higher values of WDI indicating water stress condition. The period from October 06 to Jan 07 has lower values of WDI while period from Feb07 to May 07 has higher values of WDI.

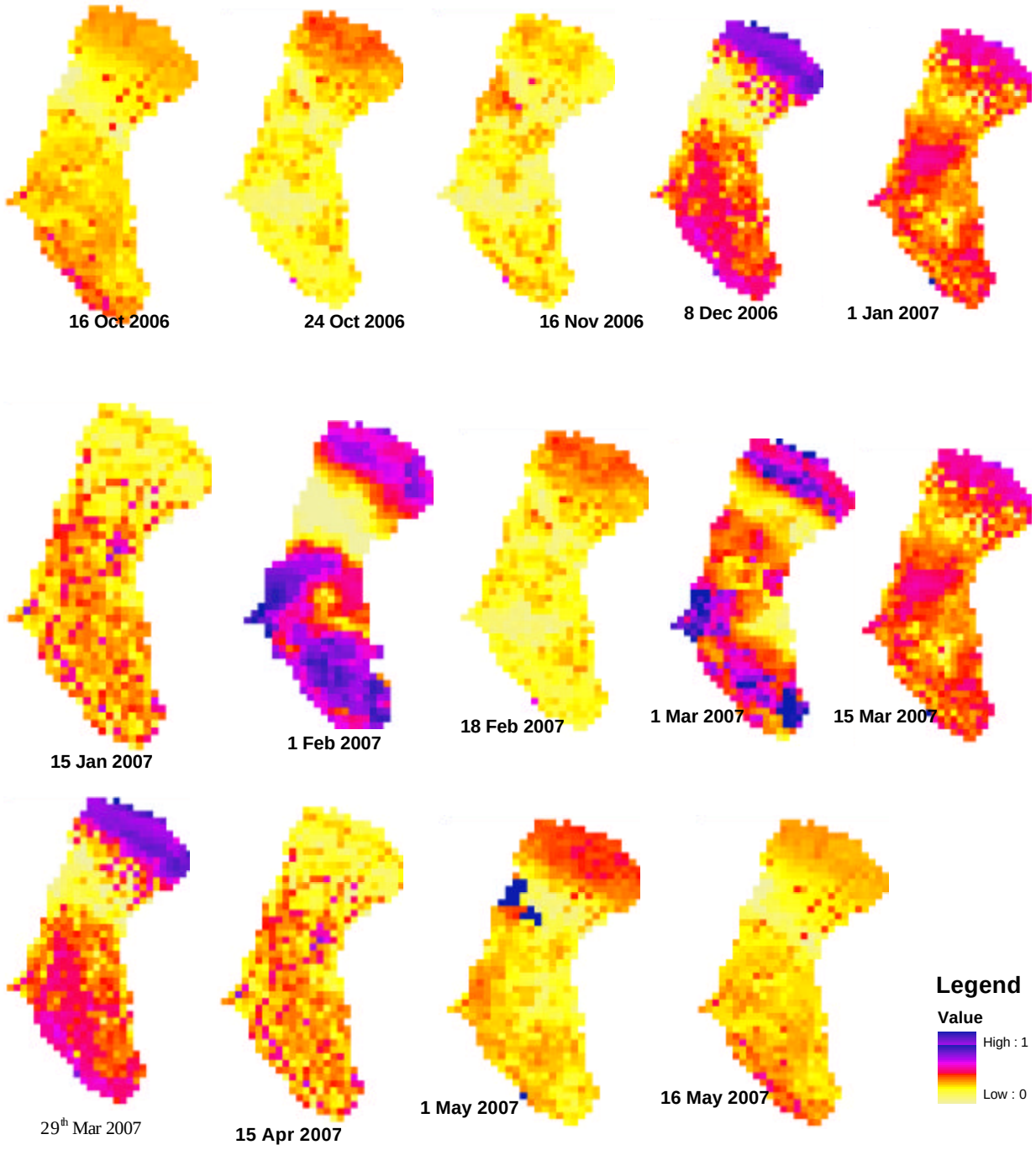

Figure 6.14 Spatial pattern of WDI in the watershed on fortnight basis from October 2006-May 2007.

6.2.3. SIWSI from MODIS

Short wave infrared water stress index was derived from MODIS SWIR and NIR bands. The spatial pattern of SIWSI is as shown in the figure 6.15. Higher the index higher is the moisture content. From the maps it can be seen that upper part has higher values of SIWSI where as lower part has lower values. The index map was divided on to four classes based up on the range of values given in the table 6.5. The values of wet pixels such as river and dense forest cover were noted during the wet months and hence the range of values was decided.

Table 6.5: Range of values of SIWSI for spatial distribution map

Range of SIWSI values	Classes
-1- -0.28	Dry areas
-0.28 – 0.51	Sparsely watered vegetation
0.51-0.61	Well watered vegetation
0.61-1.0	Wet areas

Similar to WDI maps, SIWSI maps also depicts that soil moisture in the upper part of the watershed is good compared to lower parts. This may be due to the vegetation cover and the mean temperature, which affects the moisture content in soils. Also some of the points may have contradictory results since mapping of soil moisture is difficult. Assessing near-surface soil moisture is difficult since moisture changes more quickly. Its very dynamic in nature. Huete and Warrick (1990) reported difficulty in assessing soil water content at the surface (0-5cm) with TM moisture bands (SWIR) or with various wetness indicators under partial vegetation canopies with low vegetative covers.

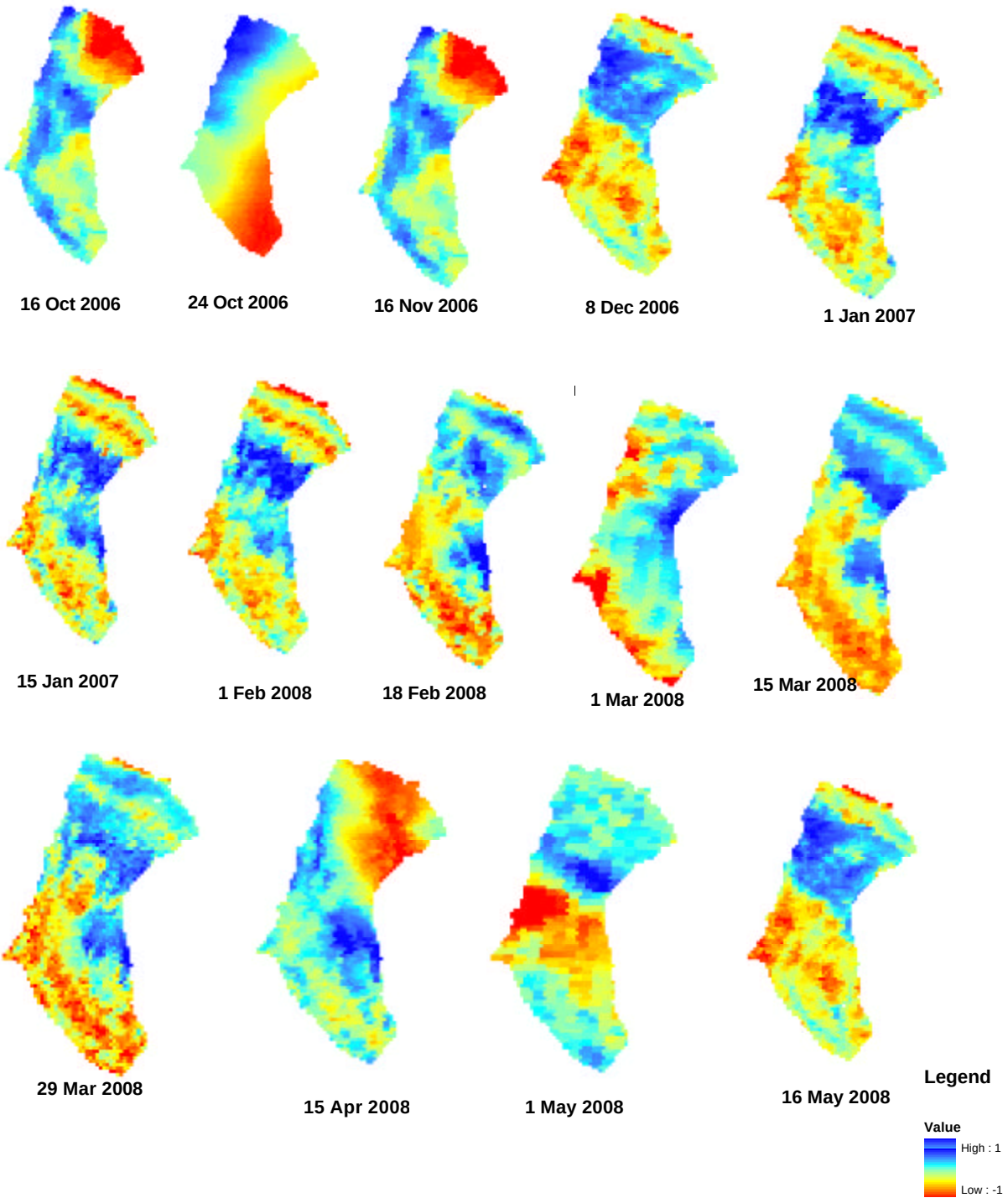

Figure 6.15 Spatial pattern of SIWSI in the watershed on fortnight basis from October 2006-May 2007.

6.2.4. STATISTICAL ANALYSIS OF THE INDICES

Regression analysis between the indices obtained and volumetric soil moisture content

Regression analysis was done between the WDI and SIWSI obtained and the in-situ soil moisture obtained from gypsum blocks for a depth of 15cm. The equations and R^2 is as shown in the tables 6.6 to 6.9.

Table 6.6: Temporal Relationship between WDI and in-situ soil moisture at six sites

Date	Equation	R2
16-Oct-06	$y = 8.4335e^{0.901x}$	0.562
24-Oct-06	$y = 9.257e^{0.6684x}$	0.358
16-Nov-06	$y = 29.968e^{-1.5872x}$	0.559
8-Dec-06	$y = 4.7814e^{1.8465x}$	0.639
1-Jan-07	$y = 11.371e^{0.6147x}$	0.504
15-Jan-07	$y = 5.7923e^{1.2792x}$	0.751
1-Feb-07	$y = 4.2181e^{1.3397x}$	0.683
18-Feb-07	$y = 126.3e^{-3.8488x}$	0.685
1-Mar-07	$y = 6.5496e^{0.8797x}$	0.505
15-Mar-07	$8.3081e^{5.5191x}$	0.580
29-Mar-07	$y = 4.9084e^{3.6277x}$	0.762
15-Apr-07	$y = 2.2376e^{4.7775x}$	0.632
1-May-07	$y = 10.076e^{0.5515x}$	0.517
16may07	$y = 5.9397e^{1.4027x}$	0.4431

Table 6.7: Spatial Relationship between WDI and in-situ soil moisture for various days

Location	Equation	R^2
Sisona	$y = 4.9863e^{1.3618x}$	0.6493
Alawalpur	$y = 10.429e^{0.3988x}$	0.3868
Tanda Misiri	$y = 15.009e^{0.8288x}$	0.3558
Mohand	$y = 7.8257e^{0.9049x}$	0.4792
AWS	$y = 9.4193e^{1.2591x}$	0.5129
Nagal MK	$y = 25.169e^{-0.5502x}$	0.3605

Table 6.8: Temporal relationship between SIWSI and in-situ soil moisture for various locations

Date	Equation	R^2
16-Oct-06	$y = 19.694e^{4.2157x}$	0.7477
24-Oct-06	$y = 50.048e^{3.2478x}$	0.358
16-Nov-06	$y = 17.166e^{3.6453x}$	0.5839
8-Dec-06	$y = 9.1003e^{-5.3668x}$	0.6326
1-Jan-07	$y = 10.872e^{2.6137x}$	0.5748
15-Jan-07	$y = 11.631e^{0.8476x}$	0.4079
1-Feb-07	$y = 7.3755e^{-1.7117x}$	0.5351
18-Feb-07	$y = 17.029e^{1.5744x}$	0.2135
1-Mar-07	$y = 264.38e^{13.476x}$	0.7069
15-Mar-07	$y = 15.206e^{1.3x}$	0.2873
29-Mar-07	$y = 15.887e^{2.3114x}$	0.3621
15-Apr-07	$y = 7.6947e^{-1.2542x}$	0.3077
1-May-07	$y = 8.6311e^{-6.8965x}$	0.5996
16may07	$y = 10.712e^{-0.875x}$	0.1357

Table 6.9: Spatial Relationship between SIWSI and in-situ soil moisture content for various days

Location	Equation	R^2
Sisona	$y = 7.064e^{-1.5523x}$	0.6175
Alawalpur	$y = 9.5043e^{-1.5098x}$	0.5113
Tanda Misiri	$y = 14.712e^{-4.1776x}$	0.4592
Mohand	$y = 11.831e^{1.8668x}$	0.3768
AWS	$y = 10.979e^{-2.2663x}$	0.6148

An exponential relationship was established between the in-situ soil moisture content and the indices. It can be seen from the table that R^2 of SIWSI obtained is better compared to WDI temporally as well as spatially. This may be because of the resolution of the data used. Using coarse resolution data for a small watershed generalizes the value to some extent.

Statistical Analysis of the Spatial map obtained from WDI and SIWSI

Spatial statistics was used evaluate the accuracy of the spatial map obtained from the data using the ground observed data. Cramer's V as described in the section 5.2.2.6 was found for the datasets for which R^2 range was 0.50 to 0.75. The maps for which spatial statistics was performed is given in the Figure 6.16. The cross matrix formed on 16th October 2006 is given in table 6.10. Similar matrix was obtained for other dates and Cramer's V was calculated along with estimated probability of correct prediction when predicting soil moisture from the indices. The values obtained are as given in table 6.11.

Table 6.10: Cross matrix for SIWSI and Observed soil moisture map on 8th December 2006

Simulated (SIWSI)	Observed			
	1	2	3	4
1	62	17	112	175
2	178	38	148	122
3	127	118	71	97
4	107	111	110	85

Table 6.11:Spatial Statistics for different dates

Date	Cramer's V (WDI)	Cramer's V (SIWSI)	Estimated probability of correct prediction	
			WDI	SIWSI
16th Oct 2006	0.496	0.60	0.5126	0.63
16th Nov 2006	0.537	0.454	0.510	0.711
1st Jan 2007	0.429	0.314	0.57	0.49
1st Feb 2007	0.396	0.540	0.38	0.60
1st Mar 2007	0.487	0.581	0.604	0.72
1st may 2007	0.491	0.663	0.718	0.792

Spatial statistics were also used evaluate the accuracy of the spatial map obtained from the LISS III and ASTER data using the ground observed data. Cramer's V for LISS III was 0.45 and for ASTER was 0.61. The estimated probability of correct prediction when predicting soil moisture map from the index was 0.50 for LISS III and 0.62 for ASTER respectively. The result of ASTER was better as compared to LISS III because ASTER has five channels in SWIR where as only one channel. The soil moisture index developed from ASTER used two SWIR bands as explained in the section 5.2.2.1, whose reflectance are sensitive to the soil moisture content whereas the index developed from LISS III used one NIR band and one SWIR band.

16th October 2006

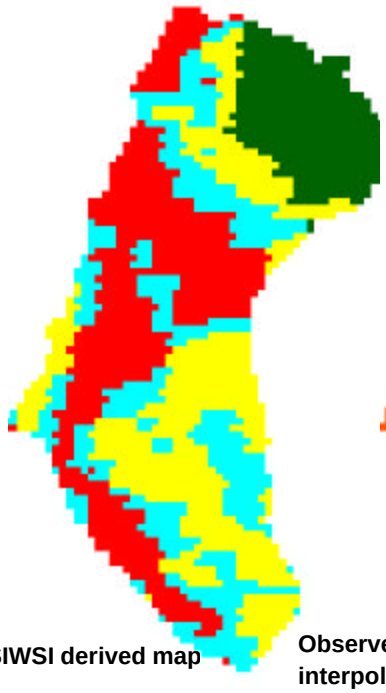

SIWSI derived map

Observed data map interpolated

WDI derived map

Legend

- Wet areas
- Well watered vegetation
- Dry areas
- Sparsely watered vegetation

16th November 2006

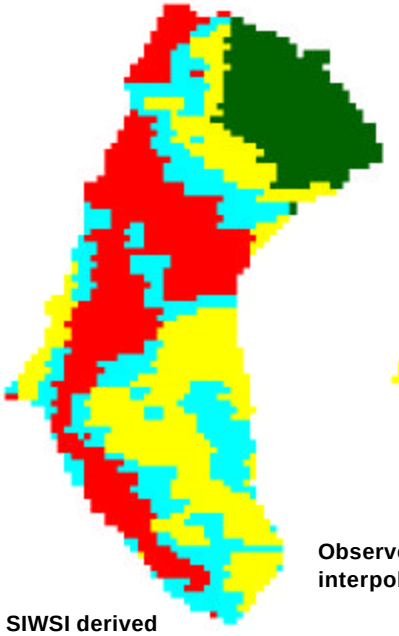

SIWSI derived

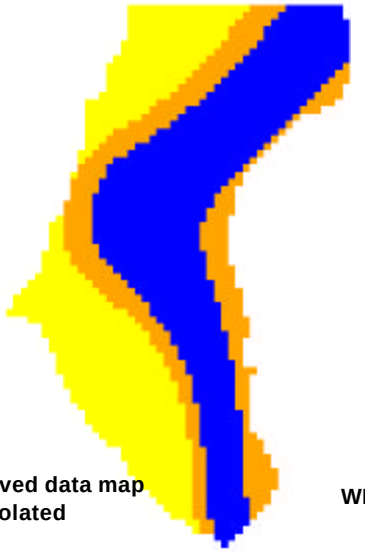

Observed data map interpolated

WDI derived

Legend

- Wet areas
- Well watered vegetation
- Dry areas
- Sparsely watered vegetation

1st January 2007

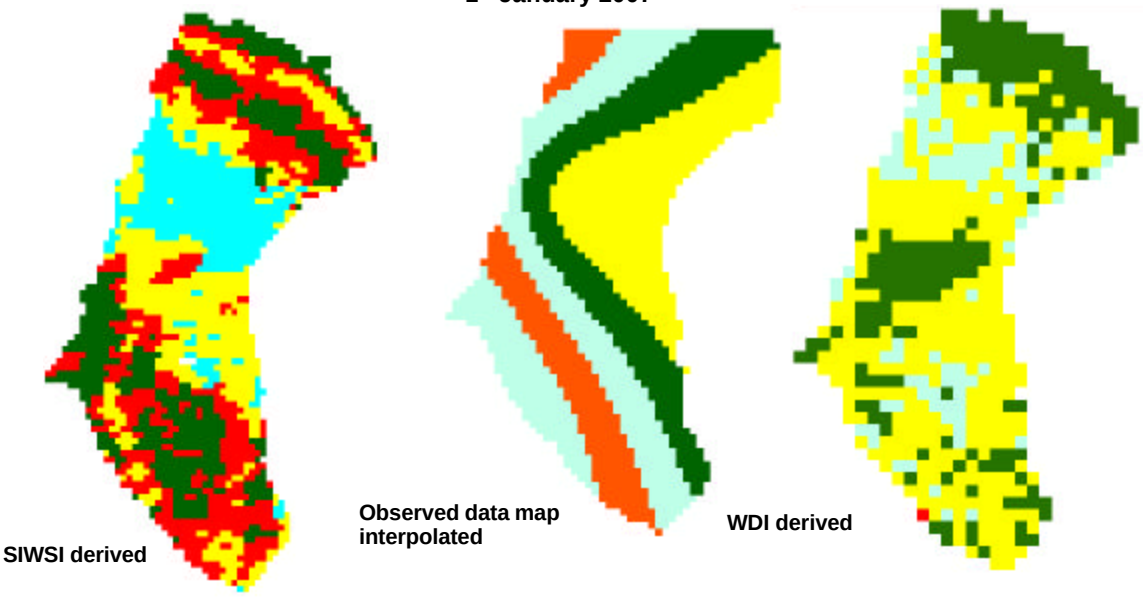

Legend

- Wet areas
- Well watered vegetation
- Dry areas
- Sparsely watered vegetation

1st February

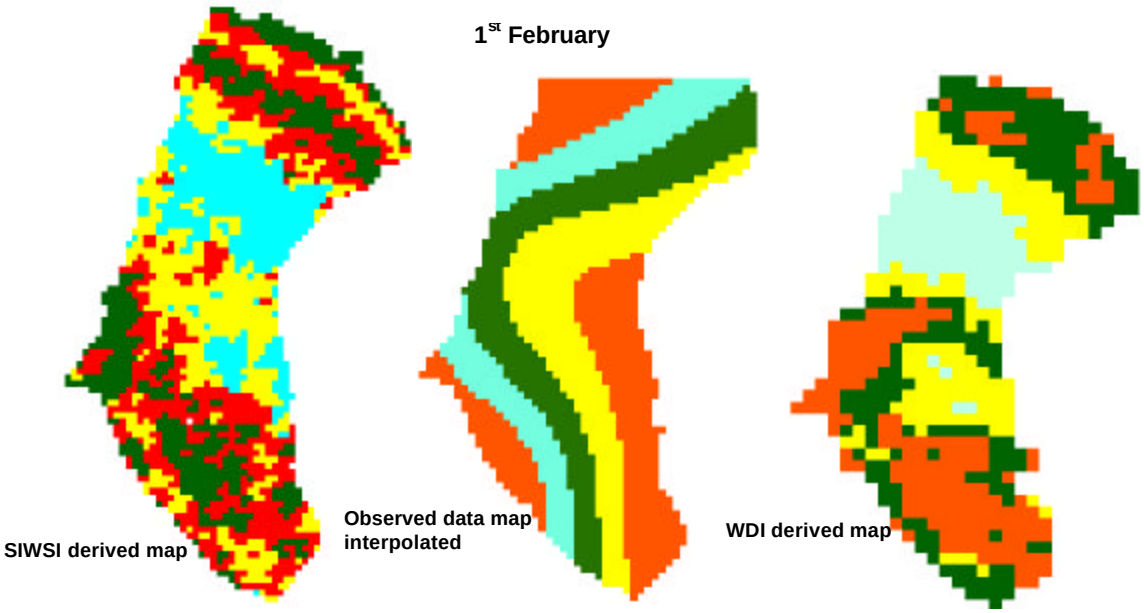

Legend

- Wet areas
- Well watered vegetation
- Dry areas
- Sparsely watered vegetation

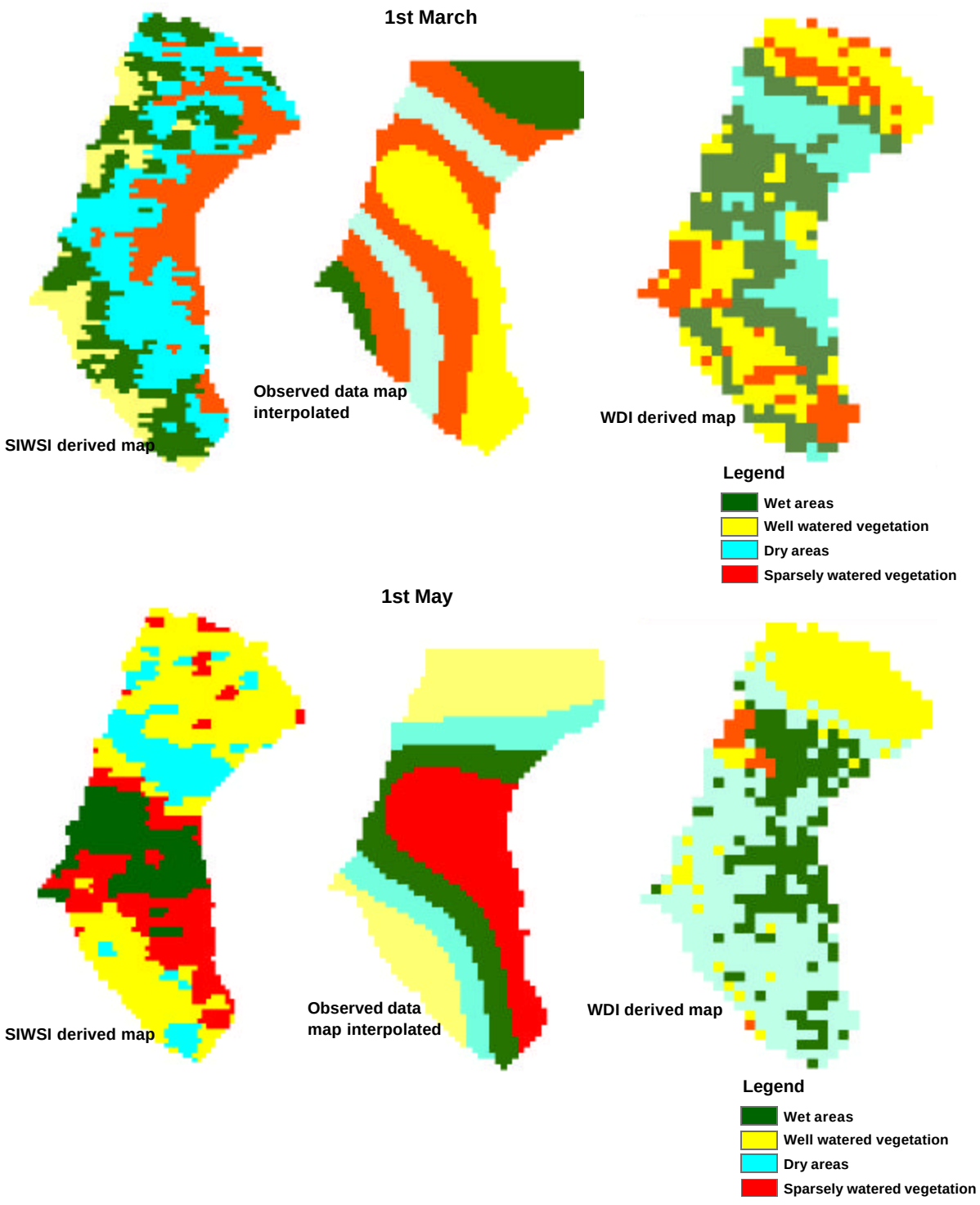

Figure 6.16Spatial maps: SIWSI, Observed and WDI classified maps

6.3. MICROWAVE REMOTE SENSING APPROACH

Microwave remote sensing techniques are most effective in deriving soil moisture of the upper surface over sparsely vegetated areas and become less reliable in measuring sub-surface soil moisture (Choudary, 1992; Jackson, 1993). Both active and passive microwave remote sensing can accurately measure surface soil moisture contents in the top 5cm of the soil. The backscattering coefficients were obtained using PCI Geomatica for both HH and HV polarization. The backscattering images obtained are shown in the Figure 6.17 respectively. The backscattering coefficient increases with the increasing amount of soil moisture content. During the satellite pass concurrent soil moisture samples are collected and analyzed for soil moisture by gravimetric method.

Since ENVISAT-ASAR data consists only for a part of the watershed, the same area is analyzed. The range of backscatter coefficient for HH polarization is -30 to 6dB and for HV polarization image is -25 to 8dB.

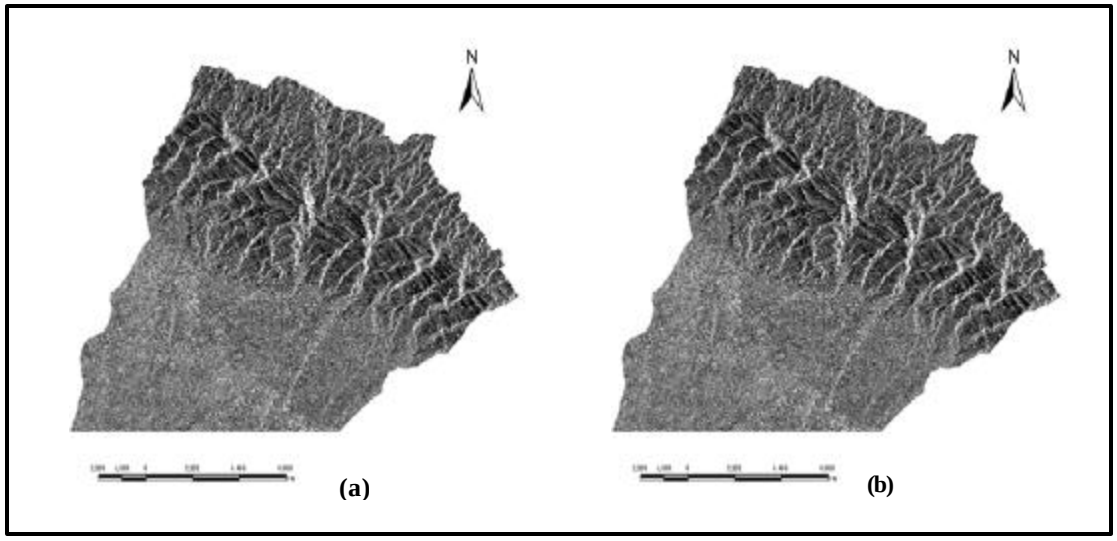

Figure 6.17Backscattering images obtained from ENVISAT-ASAR: (a)HH polarized, (b)HV polarized

Vegetation Correction for Microwave data

A Simple cloud model has been used to correct the backscattering coefficient of ASAR data. The graph between soil moisture and uncorrected back scattering co-efficient is as shown in the figure 6.18.

Table 6.12: Uncorrected backscattering co-efficient and soil moisture content with land cover

Latitude	Longitude	Land cover	s^o (dB)	M_s
$30^0$08' 06"	$77^0$52' 8.4"	small grass	-7.563	13.28
$30^0$08' 3.3"	$77^0$52' 08"	ground nut field	-9.395	14.06
$30^0$07' 56.2"	$77^0$52' 5.3"	ground nut field	-10.201	12.98
$30^0$08' 7.5"	$77^0$51' 50.9"	ground nut field	-5.179	15.62
$30^0$07' 30"	$77^0$50' 48.7"	grass	-7.233	13.95

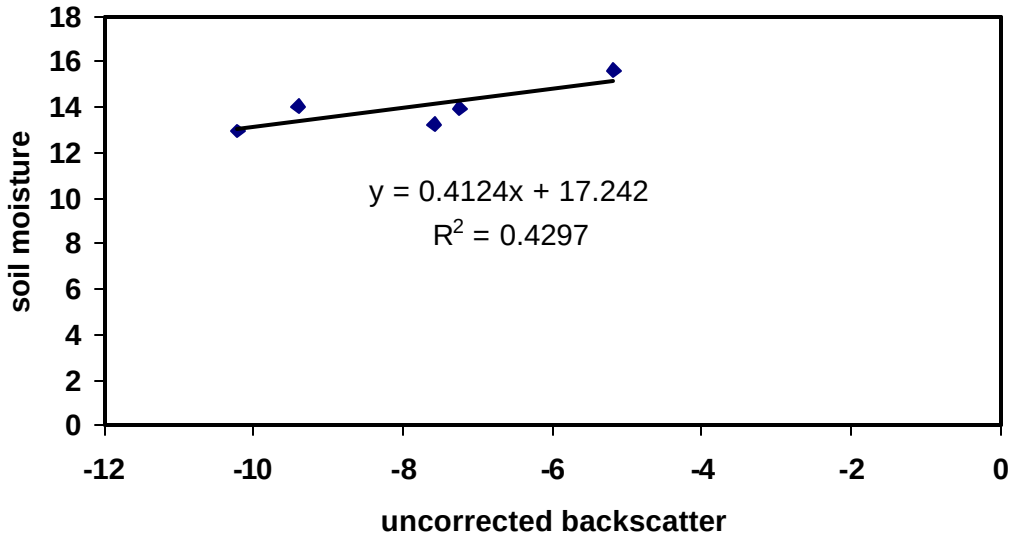

Figure 6.18Plot between In-situ Soil moisture and Uncorrected Backscattering co-efficient

The coefficient of determination is 0.429 which is quite less. Thus the backscattering coefficient needs to be corrected for vegetation effects. This correction is applied as explained in the section 5.2.2.4. The corrected backscattering coefficient is plotted against the in-situ soil moisture as shown in the figure 6.19.

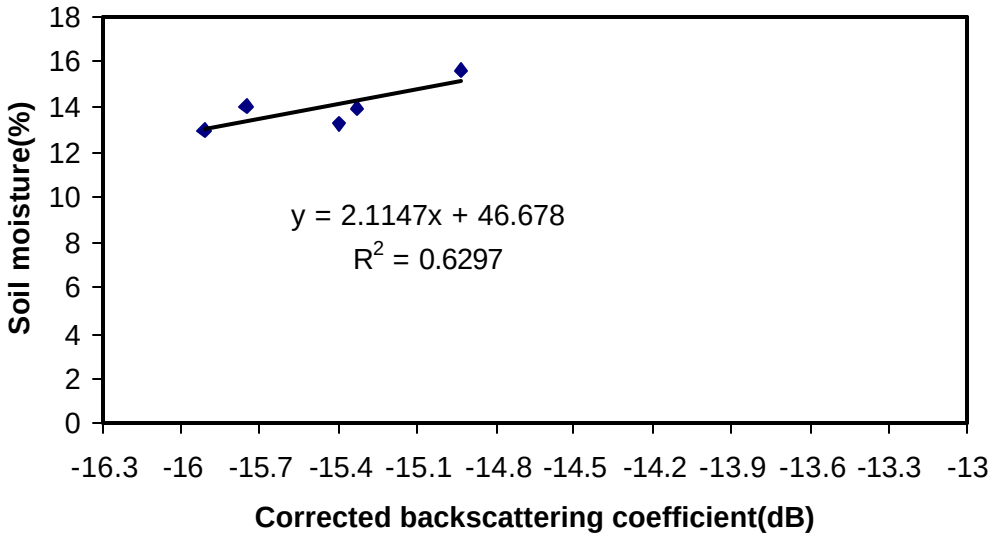

Figure 6.19Graph between soil moisture and corrected backscattering co-efficient after vegetation correction

The relationship thus obtained is validated against the relation and correlation obtained for bare soils.

Table 6.13: Backscattering values for bare soil

Latitude	Longitude	Land cover	s^o	M_s
$30^0$08' 9.1"	$77^0$51' 48.8"	unploughed land	-4.643	15.14
$30^0$07' 27.5"	$77^0$50' 45.9"	harvested crop with residue	-3.53	9.82
$30^0$07' 30"	$77^0$50' 48.7"	dense forest	-7.233	15.65

The above data is plotted and shown in figure 6.19, its relationship is linear and the same is used to correct back scatter coefficient for all vegetation densities (Figure 6.20). Also

the R^2 value has been increased after vegetation correction. The equation thus obtained has been used to obtain a spatial distribution map. The map is divided into four classes' as well watered vegetation, wet areas, sparsely watered vegetation and dry areas. The spatial map is as shown in the Figure 6.21.

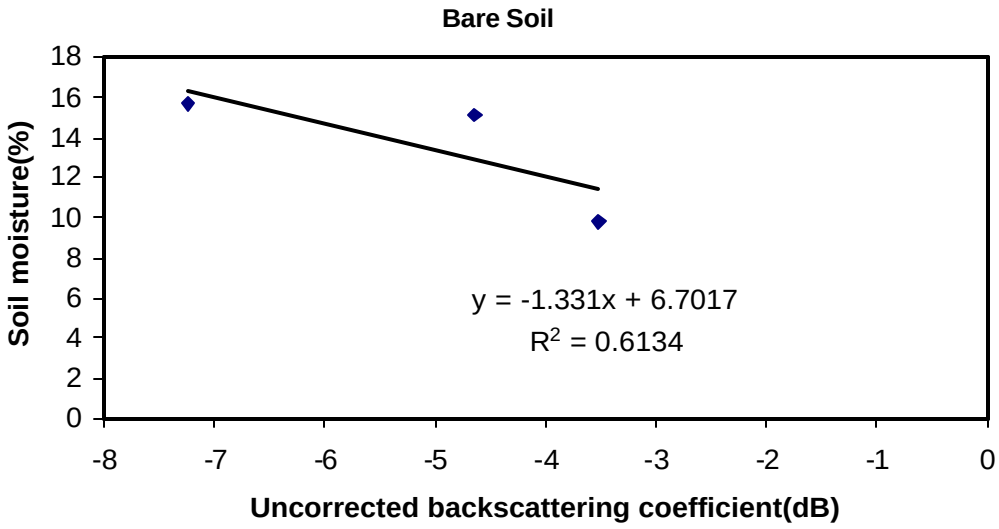

Figure 6.20Relationship between soil moisture content and backscattering co-efficient for bare soils

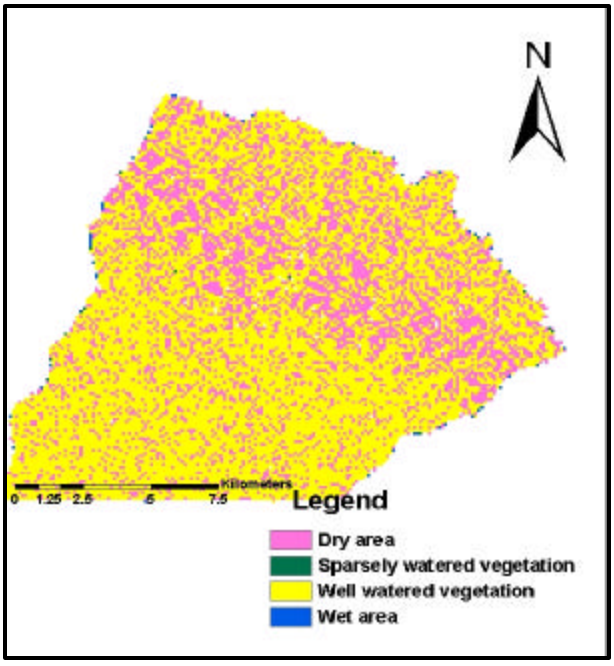

Figure 6.21Spatial Distribution of soil moisture derived using Microwave data

6.4. MIKE SHE MODEL

MIKE SHE a distributed hydrologic model was used to simulate soil moisture at different depths. The pressure gauge readings of gypsum blocks obtained were converted to volumetric soil moisture content values using the relationships developed earlier as given in Appendix A. The soil moisture values thus obtained were compared with the model results. The output of MIKE SHE was a time series file. Initial model runs were plotted and output was improved by adjusting certain parameters to better fit with observed soil moisture and stream flows. The period of simulation was June 2006 to May 2007.

Initial model runs were plotted, and output was improved by adjusting certain parameters to better fit with the observed soil moistures and stream flow. Initially model was run for a grid size of 500m. The results obtained were not satisfactory. Finally model was calibrated for a grid size of 200m. The pre-calibration graph at AWS station is as shown in the Figure 6.24. The trend of soil moisture at the station does not match the trend of observed soil moisture. RMSE was around 28% and Nash-Stucliffe co-efficient was found to be 0.23. From the graphs obtained we can see that model is values are higher than the observed values. Also RMSE is quite high. Similar graphs were obtained for other stations also.

Performance Criteria

The criteria for assessing goodness of fit between the measured and modeled soil moisture curves are qualitative as well as quantitative. The primary criterion for fit assessment was matching the shapes of the modeled to those of the measured soil moisture. Although the actual magnitudes may be different, the timing of peaks and rising limbs, the slopes of the recession curves, and the trend of the whole time series should be parallel to or “mirror”.

The calibration of the model was done for soil moisture only. While this thesis is mainly concerned with the accuracy of unsaturated zone soil moisture content plots, it is inherent that suitable unsaturated zone output should not result in poor modeled hydrographs, nor should suitable modeled hydrographs result in poor unsaturated zone output. Although adjusting various parameters in the model to improve the unsaturated zone will have an effect on the hydrographs, that effect should not be detrimental; an improvement in the unsaturated zone accounting should also be an improvement in the calculated hydrographs.

6.4.1. MODEL CALIBRATION

The model calibration involved adjusting model parameters in such a manner that simulated and measured values showed a better match. The model was calibrated for one year (June 2006 - May 2007). In this case, saturated hydraulic conductivity and initial moisture content values were adjusted so as to match simulated and observed soil moisture content. The values were obtained as per the percentage of sand and clay given by NIH, Roorkee. The values were calculated by the website(www.ficklinsoils.net/soils/soil texture.htm)

Table 6.14: Soil parameter after calibration

Soil Texture	K_s (m/s)	$?_s$	$?_r$	a
Loamy Sand	3.01x10-5	0.410	0.057	0.33
Sand	3.54x10-5	0.248	0.045	0.36
Loam	1.27x10-6	0.380	0.078	0.35
Sandy Loam	1.62x10-5	0.361	0.065	0.37
Sandy Clay	3.33x10-6	0.380	0.110	0.37
Silty Loam	1x10-5	0.411	0.065	0.36

The graphs for each station at three depths after calibration are as shown in figures 6.25 to 6.30. The trends at all the stations almost matched with the observed values. It can be seen that trend at NAGAL MK gets reversed as compared with the other stations. It can be observed that RMSE and Nash-Stucliffe co-efficient is less for a depth of 15cm as compared with other two depths. In every case the simulated values are more than the observed values i.e. over prediction. This may be due to the following possible reasons:

- ❖ The ground water depth considered for the modeling may be more in actual condition. Since topography is not same all over the watershed considering uniform well depth might have caused discrepancies in the results. Thus model may be considering seepage from ground water.
- ❖ MIKE SHE model relies on a physically based description of the rain-runoff processes, and the effects of different land cover properties defining the watershed response to

land use change. Hence, for attainment of reliable results, the ground observed parameters in vegetation parameter file and soil parameter file should be included.

- The values of LAI for forest cover and other land use types other than agriculture were taken from MODIS data (1km spatial resolution). The values get generalized at this resolution for a small watershed.

- Vertical infiltration occurs in response to rainfall. The regionalization of point measurements in case of determining area rainfall by the method of thiessen polygons may be one of the reasons because of the natural variation exhibited by the parameter has not been considered because of the unavailability of rainfall stations in the watershed.

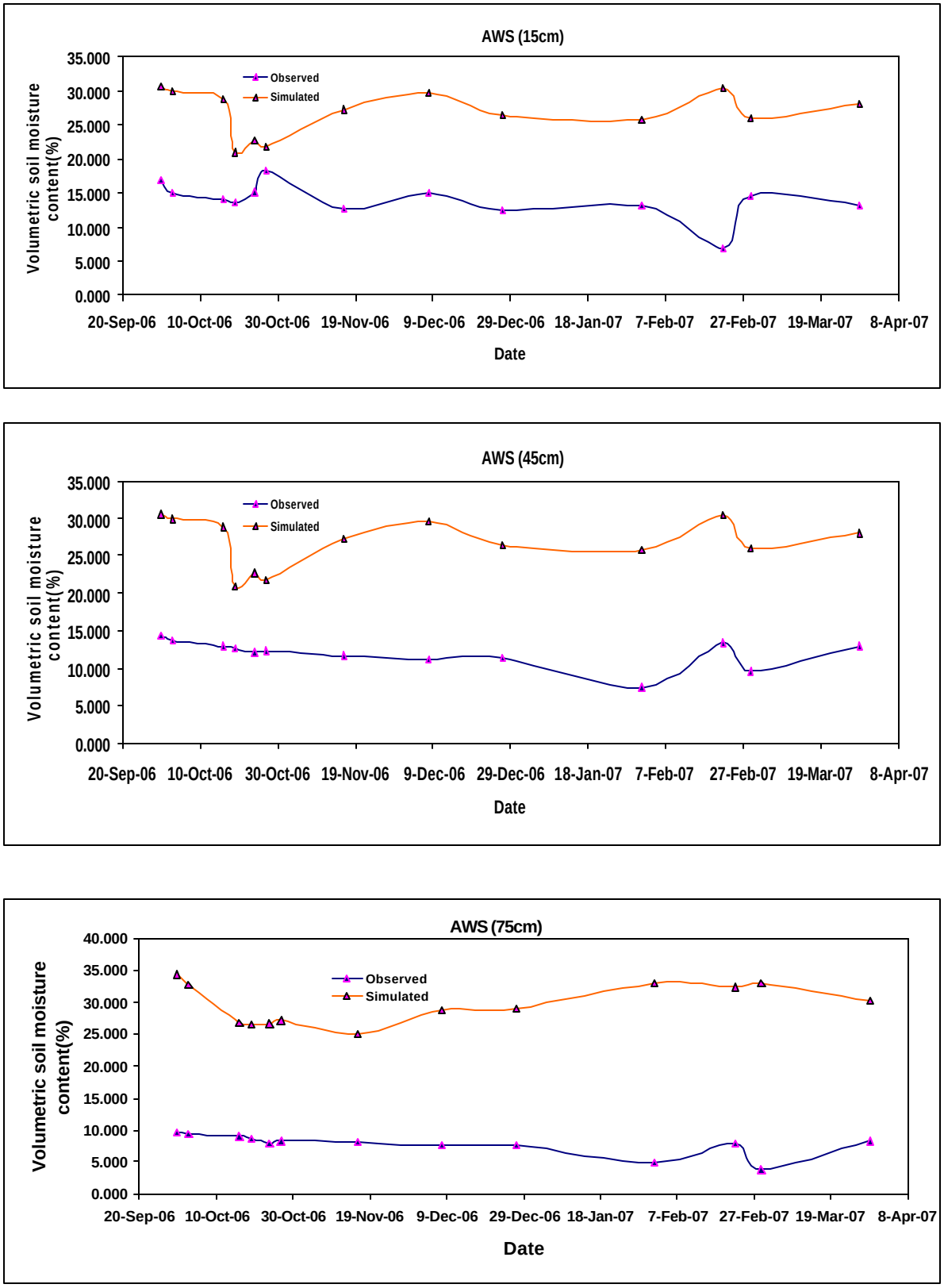

Figure 6.22 :Trend of Soil moisture at AWS before calibration

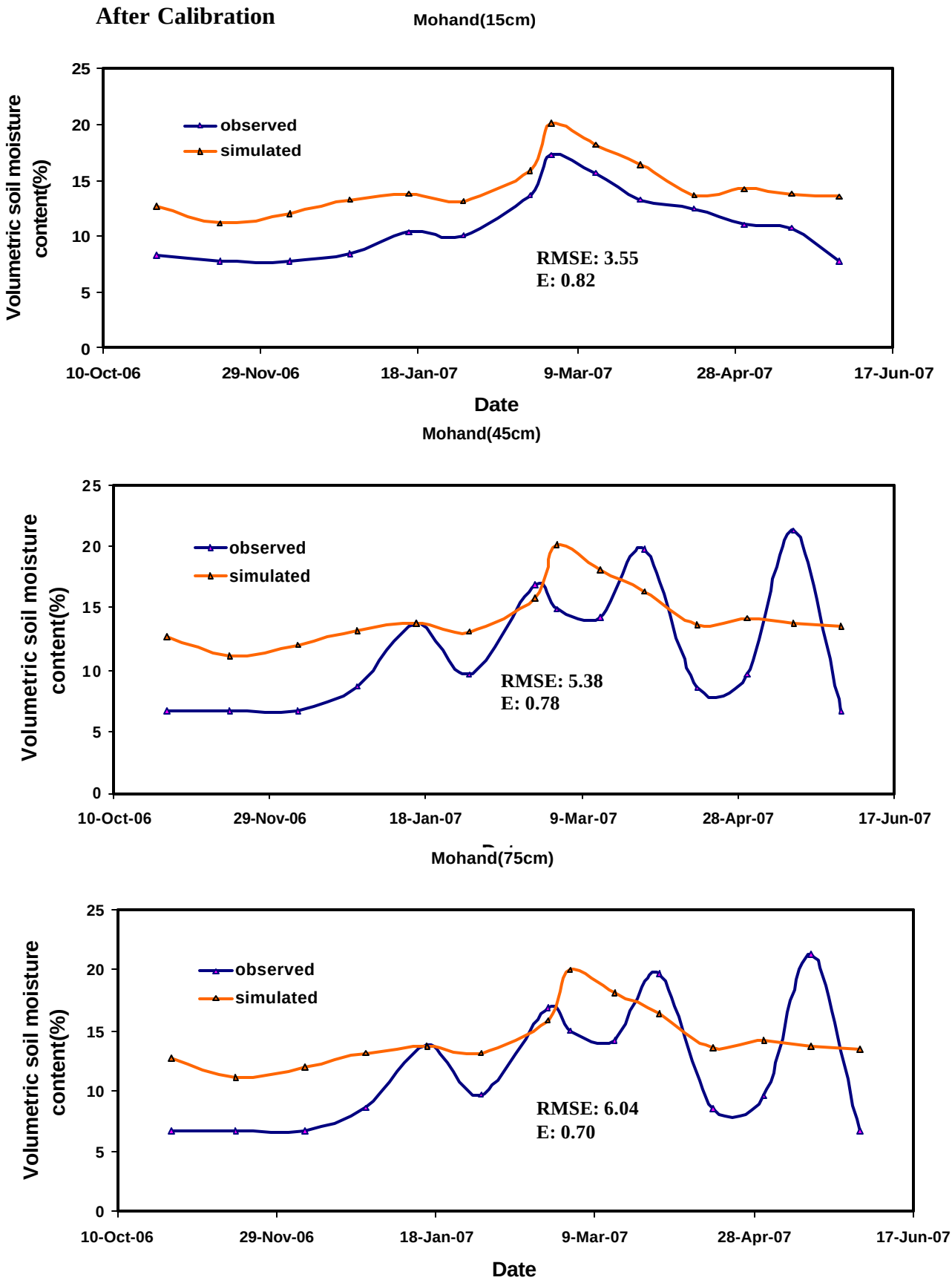

Figure 6.23: Trend of Observed and Simulated Soil Moisture at Mohand station

After Calibration

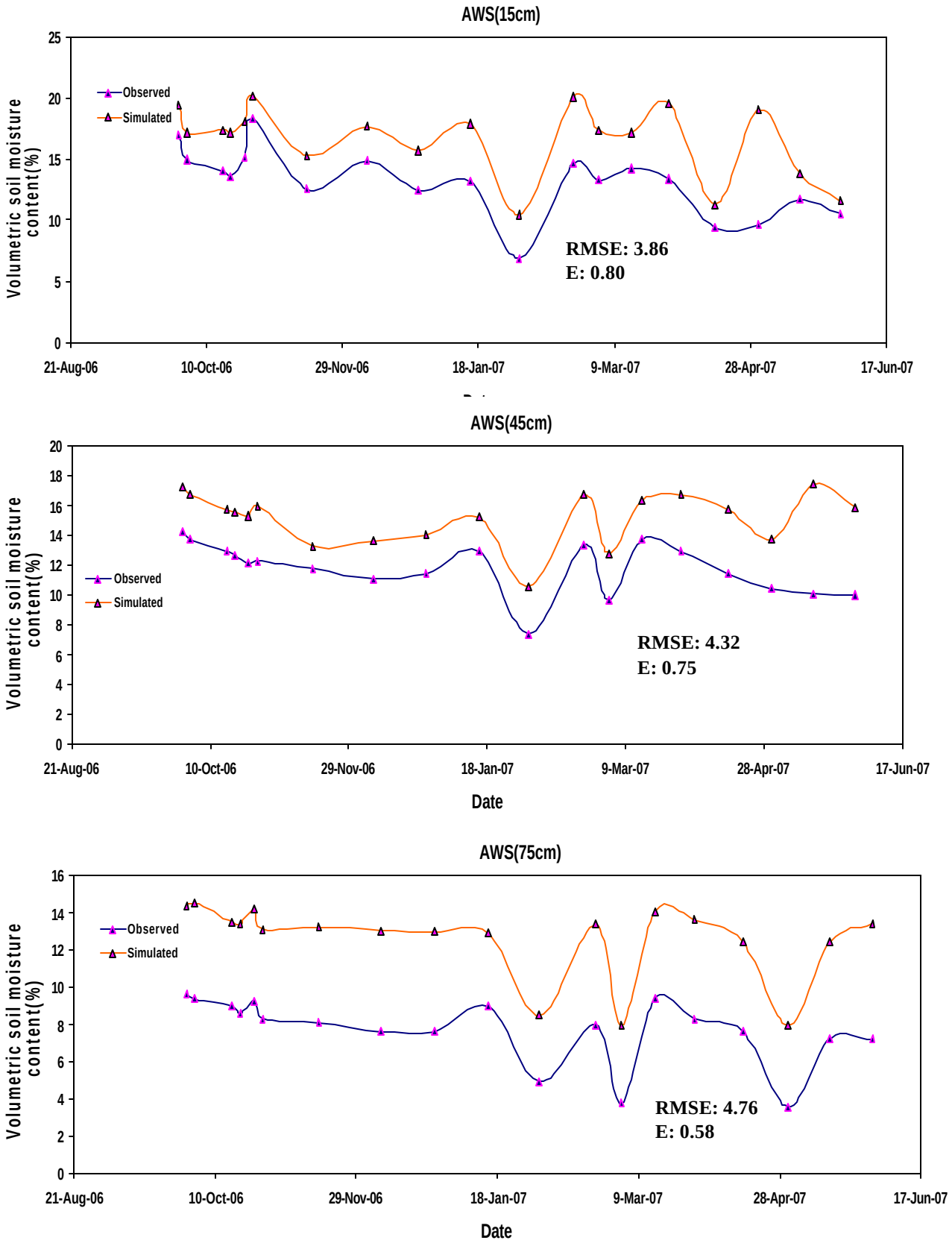

Figure 6.24 Trend of Observed and Simulated soil moisture at AWS station

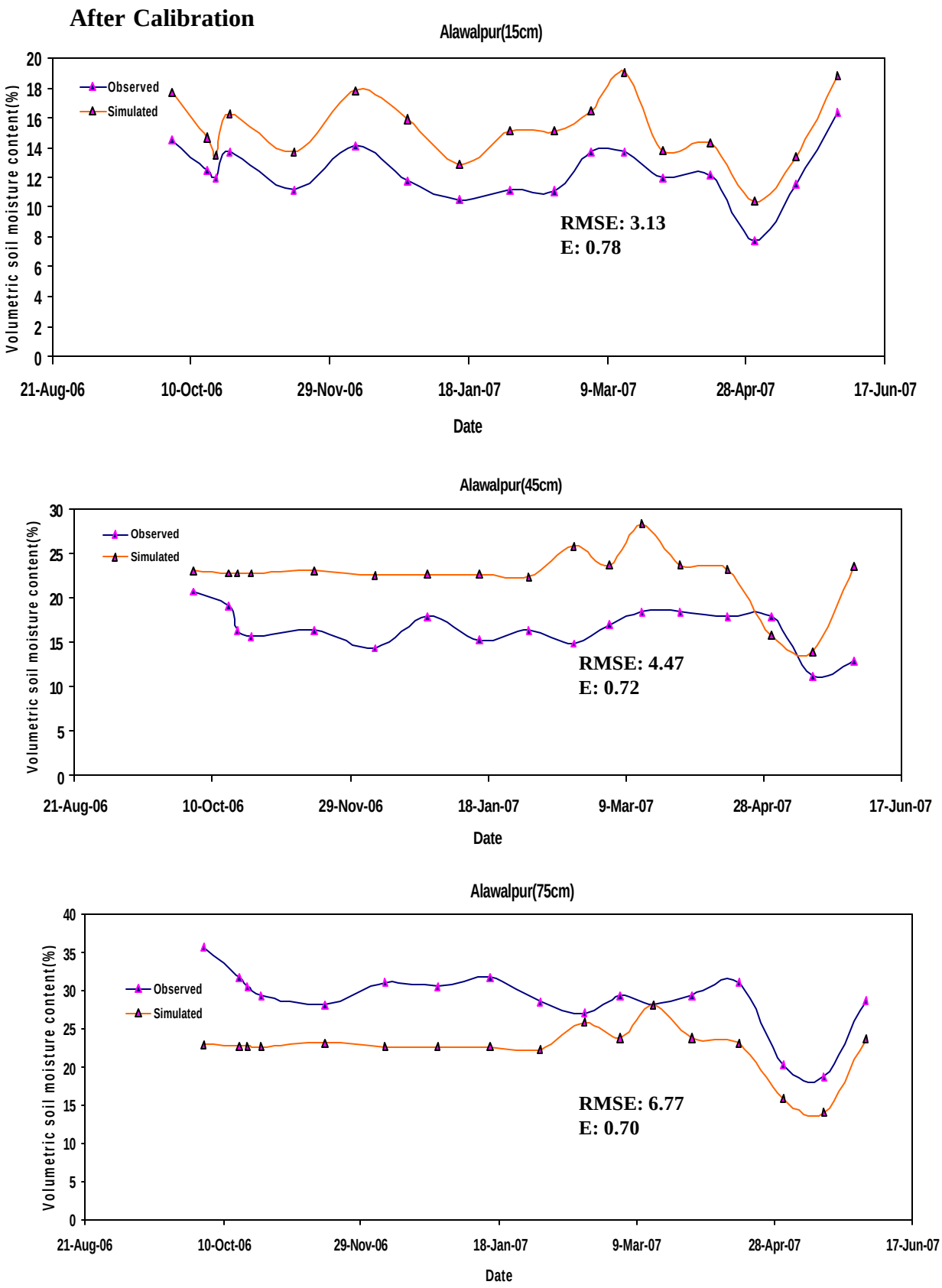

Figure 6.25 Trend of Observed and Simulated Soil Moisture at Alawalpur

After Calibration

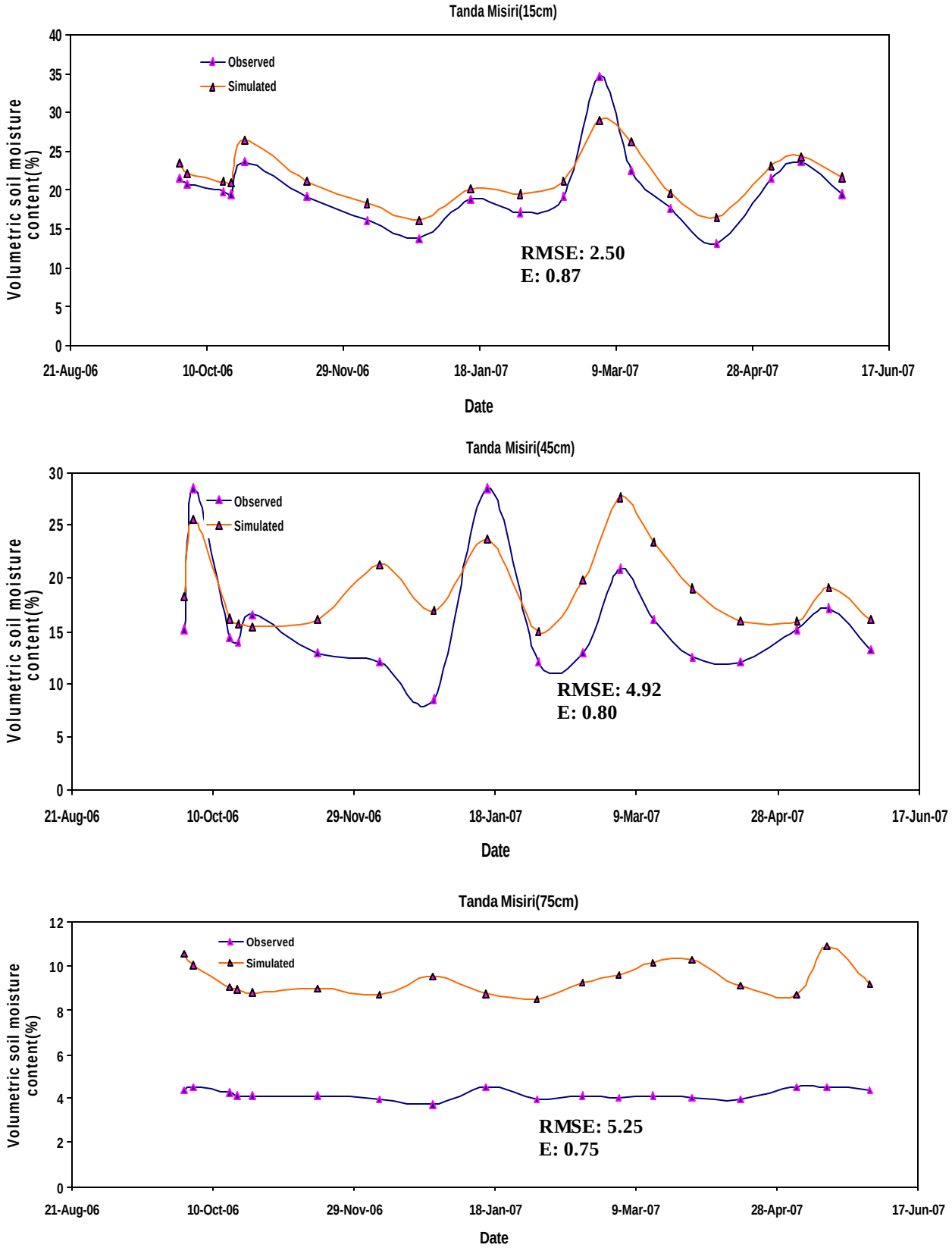

Figure 6.26 Trend of Observed and Simulated Soil moisture at Tanda Misiri

After Calibration

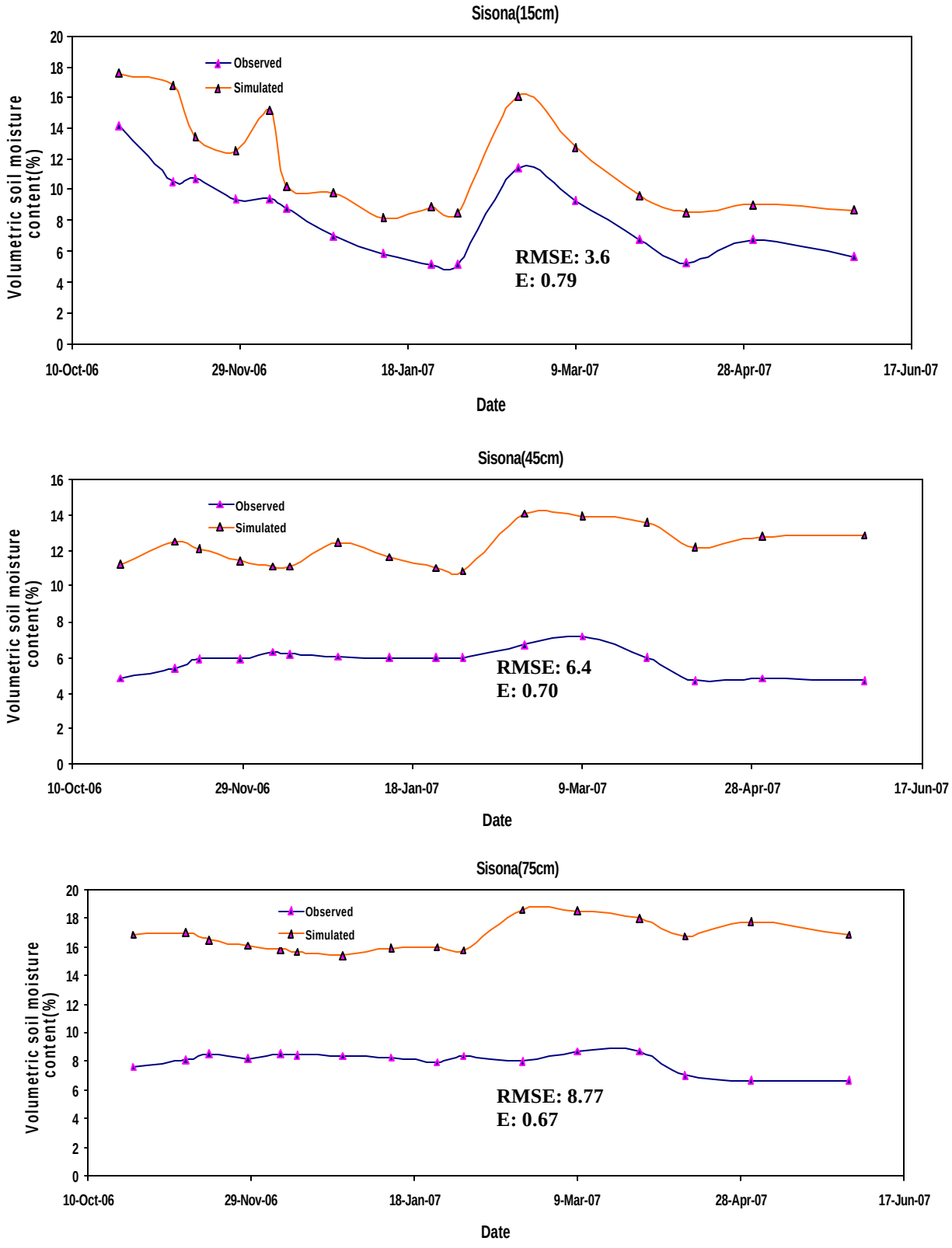

Figure 6.27 Trend of Observed and Simulated soil moisture content at Sisona

After Calibration

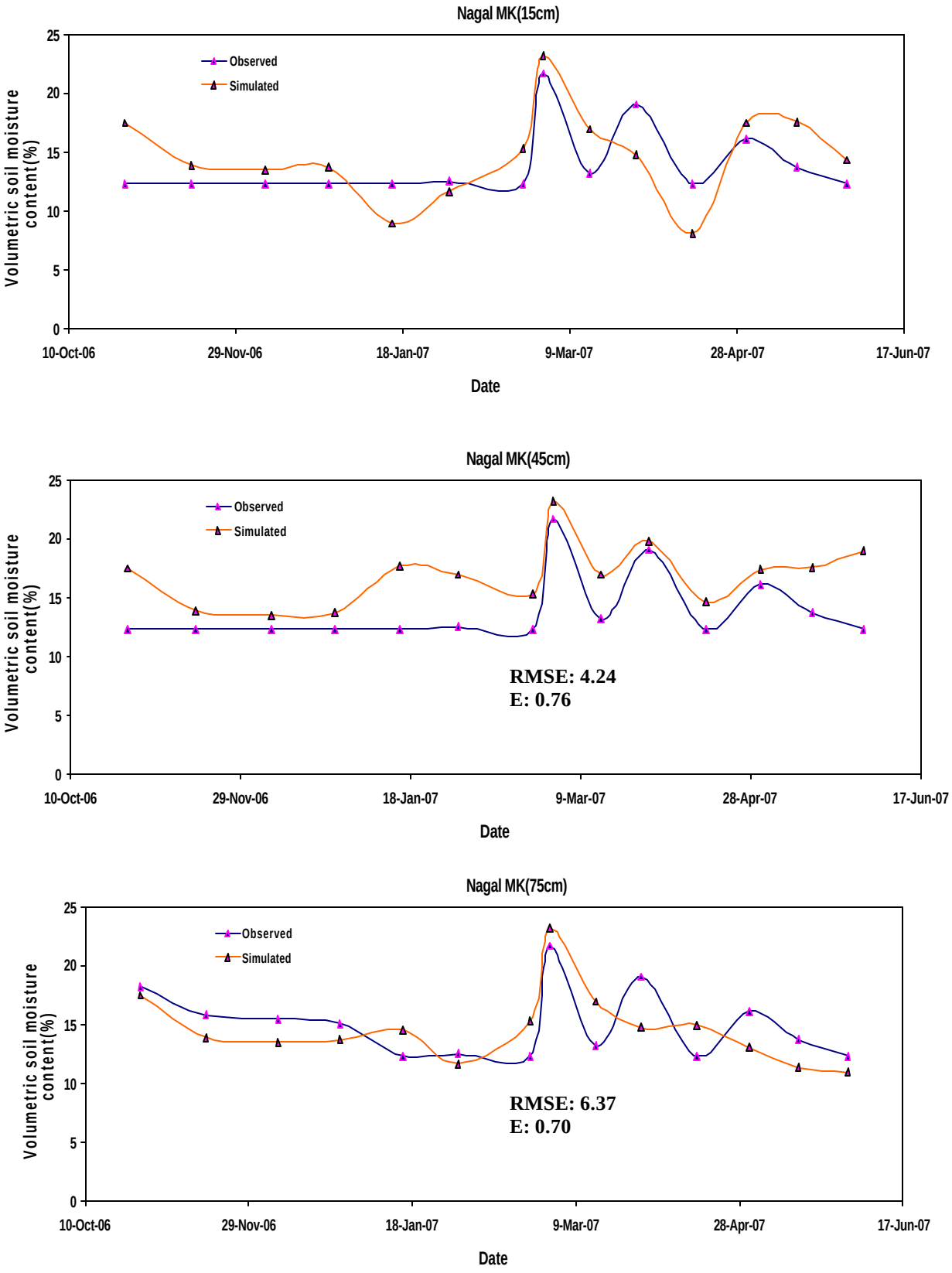

Figure 6.28 Trend of Observed and Simulated soil moisture at Nagal MK

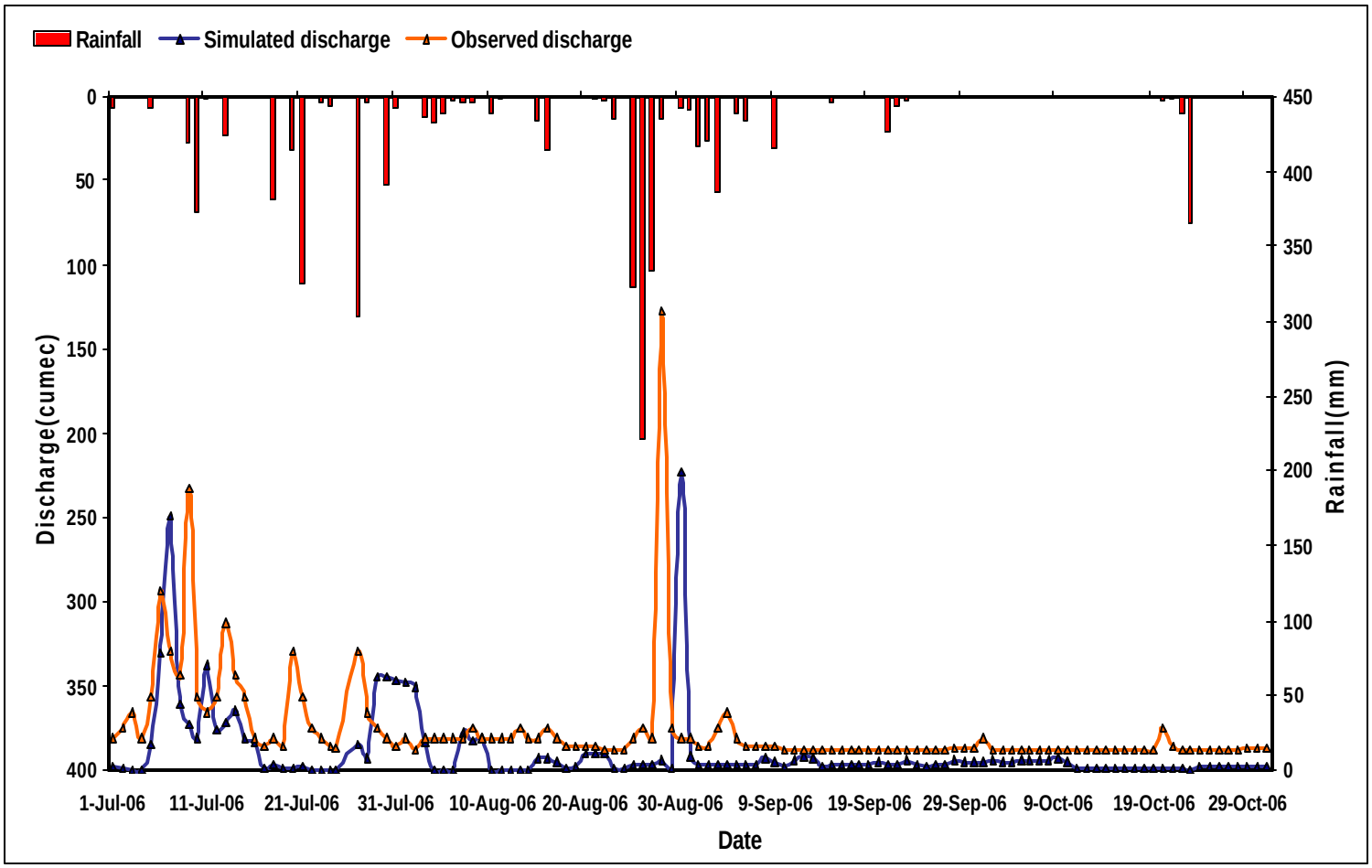

Figure 6.29Hydrograph at the outlet and Hyetograph

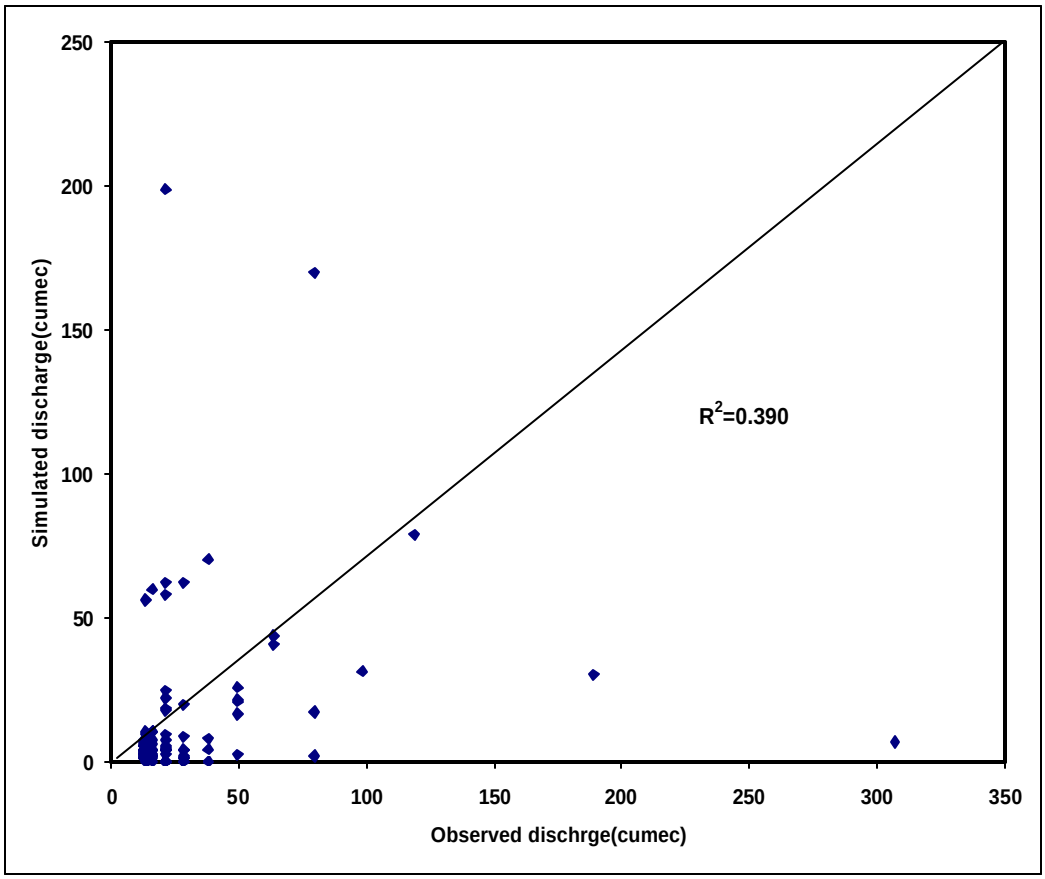

Figure 6.30Relationship between Observed and Simulated discharge at the outlet

The observed and modeled discharge showed a relatively good temporal match. Over – prediction of discharge has taken place on 2nd July 2006 in spite of low rainfall. Hyetographs along with simulated and observed hydrographs (Figure6.30 and 6.31) show that the simulated hydrographs generally matched. The timing of simulated and observed peaks matched reasonably well however, in some instances, simulated peak runoff's were slightly over or under estimated. These runoff events mostly followed precipitation events. But the relationship between simulated and observed (Figure) is not satisfactory with a R^2 of 0.39 which is less. The possible reasons for the low simulated discharge:

- The water being trapped in the depression upstream as the depression storage has been considered as 0mm.
- Also the model is over estimating soil moisture content in the unsaturated zone. This means that the precipitation over the area is being infiltrated more and hence the contribution to runoff is relatively less.

7. CONCLUSION

This chapter discusses in detail the conclusion arrived after examining the different methods and approaches adopted in the study for assessing soil moisture in the Solani watershed.

7.1 Conclusion

The main objective of the study was to assess the performance of remote sensing data and hydrologic model to infer soil moisture in the watershed. The analysis has been done on a fortnight basis during October 2006 to May 2007.

How the soil moisture in watershed varying with respect to space and time?

In this study the variation of soil moisture both spatially and temporally is derived using various parts of electromagnetic spectrum such as NIR and SWIR bands, microwave and thermal bands. Spatially varying soil moisture is derived and compared with the interpolated ground observed soil moisture data, which matches well. The same analysis is carried out temporally from during October2006 to January 2007. The MIKE SHE model results are compared with both spatial and temporal results, where there is a good agreement. Soil moisture variation at a depth of 15cm is very dynamic. Upper part of the watershed has a good amount of soil moisture as compared with the lower part. Based on this results, it is concluded that temporal remote sensing data is useful to generate spatial surface soil moisture patterns in a watershed.

Is it possible to map soil moisture using different bands of electromagnetic spectrum?

Visible bands

SWIR and NIR data was used to compute soil moisture index and SIWSI. Soil moisture indices developed from ASTER and LISS III had a good correlation of 0.64 and 0.62 respectively. Spatial statistical parameter Cramer's V was 0.64 on 1st November 2006 indicating good degree of association between the observed soil moisture map and index derived map. Correlation of coefiicient was good for wet season (Oct06-Jan07).

Thermal bands

WDI was computed for ASTER (90m) and MODIS (1km). Correlation between the soil moisture and WDI was good for wet season and for sites where there was no irrigation. Cramer's V was good for dry season indicating good degree of association between the spatial maps. The WDI value for wet pixels varied from 0.15-0.39.

Microwave

ENIVISAT-ASAR data was used to retrieve soil moisture in the watershed. Vegetation effects were also minimized. The analysis showed that HH polarization is having good coefficient of determination when compared with HV polarization. But the correlation obtained was less because of the limitation in the dataset used.

Hence remote sensing shows a potential and promising means of providing spatial and temporal distributed data at multiple scales and on a consistent and timely basis to infer soil moisture. Thus information about soil moisture condition can be derived from measurements in all parts of electromagnetic spectrum.

7.2 SCOPE OF FURTHER RESEARCH

- Analysis of soil moisture using microwave data should be done for the whole watershed with more number of ground observed points.
- Unavailability of data for validation of MIKE SHE. Validation should be done so that the model can be used in future prediction. Also other outputs from MIKE SHE should be analyzed.
- High resolution temporal images should be used to infer soil moisture as they showed good results.

REFERENCES

Abbott, M.B., Bathurst, J.C., Cunge, J.A., O'Connell, P.E. and Rasmussen, J., 1986. An Introduction to the European Hydrological System-Systeme Hydrologique European,"SHE",2:Structure of a Physically Based,Distributed Modelling System. Journal of Hydrology, 87: 61-77.

Abedinia, M.J., Dickinsonb, W.T. and Rudrab, R.P., 2006. On depressional storages: The effect of DEM spatial resolution. Journal of Hydrology, 318: 138-150.

Adegoke, J.O. and Carleton, A.M., 2001. Relations between Soil Moisture and Satellite Vegetation Indices in the U.S. Corn Belt. Journal of Hydrometrology, 3: 395-405.

Akinremi, O.O., McGinn, S.M. and Barr, A.G., 1995. Simulation of soil moisture and other components of the hydrological cycle using a water budget approach. Canadian Journal of Soil Science, 75: 133-142.

Alam, M. and Rogers, D.H., 2001. Scheduling irrigations by electrical resistance blocks, Kansas State University Agricultural Experiment Station and Cooperative Extension Service Series, Manhattan, Kansas.

Andersen, J., Dybkjaer, G., Jensen, K.H., Refsgaard, J.C. and Rasmussen, K., 2002. Use of remotely sensed precipitation and leaf area index in a distributed hydrological model. Journal of Hydrology, 264: 34-50.

Artan, G.A., Neale, C.M.U. and Tarboton, D.G., 2000. Characteristic length scale of input data in distributed models:implications for modeling grid size. Journal of Hydrology, 227: 128-139.

Baghdadi, N., Holah, N. and Zribi, M., 2006a. Calibration of the Integral Equation Model for SAR data in C-band and HH and VV polarizations. International Journal of Remote Sensing, 27(4): 805–816.

Baghdadi, N., Holah, N. and Zribi, M., 2006b. Soil moisture estimation using multi-incidence and multi-polarization ASAR data. International Journal of Remote Sensing, 27(10): 1907–1920.

Baishya, B., 2004. Hydrological modelling of Umiam catchment in Meghalaya using MIKE SHE. Unpublished Thesis, Indian Institute of Remote Sensing, Dehradun.

Bathurst, J.C., 1986. Physically Based Distributed Modelling of an upland catchment using Systeme Hydrologique European. Journal of Hydrology, 87: 79-102.

Behrens, T., Gregor, K. and Diepenbrock, W., 2005. Separation of soil and canopy reflectance signaturesof Mid German agricultural soils. Plant Soil Environ, 51(7): 296-303.

Biftu, G.F. and Gan, T.Y., 2001. Semi-distributed, physically based, hydrologic modeling of the Paddle River Basin, Alberta, using remotely sensed data. Journal of Hydrology, 244: 137-156.

Bindlish, R. and Barros, A.P., 2000. Multifrequency soil moisture inversion from SAR measurements with the use of IEM. Remote sensing of Environment, 71(1): 67-88.

Boegha, E. et al., 2004. Incorporating remote sensing data in physically based distributed agro-hydrological modelling. Journal of Hydrology, 287: 279-299.

Carlaw, S.M., 2000. Soil Moisture Accounting in Distributed Hydrologic Modelling. Master of Science Thesis, University of Waterloo, 180 pp.

Carpenter, T.M. and Georgakakos, K.P., 2006. Discretization scale dependencies of the ensemble flow range versus catchment area relationship in distributed hydrologic modeling. Journal of Hydrology, 328: 242-257.

Cashiona, J., Lakshmi, V., Boschb, D. and Jackson, T.J., 2005. Microwave remote sensing of soil moisture: evaluation of the TRMM microwave imager (TMI) satellite for the Little River Watershed Tifton, Georgia. Journal of Hydrology, 307: 242-253.

Cavazza, L., Patruno, A. and Cirillo, E., 2007. Effect of yearly oscillating water table on soil moisture retention curves. Biosystems Engineering, 98: 257 – 265.

Chakraborthy, A., 2007. Soil Moisture Estimation using C-Band Multi-Beam RADARSAT SAR data under Dynamic Surface and Vegetation Condition. Phd Thesis, Indian Agricultural Reasearch Institute, New Delhi.

Christiaens, K. and Feyen, J., 2001. Analysis of uncertanities associated with different methods to determine soil hydraulic properties and their propogation in the distributed hydrological MIKE SHE model. Journal of Hydrology, 246: 63-81.

Chubey, M.S. and Hathout, S., 2004. Integration of RADARSAT and GIS modelling for estimating future Red River flood risk. GeoJournal, 59: 237–246.

Cosh, M.H., Jackson, T.J., Starks, P. and Heathman, G., 2006. Temporal stability of surface soil moisture in the Little Washita River watershed and its applications in satellite soil moisture product validation. Journal of Hydrology, 323: 168-177.

Craig, R.F., 1992. Soil Mechanics. Chapman & Hall USA, New York, New York, USA, 427 pp.

Cuenca, R.H., 1998. Boreas hyd-01 Volumetric Soil Moisture Data Text Document. http://www-eosdis.ornl.gov/BOREAS/boreas_home_page.html.

Cuenca, R.H., Stangel, D.E. and Kelly, S.F., 1997. Soil water balance in a boreal forest. Journal of Geophysical Research, 102(D24): 29355-29365.

Dingman and Lawrence, S., 1994. Physical Hydrology. Prentice-Hall, Inc., Englewood Cliffs, New Jersey, USA, 575 pp.

Dunna, S.M. and Colohana, R.J.E., 1999. Developing the snow component of a distributed hydrological model: a step-wise approach based on multi-objective analysis. Journal of Hydrology, 223: 1-16.

Eckhardt, K. and Arnold, J.G., 2001. Automatic calibration of a distributed catchment model. Journal of Hydrology, 251: 103-109.

Ellyett, C.D. and Pratt, D.A., 1975. A review of the potential application of remote sensing techniques to hydro-geological studies in australia, Australian Water Resources Council Technical Paper, pp. 147.

Eng, D., Kolev, N. and Sci., D., 2005. "Instrumental Evaluation of Soil Physics Parameters on the Field". European Soil Bureau, 1-8 pp.

Engman, T., 1991. Application of remote sensing of soil moisture for water resources and agriculture. Remote sensing of environment, 35: 213-226.

Eni G. Njoku, Jackson, T.J., Lakshmi, V., Chan, T.K. and Nghiem, S.V., 2003. Soil moisture retrieval from AMSR-E. IEEE Transactions on Geo-Science and Remote Sensing, 141(2): 215-229.

Farrar, T.J., Nichilson, S.E. and Lare, A.R., 1994. The influence of soil type on the relationships between NDVI, rainfall and soil moisture in semi-arid Botswana.2. NDVI response to soil moisture. Remote sensing of Environment, 50: 121 -133.

Fensholt, R. and Sandholt, I., 2003. Derivation of a Shortwave Infra-red Water Stress Index from MODIS near-and shortwave Infrared Data in a Semiarid Environment. Remote Sensing of Environment, 87: 111-121.

Frances, F., Velez, J.I. and Velez, J.J., 2007. Split-parameter structure for the automatic calibration of distributed hydrological models. Journal of Hydrology, 332: 226-240.

Gotzinger, J. and Bardossy, A., 2007. Comparison of four regionalisation methods for a distributed hydrological model. Journal of Hydrology, 333: 374-384.

Goyal, V.C., Gupta, P.K., Seth, S.M. and Singh, V.N., 1998. Estimation of Temporal Changes in Soil Moisture Using Resistivity Method. Hydrological Processes, 10(9): 1147 - 1154.

Haider, S.S., Said, S., Kothyari, U.C. and Arora, M.K., 2004. Soil moisture estimation using ERS-2 SAR data: a case study in the Solani river catchment. Hydrological Science Journal, 49(2): 323-334.

Hanson, B., Peters, D. and Orloff, S., 2000. Effectiveness of tensiometers and electrical resistance sensors varies with soil conditions. California Agriculture, 54(3): 47-50.

Helmers, M.J. and Eisenhauer, D.E., 2006. Overland flow modeling in a vegetative filter considering non-planar topography and spatial variability of soil hydraulic properties and vegetation density. Journal of Hydrology, 328: 267-282.

Huang, M. and Liang, X., 2006. On the assessment of the impact of reducing parameters and identification of parameter uncertainties for a hydrologic model with applications to ungauged basins. Journal of Hydrology, 320: 37-61.

Hundecha, Y. and Bardossy, A., 2004. Modeling of the effect of land use changes on the runoff generation of a river basin through parameter regionalization of a watershed model. Journal of Hydrology, 292: 281-295.

Hutjesa, R.W.A. et al., 1998. Biospheric Aspects of the Hydrological Cycle. Journal of Hydrology, 212-213: 1-21.

Idso, S.B., Jackson, R.D. and Reginato, R.J., 1976. Calculation of evaporation rates during the transistion from energy-limiting to soil limiting phases using albedo data. Water Resource Reasearch, 12(1): 23-26.

Jackson, T.J., Schmugge, T.J. and Engman, E.T., 1996. Remote Sensing Applications to Hydrology: Soil Moisture. Hydrological Sciences Journal, 41: 517-530.

Jacques, D., Simunek, J., Timmerman, A. and Feyen, J., 2002. Calibration of Richards' and convection-dispersion equations to field-scale water flow solute transport under rainfall conditions. Journal of Hydrology, 259: 15-31.

Jain, S.K., Storm, B., Bathurst, J.C., Refsgaard, J.C. and Singh, R.D., 1992. Application of the SHE to catchments in India Part2.Field experiments and Simulation Studies with the SHE on the Kolar subcatchment of the Narmada River. Journal of Hydrology, 140: 25-47.

Jaina, M.K., Kothyarib, U.C. and Raju, K.G.R., 2004. A GIS based distributed rainfall–runoff model. Journal of Hydrology, 299: 107-135.

Jayatilaka, C.J., Storm, B. and Mudgway, L.B., 1998. Simulation of water flow on irrigation bay scale with MIKE SHE. Journal of Hydrology, 208: 108-130.

Jonsdottir, H., Madsen, H. and Palsson, O.P., 2006. Parameter estimation in stochastic rainfall-runoff models. Journal of Hydrology, 326: 379-393.

Katra, I., Blumberg, D.G., Lavee, H. and Sarah, P., 2007. Topsoil moisture patterns on arid hillsides – Micro-scale mapping by thermal infrared images. Journal of Hydrology, 334: 359-367.

Kim, S. and Kim, H., 2007. Stochastic analysis of soil moisture to understand spatial and temporal variations of soil wetness at a steep hillside. Journal of Hydrology, 341: 1-11.

Kirda, C. and Reichardt, K., 1992. Comparison of Neutron Moisture Gauges with Nonnuclear Methods to Measure Field Soil Water Status. Scientia Agricola, Piracicaba-SP, 49(1): 111-121.

Kolev et al., 1994. Remote sensing and synchronous land surface measurements forestimation of soil moisture and temperature, Geoscience and Remote Sensing Symposium, 1994. IGARSS '94. Surface and Atmospheric Remote Sensing: Technologies, Data Analysis and Interpretation, Pasadena, CA, USA, pp. 1442-1444.

Kumar, C.P., 1991. Application of SHE Model to Hemavati (up to Sakleshpur) Basin. Hydrology Journal of IAH, XIV(No.4): 209-227.

Kumar, P., 2004. Layer averaged Richard's equation with lateral flow. Advances in Water Resources, 27: 521-531.

Kumar, R., S.M.Seth and R.D.Singh, 1996. Sensitivity Analysis of the SHE Model for a Typical Grid of Ganjal Sub-Basin of River Narmada. Hydrology Journal, XIX(1): 72-84.

Lakshmi, V., Wood, E.F. and Choudhury, B.J., 1997. Evaluation of Special Sensor Microwave/Imager Satellite Data for Regional Soil Moisture Estimation over the Red River Basin. Journal of Applied Metrology, 36: 1305-1328.

Li, J. and Islam, S., 2002. Estimation of root zone soil moisture and surface fluxes partitioning using near surface soil moisture measurements. Journal of Hydrology, 259: 1-14.

Liu, Y., Hiyama, T. and Yamaguchi, Y., 2006. Scaling of land surface temperature using satellite data:A case examination on ASTER and MODIS products over a heterogeneous terrain area. Remote Sensing of Environment, 105(115-128).

Lobell, D.B. and Asner, G.P., 2002. Moisture Effects on Soil Reflectance. Soil Science Society of America Journal, 66: 722-727.

Lunt, I.A., S.S.Hubbard and Y.Rubin, 2005. Soil moisture content estimation using ground-penetrating radar reflection data. Journal of Hydrology, 307: 254-269.

Madsen, H., 2003. Parameter estimation in distributed hydrological catchment modelling using automatic calibration with multiple objectives. Advances in Water Resources, 26: 205-216.

Maeda, K., Tanaka, T., Park, H. and Hattori, S., 2006. Spatial distribution of soil structure in a suburban forest catchment and its effect on spatio-temporal soil moisture and runoff fluctuations. Journal of Hydrology, 321: 232-256.

Maidment and R, D., 1993. Handbook of Hydrology. McGraw-Hill Inc., USA.

Manfreda, S., McCabe, M.F., Fiorentino, M., Rodrý´guez-Iturbe, I. and Wood, E.F., 2007. Scaling characteristics of spatial patterns of soil moisture from distributed modelling. Advances in Water Resources, 30: 2145–2150.

Martinez-Fernandez, J. and Ceballos, A., 2005. Mean soil moisture estimation using temporal stability analysis. Journal of Hydrology, 312: 28-38.

McCabe, G.J., 1999. Evaluating the use of "goodness of fit" measures in hydrologic and hydroclimatic model validation. Water Resources Research, 35: 233-241.

McMichaela, C.E., Hopeb, A.S. and Loaiciga, H.A., 2006. Distributed hydrological modelling in California semi-arid shrublands:MIKESHEmodel calibration and uncertainty estimation. Journal of Hydrology, 317: 307-324.

McVicar, T.R. and Jupp, D.L.B., 1998. The current and potential operational uses of remote sensing to aid decisions on drought exceptional circumstances in Australia: A review. Agricultural Systems, 57(3): 399-468.

Mertens, J., Madsen, H., L, F., Jacques, D. and Feyen, J., 2004. Including prior information in the estimation of effective soil parameters in unsaturated zone modelli. Journal of Hydrology, 294(4): 251-269.

Moreda, F., Koren, V., Zhang, Z., Reed, S. and Smith, M., 2006. Parameterization of distributed hydrological models: learning from the experiences of lumped modeling. Journal of Hydrology, 320: 218-237.

Mukund, A., 2007. Analysing Performance of Optical and Passive Microwave data to Infer Soil Moisture in the Upper Soil Layers for the Prominent Crops in Eastern Part of Rajasthan,India, ITC & IIRS, Dehradun.

Muleta, M.K. and Nicklow, J.W., 2005. Sensitivity and uncertanity analysis coupled with automatic calibration for a distributed watershed model. Journal of Hydrology, 306: 127-145.

oevelen, P.J.V., 2000. Estimation of aerial soil water content through microwave remote sensing,Doctoral Thesis, Wageningen University, 227 pp.

Oldak, A., Pachepsky, Y., Jackson, T.J. and Rawls, W.J., 2002. Stastical properties of soil moisture images revisited. Journal of Hydrology, 255: 12-24.

Olyphant, G.A., 2003. Temporal and spatial (down profile) variability of unsaturated soil hydraulic properties determined from a combination of repeated field experiments and inverse modeling. Journal of Hydrology, 281: 23-35.

Oogathoo, S., 2006. Runoff simulation in the canagagigue creek watershed using the mike she model. MS Thesis, McGill University, Canada, 121 pp.

Pachepskya, Y., Timlinb, D. and Rawls, W., 2003. Generalized Richards' equation to simulate water transport in unsaturated soils. Journal of Hydrology, 272: 3-13.

Panday, S. and Huyakorn, P.S., 2004. A fully coupled physically-based spatially-distributed model for evaluating surface/subsurface flow. Advances in Water Resources, 27: 361–382.

Parent, A.-C., Anctil, F. and Parent, L.-E.t., 2006. Characterization of temporal variability in near-surface soil moisture at scales from 1 h to 2 weeks. Journal of Hydrology, 325: 56-66.

Parida, B.R., 2006. Analysing the effect of severity and duration of Agricultural drought on crop performance using Terra/MODIS Satellite data and Meteorological data. MSc Thesis, IIRS and ITC, 104 pp.

Prasad, V.H., Agarawal, S. and A.K.Chakraborti, 1997. Surface Soil Moisture Assessment using Landsat TM Middle Infrared Band Data. Asian-Pacific Remote Sensing and GIS Journal, 9(2): 63-68.

R.Subbaiah, 1996. Development and Validation of a Simple Soil Moisture Status Model. Hydrology Journal, XIX(1): 19-31.

Roth, K., Schulin, R., Fluhler, H. and Attinger, W., 1990. Calibration of Time Domain Reflectometry for Water Content Measurement Using a Composite Dielectric Approach. Water Resources Research, 26(10): 2267-2273.

Sadeghi, A.M., Hancock, G.D., Waite, W.P., Scott, H.D. and Rand, J.A., 1984. Microwave measurements of moisture distributions in the upper soil profile. Water Resource research, 20(7): 927-934.

Sahoo, G.B., Ray, C. and Carlo, E.H.D., 2006. Calibration and validation of physically distributed hydrological model, MIKE SHE, to predict streamflow at high frequency in a flashy mountainous Hawaii stream. Journal of Hydrology, 327: 94-109.

Sandholt, I., Rasmussen, K. and Anderson, J., 2002. A simple interpretation of the surface temperature vegetation index space for assessment of surface moisture status. Remote sensing of Environment, 79: 213-224.

Santanello, J.A. et al., 2007. Using remotely-sensed estimates of soil moisture to infer soil texture and hydraulic properties across a semi-arid watershed. Remote Sensing of Environment, 110: 79–97.

Schaefli, B., Talamba, D.B. and Musy, A., 2007. Quantifying hydrological modeling errors through a mixture of normal distributions. Journal of Hydrology, 332: 303-315.

Schumann, A.H., Funke, R. and Schultz, G.A., 2000. Application of a geographic information system for conceptual rainfall-runoff modeling. Journal of Hydrology, 240: 45-61.

Schwab, G.O., Fangmeier, D.D., Elliot, W.J. and Frevert., R.K., 1993. Soil and Water Conservation Engineering. 4th ed. New York: Wiley.

Serrano, S.E. and Workman, S.R., 1998. Modeling transient stream/aquifer interaction with the non-linear Boussinesq equation and its analytical solution. Journal of Hydrology, 206: 245-255.

Severino, G., Santini, A. and Sommella, A., 2003. Determining the soil hydraulic conductivity by means of a field scale internal drainage. Journal of Hydrology, xx: 1-15.

Simpsona, M.J. and Clement, T.P., 2003. Comparison of finite difference and finite element solutions to the variably saturated flow equation. Journal of Hydrology, 270: 49-64.

Singh, R.P., S.R.Oza, K.N.Chaudhari and V.K.Dhadwal, 2005. Spatial and Temporal Patterns of Surface Soil Moisture over India Estimated using Surface Wetness Index from SSM/I Microwave Radiometer. International Journal of Remote Sensing, 26(6): 1269-1276.

Srinivasulu, J. and Kulkarni, A.V., 2004. Estimation of spectral reflectance of snow from IRS-1D LISS-III sensor over the Himalayan terrain, Proc. Indian Acad. Sci. (Earth Planet. Sci.),, pp. 117-128.

Starks, P.J., Heathman, G.C., Ahuja, L.R. and Ma, L., 2003. Use of limited soil property data and modeling to estimate root zone soil water content. Journal of Hydrology, 272.

Starks, P.J., Heathman, G.C., Jackson, T.J. and Cosh, M.H., 2006. Temporal stability of soil moisture profile. Journal of Hydrology, 324: 400-411.

Svetlitchnyi, A.A., Plotnitskiy, S.V. and Stepovaya, O.Y., 2003. Spatial distribution of soil moisture content within catchments and its modelling on the basis of topographic data. Journal of Hydrology, 277: 50-60.

Tansey, K.J., Millington, A.C., Battikhi, A.M. and White, K.H., 1999. Monitoring soil moisture dynamics using satellite imaging radar in northeastern Jordan. Applied Geography, 19(325-344).

Tartakovsky, D.M., Lu, Z., Guadagnini, A. and Tartakovsky, A.M., 2003. Unsaturated flow in heterogeneous soils with spatially distributed uncertain hydraulic parameters. Journal of Hydrology, 275: 182-193.

Temimi, M., Leconte, R., Brissette, F. and Chaouch, N., 2007. Flood and soil wetness monitoring over the Mackenzie River Basin using AMSR-E 37 GHz brightness temperature. Journal of Hydrology, 333: 317-328.

Thompson, J.R., Sorenson, H.R., Gavin, H. and Refsgaard, A., 2004. Application of the coupled MIKE SHE/MIKE 11 modelling system to a lowland wet grassland in southeast England. Journal of Hydrology, 294: 151-179.

Topp, G.C., Davis, J.L. and Annan, A.P., 1980. Electromagnetic Determination of Soil Water Content: Measurements in Coaxial Transmission Lines. Water Resources Research, 16(3): 574-582.

Troch, P.A., Troch, F.P.d., Debruyckere, L. and Cosyn, B., 1994. Organization of the summer 94 Field Campaigns in the Zwalm Test Site, Proceedings of the first workshop on data collection and data analysis issues for spatial and temporal soil moisture mapping from ERS-1 and JERS-1 SAR data and macroscale hydrologic modeling (EV5V-CT9-0446), Institute for agricultural Hydraulics, University of Naples, Italy, pp. 14-24.

Troofleau, D. and Segaard, H., 1998. Deriving surface water status in the sahel from the pathfinder AVHRR Land data set. Physics , Chemistry , Earth, 23(4): 421-426.

Trung, L.V. and Minch, N.T., Mapping land surface temperature(LST) from satellite imageries. Case study in Hochiminh city.

Uhlenbrook, S., Roser, S. and Tilch, N., 2004. Hydrological process representation at the meso-scale: the potential of a distributed, conceptual catchment model. Journal of Hydrology, 291: 278-296.

Ulaby, F.T., Dubois, P.C. and Zyl, J.v., 1996. Radar mapping of surface soil moisture. Journal of Hydrology, 184: 57-84.

V´azquez, R.F., Feyen, L., Feyen, J. and Refsgaard, J.C., 2002. Effect of grid size on effective parameters and model performance of the MIKE-SHE code. Hydrological Processes, 16: 355–372.

VanDam, J.C. and Feddes, R.A., 2000. Numerical simulation of infiltration, evaporation and shallow groundwater levels with the Richards equation. Journal of Hydrology, 233: 72-85.

Varado, N., Braud, I., Ross, P.J. and Haverkamp, R., 2006. Assessment of an efficient numerical solution of the 1D Richards' equation on bare soil. Journal of Hydrology, 323: 244-257.

Vazquez, R.F. and Feyen, J., 2003. Effect of potential evapotranspiration estimates on effective parameters and performance of the MIKE SHE-code applied to a medium-size catchment. Journal of Hydrology, 270: 309-327.

Vazquez, R.F. and Feyen, J., 2007. Assessment of the effects of DEM gridding on the predictions of basin runoff using MIKE sHE and a modelling resolution of 600m. Journal of Hydrology, 334: 73-87.

Verhoef, A., Fernandez-Galvez, J., Diaz-Espejo, A., Main, B.E. and El-Bishti, M., 2006. The diurnal course of soil moisture as measured by various dielectric sensors: Effects of soil temperature and the implications for evaporation estimates. Journal of Hydrology, 321: 147-162.

Walker, J.P., Willgoose, G.R. and Kalma, J.D., 2004. In situ measurement of soil moisture: a comparison of techniques. Journal of Hydrology, 293: 85-99.

Wang, X., Xie, H., Guan, H. and Zhou, X., 2007. Different responses of MODIS-derived NDVI to root-zone soil moisture in semi-arid and humid regions. Journal of Hydrology, 340: 12-24.

Wei, L., Zhang, B. and Wang, M., 2007. Effects of antecedent soil moisture on runoff and soil erosion in alley cropping systems. Agricultuaral Water Management, 94: 54-62.

Western, A.W., Grayson, R.B. and Green, T.R., 1999. The Tarrawarra project: high resolution spatial measurement, modelling and analysis of soil moisture and hydrological response. Hydrological Processes, 13: 633-652.

Western, A.W. et al., 2004. Spatial correlation of soil moisture in small catchments and its relationship to dominant spatial hydrological processes. Journal of Hydrology, 286: 113-134.

Wetzel, P.J., Atlas, D. and Woodward, R.H., 1984. Determining soil moisture from geosynchronous satellite infrared data; A feasibility study. Journal of Climatology and Applied Meterology, 23: 375-391.

Wongprayoon, S., Vieira, C.A.O. and Leach, J.H.J., 2007. Spatial Accuracy Assessment for Coral Reef Classifications, Anais XIII Simpósio Brasileiro de Sensoriamento Remoto, Florianópolis, Brasil, pp. 6273-6281.

Wooldridge, S., Kalma, J. and Kuczera, G., 2001. Parameterization of a simple semi-distributed model for assessing the impact of land-use on hydrologic response. Journal of Hydrology, 254: 16-32.

Yang, H., Shi, J., Li, Z. and Guo, H., 2006. Temporal and spatial soil moisture change pattern detection in an agricultural area using multi-temporal Radarsat ScanSAR data. International Journal of Remote Sensing, 27(19): 4199–4212.

Yu, Z., Pollard, D. and Cheng, L., 2006. On continental-scale hydrologic simulations with a coupled hydrologic model. Journal of Hydrology, 331: 110-124.

Zazueta, F.S. and Xin, J., 1994. Soil Moisture Sensors, Florida Cooperative Extension Service, Institute of Food and Agricultural Sciences,, pp. 1-11.

Zhang, Y.-K. and Schilling, K.E., 2006. Effects of land cover on water table, soil moisture, evapotranspiration, and groundwater recharge: A Field observation and analysis. Journal of Hydrology, 319: 328-338.

Zhou, X., Lin, H.S. and White, E.A., 2007. Surface soil hydraulic properties in four soil series under different land uses and their temporal changes, CATENA, pp. 1-9.

Zribi, M., Bagdadi, N., Holah, N. and Fafin, O., 2005a. New methodology for soil surface moisture estimation and its application to ENVISAT-ASAR multi-incidence data inversion. Remote sensing of Environment, 96: 485-496.

APPENDIX A

SOIL MOISTURE CHARACTERSTIC CURVES FOR DIFFERENT SITES

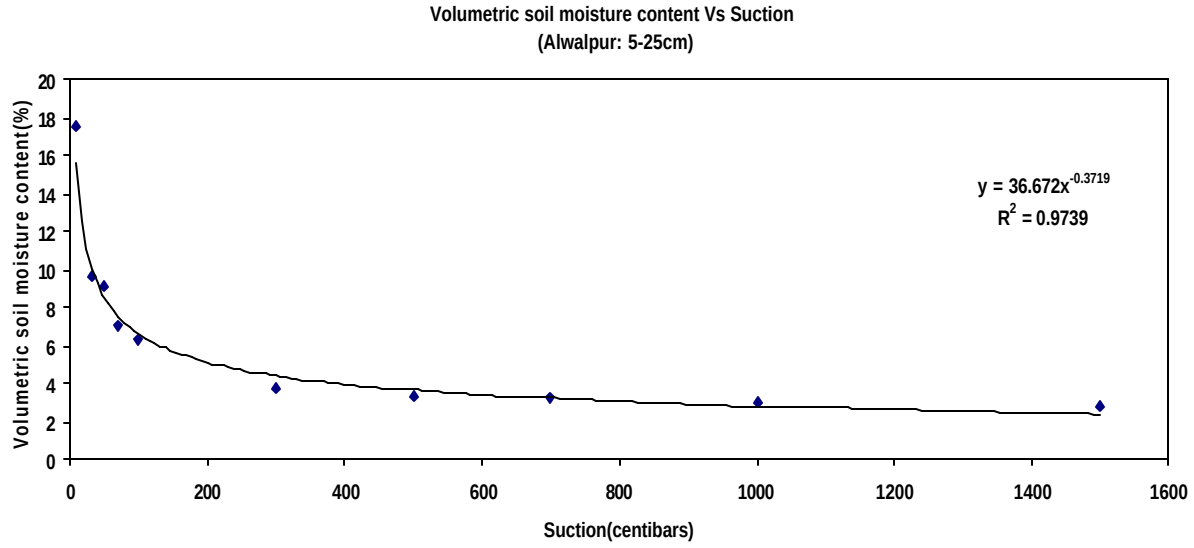

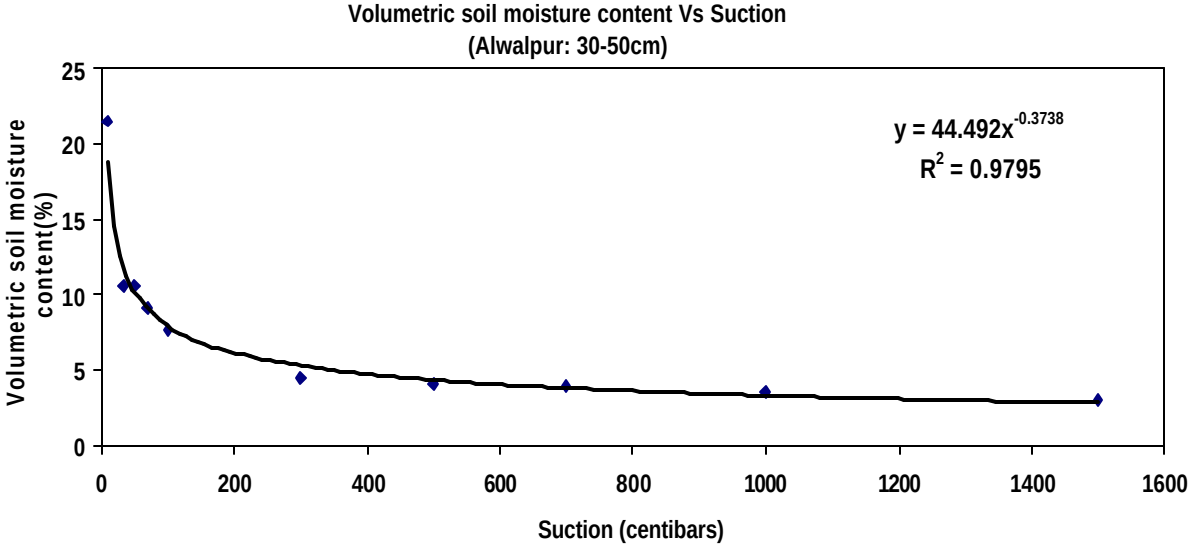

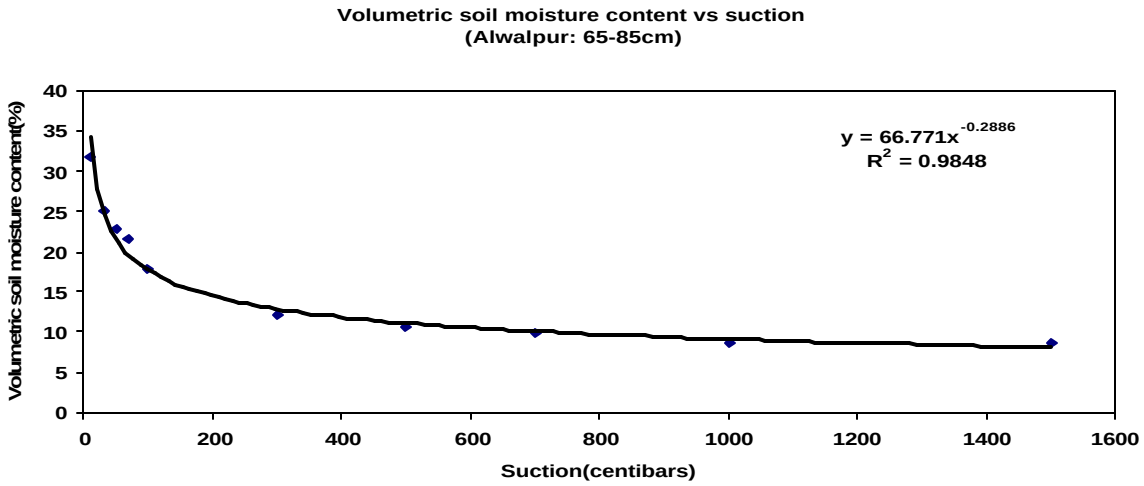

Soil moisture characteristic curve at Alawalpur

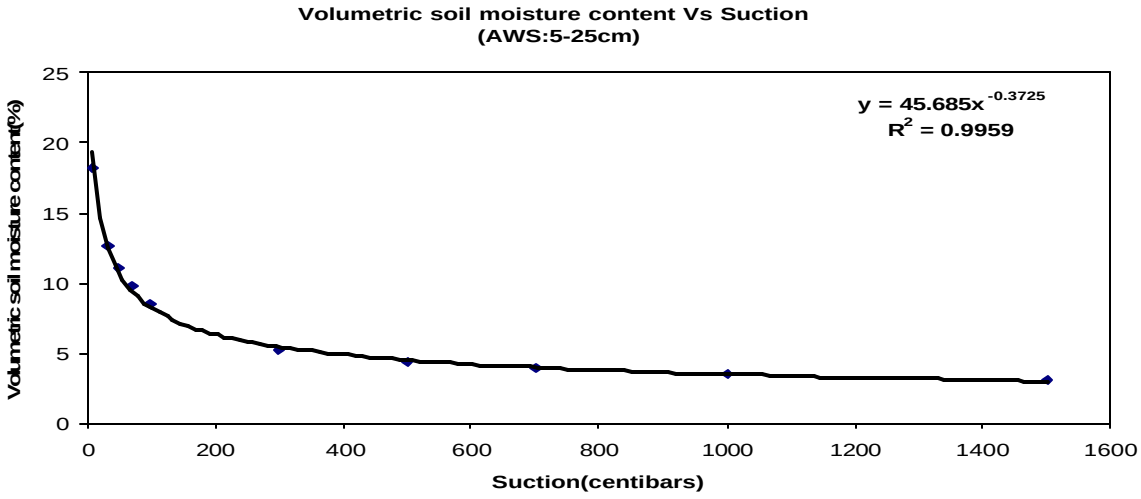

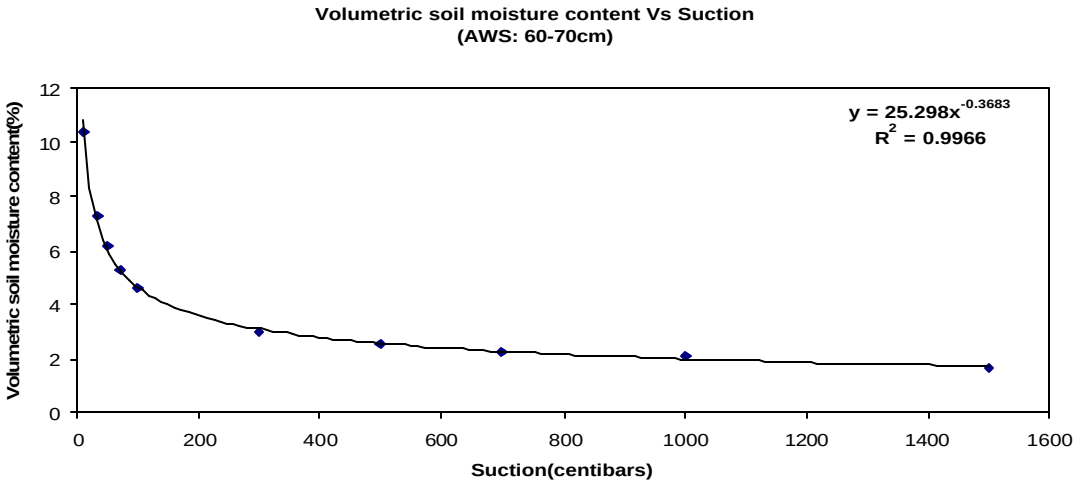

Soil moisture characterstic curve at AWS

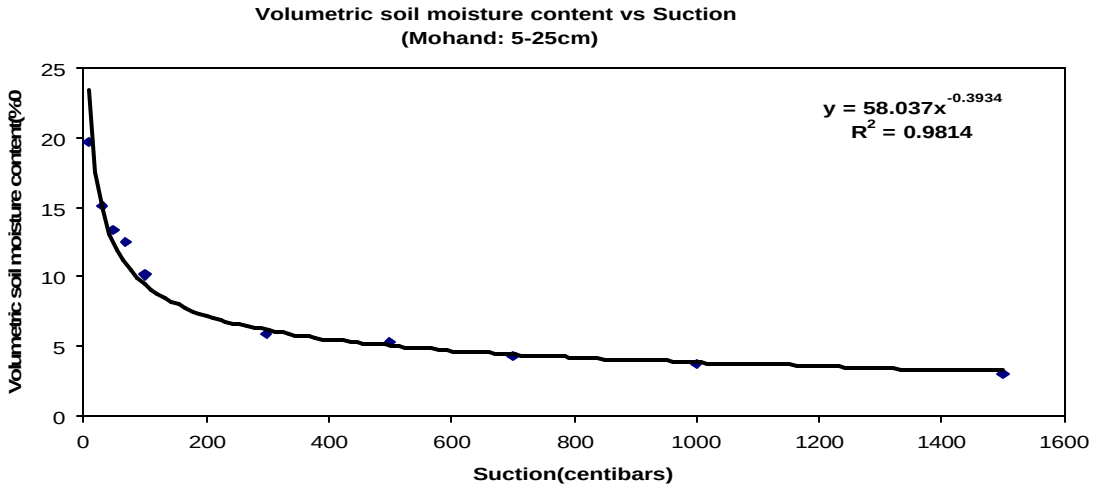

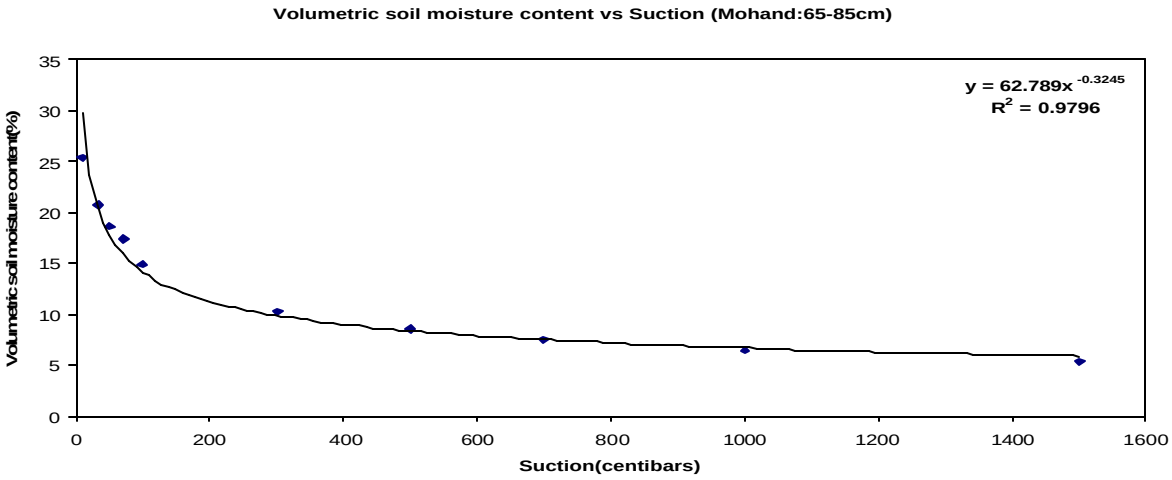

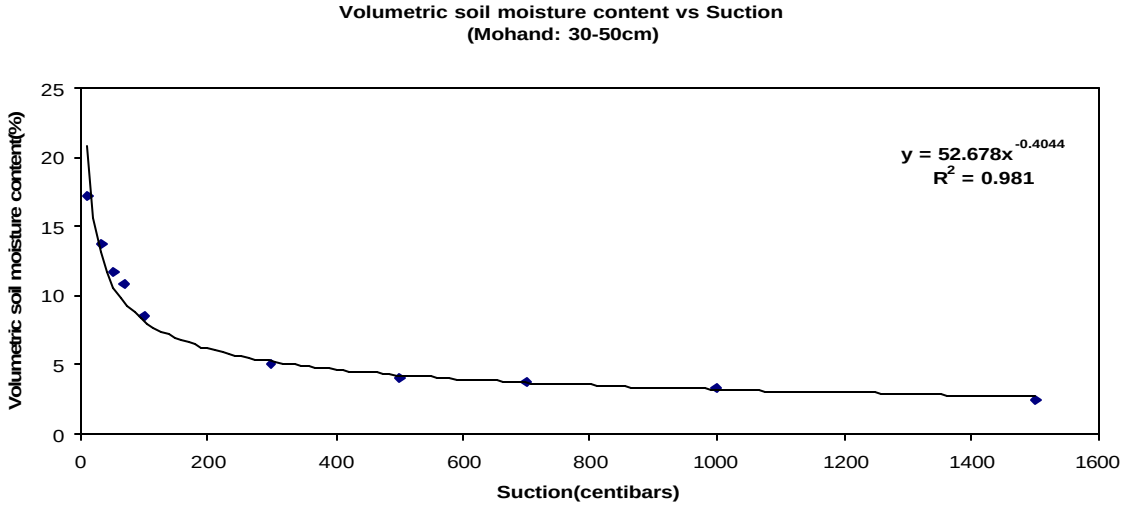

Soil moisture characteristic curve at Mohand

Tanda Misiri

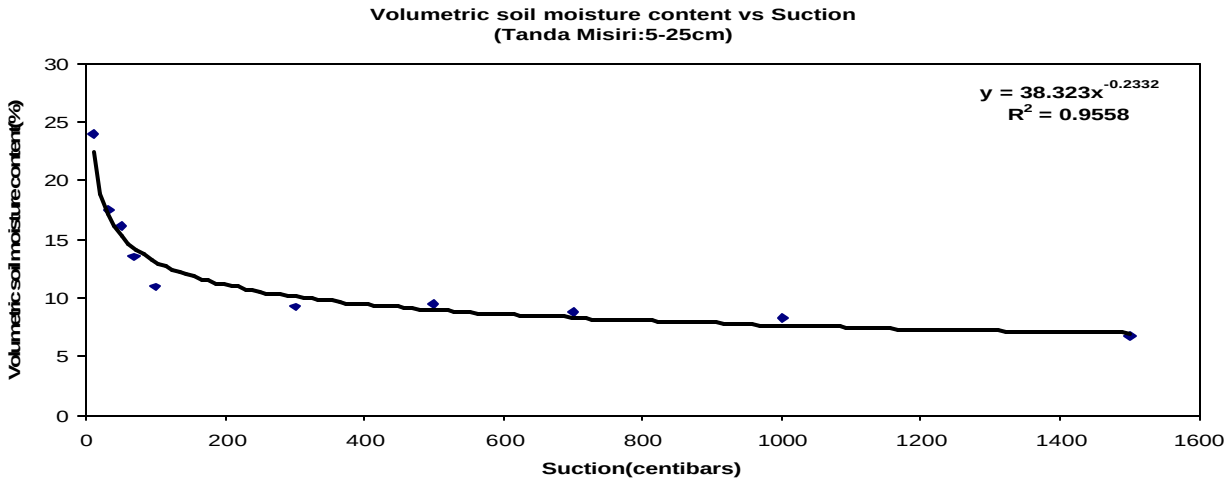

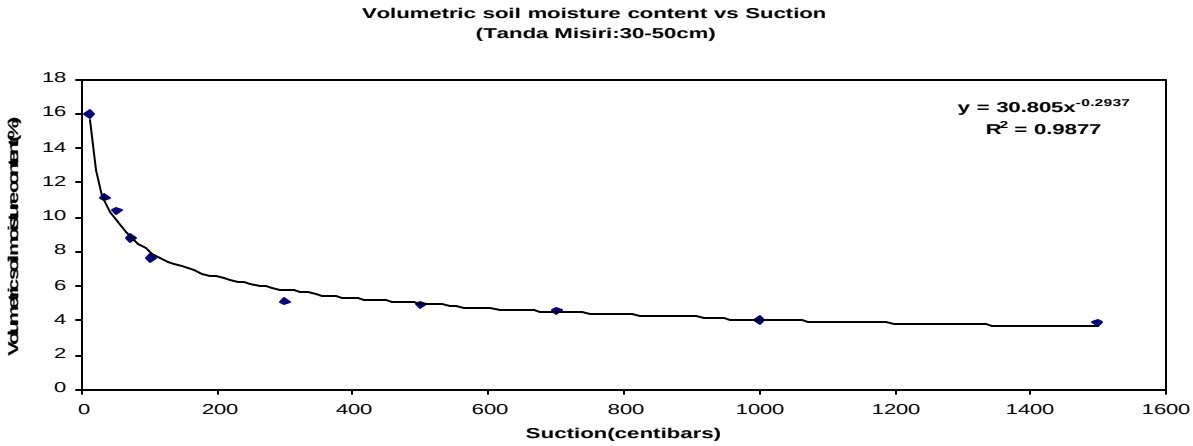

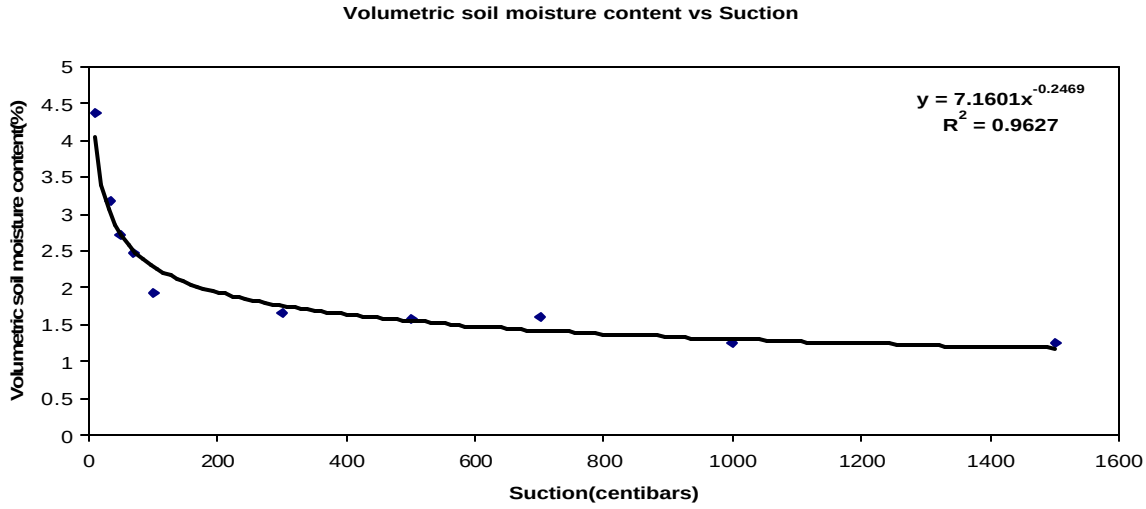

Soil moisture characterstic curve at Tanda Misiri

Sisona

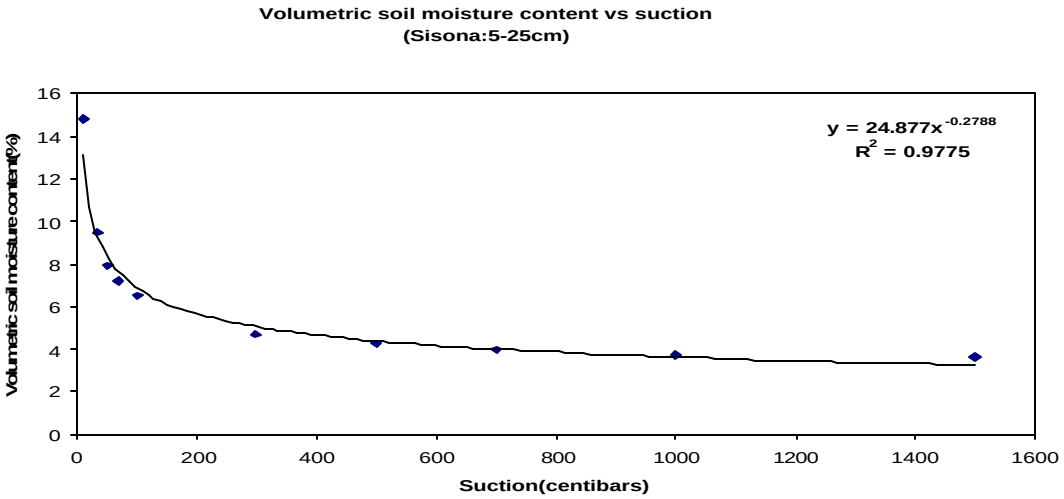

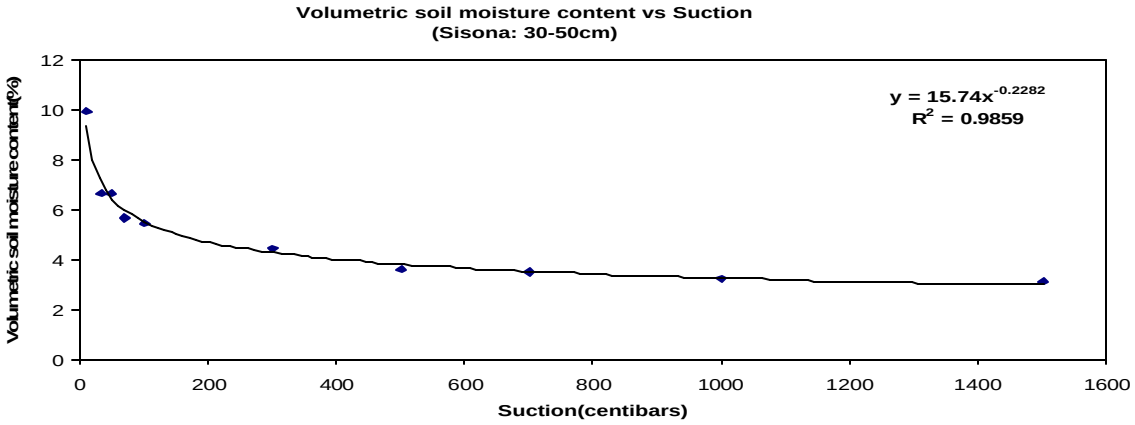

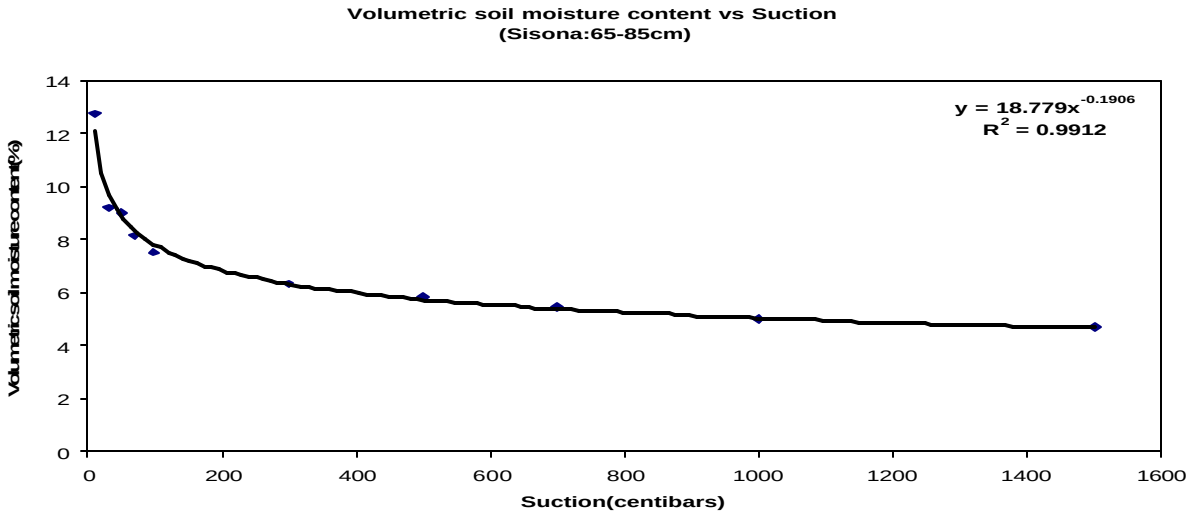

Soil moisture characteristic curve at Sisona

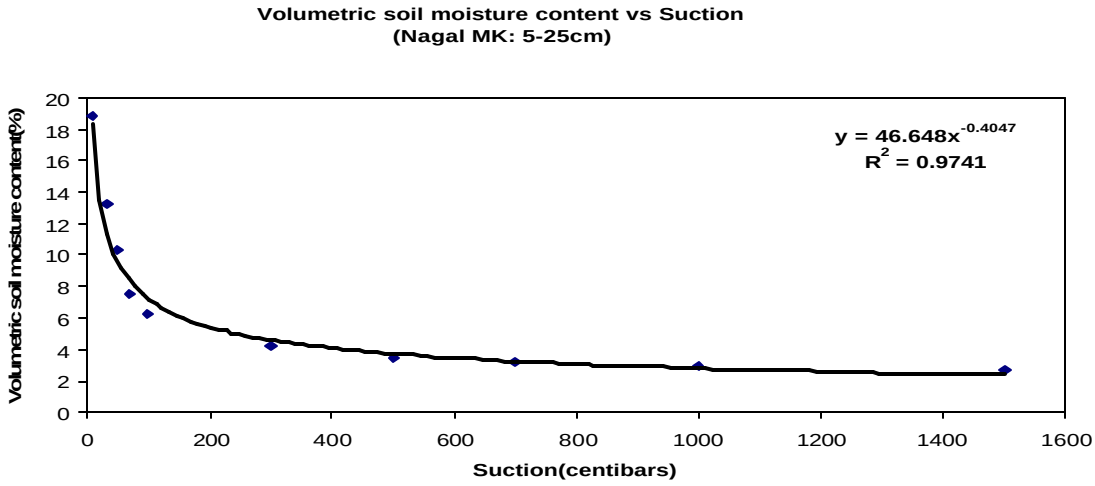

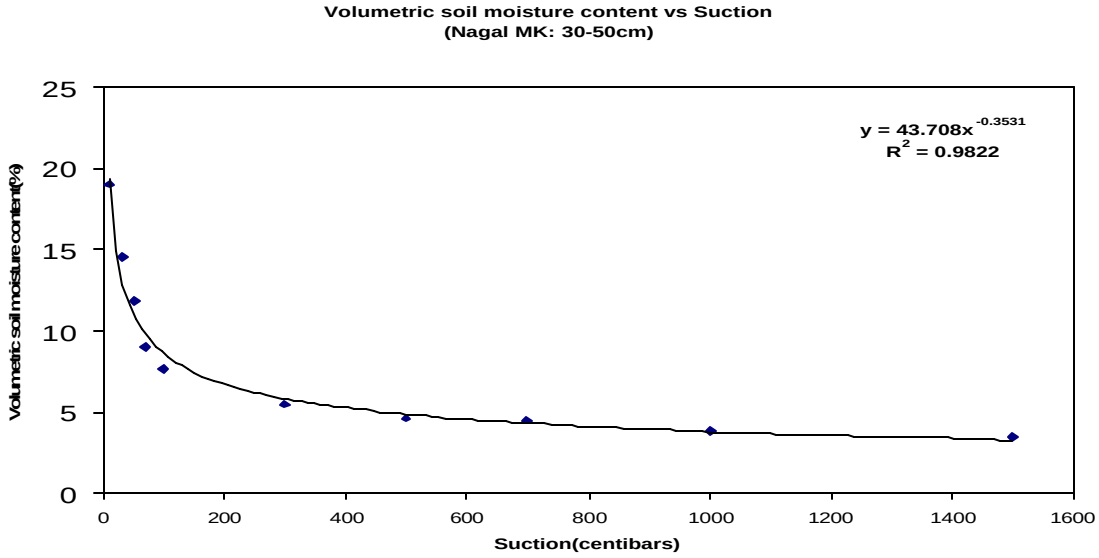

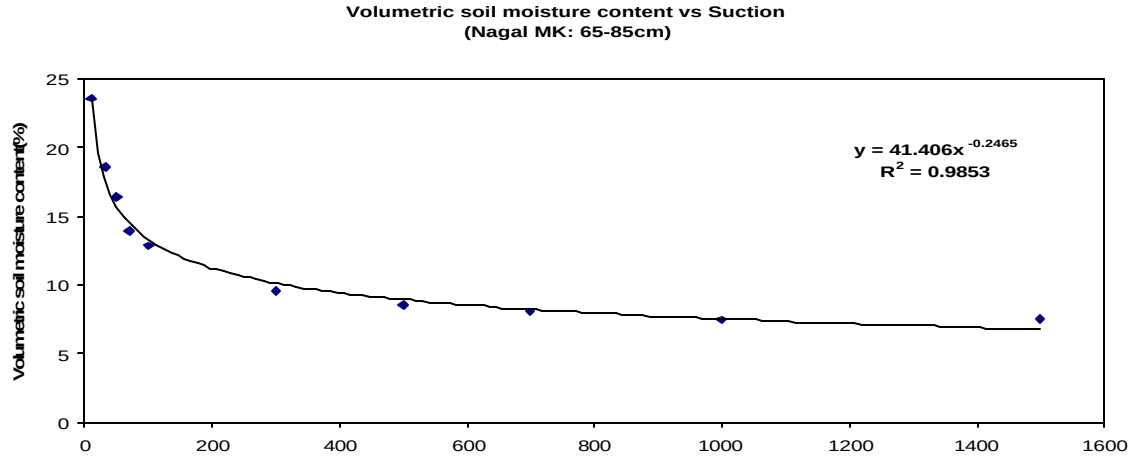

Soil characterstic curve at Nagal MK